

**REPUBLIC OF TURKEY
YILDIZ TECHNICAL UNIVERSITY
GRADUATE SCHOOL OF NATURAL AND APPLIED SCIENCES**

**RADIATIVE TRANSITIONS OF CHARMED BARYONS IN
LATTICE QUANTUM CHROMODYNAMICS (QCD)**

HÜSEYİN BAHTİYAR

**Ph.D. THESIS
DEPARTMENT OF PHYSICS
PROGRAM OF PHYSICS**

**ADVISER
ASSOC. PROF. DR. TAYLAN YETKİN**

**CO-ADVISER
PROF. DR. GÜRAY ERKOL**

İSTANBUL, 2017

REPUBLIC OF TURKEY
YILDIZ TECHNICAL UNIVERSITY
GRADUATE SCHOOL OF NATURAL AND APPLIED SCIENCES

**RADIATIVE TRANSITIONS OF CHARMED BARYONS IN LATTICE
QUANTUM CHROMODYNAMICS (QCD)**

A thesis submitted by HÜSEYİN BAHTİYAR in partial fulfillment of the requirements for the degree of **DOCTOR OF PHILOSOPHY** is approved by the committee on 16.05.2017 in Department of Physics.

Thesis Adviser

Assoc. Prof. Dr. Taylan YETKİN
Yıldız Technical University

Co-Adviser

Prof. Dr. Güray ERKOL
Özyeğin University

Approved by the Examining Committee

Assoc. Prof. Dr. Taylan YETKİN
Yıldız Technical University

Prof. Dr. Cenap ÖZBEN
İstanbul Technical University

Prof. Dr. Altuğ ÖZPİNECİ
Middle East Technical University

Assoc. Prof. Dr. Kutsal BOZKURT
Yıldız Technical University

Assist. Prof. Dr. Murat HÜDAVERDİ
Yıldız Technical University

ACKNOWLEDGEMENTS

Everything that has a beginning, has an end. Even a PhD thesis! Completing my PhD was a very important but challenging journey for me to become a physicist. It was impossible for me to complete this process without the help of my respectable supervisors, instructors, my friends and family.

First of all, I am really grateful to my co-supervisor Prof. Dr. Güray Erkol for leading me to work in Lattice QCD and I also would like to express him my sincere gratitude for always being there for me. I am very fortunate to have worked with such a valuable physicist, benefit from his scientific expertise and his profound knowledge. It would not have been possible to complete this process without the time and help that he spent with me. I would also like to give my deepest thanks to my supervisor Assoc. Prof. Dr. Taylan Yetkin for endless support and understanding. I am grateful that he is always there for me not only in my academic life but also in my personal life.

I would like to thank to my friend and colleague Dr. Kadir Utku Can for his continuous helps to both theoretical and numerical part of my study. I am grateful for his very valuable comments on this thesis. I feel very privileged to have taken QFT and Group Theory courses from Prof. Dr. Cemsinan Deliduman. These courses helped me tremendously in the theoretical part of my work. I can not thank him enough for taking me one step further by asking questions and comments, and sharing his knowledge and experience. I would like to thank to my thesis committee Prof. Dr. Cenap Özben, Prof. Dr. Altuğ Özpineci, Assoc. Prof. Dr. Kutsal Bozkurt and Assist. Prof. Dr. Murat Hüdaverdi for accepting to be a member on my jury. I would like to extend my sincerest thanks and appreciation to these wonderful four scientists for their insightful comments and suggestions.

I am grateful to Assist. Prof. Dr. Bora Işıldak for his valuable and helpful suggestions. His feedback has been a great help to overcome numerical problems on ROOT. I would like to thank my dear friend Özlem Özlüdil for the discussions, and for all the fun we have had in the last years. It is a pleasure to thank my friends who were present at my defense. We performed our computations using a modified version of Chroma software system [1] on CPU clusters and with QUDA [2, 3] for propagator inversion on GPUs. We use lattice configurations generated by the PACS-CS collaboration [4], with $O(a)$ -improved Wilson quark action and the Iwasaki gauge action.

I would like to thank my family for supporting me throughout writing this thesis and my life in general. Finally, and most importantly, I would like to thank my beloved wife Başak for her unwavering love, encouragement and understanding. She is my inspiration and motivation to never stop improving my knowledge.

This thesis is dedicated to my father and my wife.

May, 2017

Hüseyin BAHTİYAR

TABLE OF CONTENTS

	Page
LIST OF SYMBOLS	vii
LIST OF ABBREVIATIONS	viii
LIST OF FIGURES	xii
LIST OF TABLES	xii
ABSTRACT	xiv
ÖZET	xvi
CHAPTER 1	
INTRODUCTION	1
1.1 Literature Review	1
1.2 Objective of the Thesis	2
1.3 Hypothesis	4
CHAPTER 2	
STANDARD MODEL AND LATTICE QCD	6
2.1 Introduction	6
2.1.1 Quantum Electrodynamics	8
2.1.2 Weak Interaction	11
2.1.3 Quantum Chromodynamics	11
2.1.4 Non-Perturbative Methods	13
2.2 Lattice Quantum Chromodynamics	15
2.2.1 Path Integral in Lattice QCD	16
2.2.2 Discretization of the Gauge Fields	17
2.2.3 Naive Discretization of Fermions	20
2.2.4 Fermion Doubling Problem	22
2.2.5 Wilson's Fermions	25
2.2.6 Other Lattice Fermion Actions	26
2.2.6.1 Staggered Fermions	26

2.2.6.2	Twisted Mass Fermions	27
2.2.6.3	Domain Wall Fermions	27
2.2.7	Hopping Expansion	28
2.2.7.1	Hopping Expansion of the Quark Propagator	28
2.2.7.2	Hopping Expansion of the Fermion Determinant	30
2.2.8	Symanzik Improvement of Quark Propagator	30
2.3	Discrete Symmetries	33
2.3.1	Parity	33
2.3.2	Charge Conjugation	34
2.3.3	Time-Reversal and γ_5 -hermicity	35
CHAPTER 3		
TECHNICALITIES		36
3.1	Correlators in Lattice QCD	36
3.1.1	Interpolating Fields	36
3.1.2	Two-Point Correlators	38
3.2	Lattice Simulations	42
3.2.1	Quark Sources	43
3.2.1.1	Wall Smearing	45
3.2.2	CHROMA Software	45
3.3	Baryon Spectroscopy and Form Factors	46
3.3.1	Effective Mass	46
3.3.2	Form Factors	48
3.3.2.1	Form Factors in Lattice QCD	54
3.3.3	Baryons in Lattice QCD	57
3.3.3.1	Charmed Baryons	58
CHAPTER 4		
$\Omega_c \gamma \rightarrow \Omega_c^*$	TRANSITION IN LATTICE QCD	63
4.1	Lattice Formulation	63
4.2	Numerical Results	70
CHAPTER 5		
$\Xi_c \gamma \rightarrow \Xi_c'$	TRANSITION IN LATTICE QCD	76
5.1	Lattice Formulation	76
5.1.1	Lattice Setup	81
5.2	Numerical Results	82
CHAPTER 6		
RESULTS AND DISCUSSION		93

REFERENCES	96
APPENDIX-A	
DEFINITIONS AND ALGEBRAS	106
A.1 Gamma Matrices	106
A.2 Grassmann Algebra and Grassmann Integrals	106
A.3 Jackknife Resampling Method	110
APPENDIX-B	
PATH INTEGRAL ON THE LATTICE	111
APPENDIX-C	
U-SPIN SYMMETRY	115
APPENDIX-D	
HOPPING PART	120
D.1 Hopping Part Invariance Under Parity Transformation	120
D.2 Hopping Part Invariance Under Charge Conjugation Transformation ..	121
D.3 Hopping Part Invariance Under Time-Reversal	122
APPENDIX-E	
VERTEX FUNCTION AND FORM FACTORS	123
E.1 Calculation of Vertex Function	123
E.2 Form Factors of spin $\frac{1}{2}$ particles in Lattice QCD	123
E.3 $N\gamma \rightarrow \Delta$ Electromagnetic Form Factors	126
APPENDIX-F	
TABLES FOR ALL PROBABLE Q^2 VALUES	130
CURRICULUM VITAE	132

LIST OF SYMBOLS

$U_{\mu\nu}$	Plaquette
$F_{\mu\nu}$	Field strength tensor
U_μ	Link variable
γ	Photon
g	Gluon
Ω_c	Omega (css) baryon
Ω_c^*	Omega star (css) baryon
Ξ_c	Xi (ucs) baryon
Ξ_c'	Xi prime (ucs) baryon
α_s	Strong coupling constant
$Q_{\mu\nu}$	Sum of plaquettes in the $\mu - \nu$ plane

LIST OF ABBREVIATIONS

1-D	One-Dimensional
2-D	Two-Dimensional
3-D	Three-Dimensional
4-D	Four-Dimensional
Dof	Degree of Freedom
QCD	Quantum Chromodynamics
QED	Quantum Electrodynamics
Lattice QCD	Lattice Quantum Chromodynamics

LIST OF FIGURES

	Page
Figure 2.1 The fundamental particles and their interactions [54].	9
Figure 2.2 Strong Coupling Constant as a function of the energy [17].....	14
Figure 2.3 Illustration of Lattice, red dots $\psi(n)$ denotes <i>fermions</i> , lines that connecting the fermions are <i>link variables</i> and the simplest closed loop <i>plaquette</i> is illustrated as blue arrows.	15
Figure 2.4 1×1 Plaquette $U_{\mu\nu}$	20
Figure 2.5 Forward and backward link variables.	22
Figure 2.6 Sum of plaquettes in the $\mu - \nu$ plane ($Q_{\mu\nu}$).	32
Figure 3.1 Illustration of a two-point function: Arrows are the quark propagators. Node (m) is the source point and node (n) is the sink point.....	38
Figure 3.2 Illustration of wall smeared three-point function. J_μ is the inserted current, x_1 and t_1 is spatial and temporal points respectively.....	45
Figure 3.3 Illustration of vertex function at tree level.	49
Figure 3.4 Illustration of vertex function as sum of all contributions.	50
Figure 3.5 Electron proton scattering, a virtual photon exchange approximation, k is momentum of incoming electron, k' is momentum of outgoing electron.....	51
Figure 3.6 Illustration of three-point function. J_μ is the inserted current, x_1 and t_1 is spatial and temporal points respectively.	54
Figure 3.7 Illustration of current insertion to the propagators one by one.	55
Figure 3.8 Light hadron spectrum extrapolated to the physical point (red circles) calculated by PACS-CS Collaboration [93] in comparison with the experimental values (black bars).	57
Figure 3.9 Octet baryons.	58
Figure 3.10 Decuplet baryons.....	58
Figure 3.11 Experimentally observed charmed baryons and their decay channels [17].	60
Figure 3.12 Charmed baryon spectrum comparison with LQCD results [40].	61
Figure 3.13 SU(4) multiplets of spin- $\frac{1}{2}$	62
Figure 3.14 20-plet of SU(4) for spin- $\frac{3}{2}$	62
Figure 4.1 Two-point functions of Ω_c and Ω_c^* , red horizontal line indicates the fit region.....	71
Figure 4.2 The correlation function ratios Π_1 and Π_2 as functions of the current insertion time. $G_{M1}^{s,c}$ were obtained. The squares denote the kinematical case when Ω_c^* at rest and triangles denote the kinematical case when Ω_c at rest.....	71

Figure 5.1	Effective mass plots of Ξ_c and Ξ'_c , red horizontal line indicates the fit region.....	82
Figure 5.2	Constant fits for the electric form factors (a) Charged transitions of Ξ_c and Ξ'_c . (b) Neutral transitions of Ξ_c and Ξ'_c the fits made between 3-5 timesteps.....	84
Figure 5.3	Dipole fits for Ξ'_c and Ξ_c . Red line indicates the fit function, black shadow indicates one σ error band.	85
Figure 5.4	Constant fits for the electric form factors (a) Charged transitions of Ξ_c and Ξ'_c . (b) Neutral transitions of Ξ_c and Ξ'_c . The fits made between 3-5 timesteps.	86
Figure 5.5	Individual quark (u/d , s and c) contributions of $\Xi'_c \gamma \rightarrow \Xi'_c$ (left), $\Xi_c \gamma \rightarrow \Xi_c$ (middle), $\Xi_c \gamma \rightarrow \Xi'_c$ (right) transitions. Black shadow indicates one σ error band.	87
Figure 5.6	Q^2 dependence of the magnetic form factors. Red line indicates the fit function, red dotted line indicates extrapolation. Black shadow indicates one σ error band.....	89
Figure C.1	U-spin and I-spin for octet baryons.....	117

LIST OF TABLES

		Page
Table 2.1	The four fundamental forces [50].....	6
Table 2.2	Symmetries and conservation laws [50].....	33
Table 2.3	Table of discrete symmetry operators on Lattice [78].....	35
Table 3.1	Interpolating fields of spin- $\frac{1}{2}$ baryons.	37
Table 4.1	The details of the gauge configurations used in the analysis [4]. N_s and N_t are the spatial and temporal sizes of the lattice, respectively, N_f is the number of flavors, a is the lattice spacing, L is the volume of the lattice, β is the inverse gauge coupling, c_{sw} is the Clover coefficient, κ_{sea}^f is the hopping parameter of the quark with flavor f and m_π is the pion mass.	68
Table 4.2	The Ω_c and Ω_c^* masses at $m_\pi = 156$ MeV.....	71
Table 4.3	The results for form factors at the lowest allowed four momentum transfer and zero momentum transfer for the two kinematical cases [12].	73
Table 4.4	The results for helicity amplitudes in the rest frame of Ω_c^* [12].	74
Table 5.1	The details of the gauge configurations used in the analysis [4]. N_s and N_t are the spatial and temporal sizes of the lattice, respectively, N_f is the number of flavors, a is the lattice spacing, L is the volume of the lattice, β is the inverse gauge coupling, c_{sw} is the Clover coefficient, κ_{sea}^f is the hopping parameter of the quark with flavor f and m_π is the pion mass.	81
Table 5.2	The Ξ_c and Ξ_c' masses together with experimental values and those of other lattice collaborations.	83
Table 5.3	Individual quark contributions of $\Xi_c \gamma \rightarrow \Xi_c'$ transition to the magnetic form factor at different Q^2 values of all transitions.....	88
Table 5.4	Individual quark contributions of $\Xi_c \gamma \rightarrow \Xi_c$ transition to the magnetic form factor at different Q^2 values of all transitions.....	88
Table 5.5	Individual contributions of $\Xi_c' \gamma \rightarrow \Xi_c'$ transition to the magnetic form factor at different Q^2 values of all transitions.	90

Table 5.6	The combined form factor as obtained using Eq. (5.25) and extrapolated to $Q^2 = 0$, together with the magnetic moments in units of nuclear magneton.	91
Table C.1	U-spin numbers for octet baryons.	118
Table C.2	U-spin numbers for decuplet baryons.	118
Table C.3	U-spin numbers for triply charmed, doubly charmed and single charmed spin $\frac{1}{2}$ baryons	118
Table C.4	U-spin numbers for triply charmed, doubly charmed and single charmed spin $\frac{3}{2}$ baryons	119
Table F.1	Table for probabilities q^2 up to 6.....	130
Table F.2	Table for probabilities q^2 7-8	131



ABSTRACT

RADIATIVE TRANSITIONS OF CHARMED BARYONS IN LATTICE QUANTUM CHROMODYNAMICS (QCD)

HÜSEYİN BAHTİYAR

Department of Physics

Ph.D. Thesis

Adviser: Assoc. Prof. Dr. Taylan YETKİN

Co-Adviser: Prof. Dr. Güray ERKOL

Lattice QCD (LQCD) is a discretized version of Quantum Chromo Dynamics and it is the only approach that uses the QCD Lagrangian directly. With this approach we have an excellent opportunity to solve QCD in the energy region starting from very low energies where chiral perturbation theory can be used to high energies that only perturbative theories are applicable. This region is commonly referred to as non-perturbative QCD.

The idea of calculating QCD numerically on a lattice was introduced nearly forty years ago and it turned into very powerful approach to understand the strongly interacting particles. The main idea of LQCD is the path-integral representation of quantum mechanics and quantum field theory. This approach allows a calculation, based on simulation of direct the original theory. In this process, however, there are systematical problems called lattice artifacts. These artifacts need to be investigated before LQCD results can be compared to observables [5].

The first calculations of electromagnetic form factors were made about thirty years ago [6]. The study of electromagnetic properties of baryons gives excellent opportunity to understand more about the non-perturbative Quantum Chromo Dynamics (QCD). The baryon electromagnetic form factors are fundamental quantities which describe the internal structure of the nucleon, like the spatial distributions of electric charge and current inside the nucleon; these form factors are among the most basic observables of the nucleon. Baryons' charge radii, distribution of baryons' charge, the origin of magnetizations, magnetic moments, and shapes can be studied by calculating baryon form factors.

The observables can be determined by using baryon matrix elements. Furthermore these matrix elements can be written in the form of QCD path integrals, which enables the methods of lattice gauge theory to be used. The path integrals are numerically and fully nonperturbatively calculated by using a discretized finite Euclidean space-time lattice.

We concentrate on heavy flavor baryons, since baryons that contain heavy quarks provide an exciting field to study QCD. They are combinations of the slow heavy quarks with a relativistic light quark. The energies, detectors and luminosities at the modern experiments made possible the observation of heavy baryons with one heavy quark [7]. In this thesis we present our results for the two observed $\Omega_c \gamma \rightarrow \Omega_c^*$ and $\Xi_c \gamma \rightarrow \Xi_c'$ transitions.

We have run our the simulations on $32^3 \times 64$, unquenched 2 + 1-flavor lattices generated by PACS-CS collaboration [4] with the nonperturbatively $O(a)$ -improved Wilson quark action and the Iwasaki gauge action. For the $\Omega_c \gamma \rightarrow \Omega_c^*$ transition, we calculate magnetic dipole and electric quadrupole form factors. The magnetic dipole form factor is found to be mainly determined by the strange quark and the electric quadrupole form factor to be negligibly small, in consistency with the quark model. We also evaluate the decay rate and lifetime.

We also study the electromagnetic $\Xi_c \gamma \rightarrow \Xi_c'$ transition on 2+1 flavor lattices. We calculate the magnetic Sachs and Pauli form factors which give the Ξ_c - Ξ_c' transition magnetic moment and the decay widths of Ξ_c' baryons. We did not find a signal for the magnetic form factor of the neutral transition $\Xi_c^0 \gamma \rightarrow \Xi_c'^0$, neutral transition is suppressed by the U-spin flavor symmetry. We calculate the magnetic form factors and the magnetic moments of Ξ_c and Ξ_c' baryons as a byproduct. This study gives an insight to the dynamics of u/d , s and c quarks having masses at different scales.

Many theoretical approaches have been used to examine the existing spectra of heavy quark containing baryons and predict new states such as quark models [8], QCD sum rules [9], heavy quark effective theory based models [10], and lattice QCD [11]. We compare our results with those of other approaches.

The results have been published in $\Omega_c \gamma \rightarrow \Omega_c^*$ in Lattice QCD [12], $\Xi_c \gamma \rightarrow \Xi_c'$ in Lattice QCD [13].

Keywords: Charmed baryons; Electric and magnetic form factor; Lattice QCD; Decay width.

TILSIMLI BARYONLARIN RADYATİF GEÇİŞLERİNİN ÖRGÜ KUANTUM RENK DİNAMİĞİNDE İNCELENMESİ

HÜSEYİN BAHTİYAR

Fizik Anabilim Dalı

Doktora Tezi

Tez danışmanı: Doç. Dr. Taylan YETKİN

Eş-danışmanı: Prof. Dr. Güray ERKOL

Örgü KRD (ÖKRD) kuantum renk dinamiğinin (KRD) kesikli hale getirilmiş şeklidir ve KRD Lagrangian'ını direk olarak kullanan tek yaklaşımdır. Bu yaklaşım sayesinde kiral pertürbasyon teorisinin kullanıldığı düşük enerjilerden başlayan ve pertürbasyon teorisi kullanılan yüksek enerji aralığına kadar olan pertürbatif olmayan KRD enerji bölgesini anlamamız için mükemmel bir fırsattır.

KRD hesaplarını örgü üzerinde nümerik olarak çözme fikri yaklaşık kırk yıl önce önerildi ve bu yaklaşık kuvvetli etkileşim ile etkileşen parçacıkların anlaşılması için çok güçlü bir yönteme dönüştü. ÖKRD'nin ana fikri, kuantum mekaniğinin ve kuantum alan teorisinin yol-integral gösterimidir. Bu yaklaşım orijinal teorisinin doğrudan simülasyonuna dayanan bir hesaplama izni verir. Bununla birlikte, bu süreçte, örgü kalıntıları olarak adlandırılan sistematik problemler vardır. ÖKRD sonuçları gözlenebilirlerle karşılaştırılmadan önce bu kalıntılar araştırılmalıdır [5].

Elektromanyetik form faktörlerinin ilk hesaplamaları yaklaşık otuz yıl önce yapılmıştır [6]. Baryonların elektromanyetik özelliklerinin incelenmesi, pertürbatif olmayan KRD hakkında daha fazla bilgi edinmek için mükemmel bir fırsattır. Nükleon elektromanyetik form faktörleri, nükleon içindeki elektrik yükünün ve akımının uzaysal dağılımları gibi, nükleonun iç yapısını tanımlayan temel değişkenlerdir. Bu form faktörleri nükleonun en temel gözlemlenebilirleri arasındadır. Baryon'un yük yarıçapları, baryon yükünün dağılımı, manyetizasyonları, manyetik momentler ve şekilleri form faktörlerinin hesaplanmasıyla incelenebilir.

Gözlenebilirler baryon matris elemanları kullanılarak saptanabilir. Ayrıca, bu matris elemanları, ÖKRD yöntemlerinin kullanılmasını sağlayan KRD yol integralleri formunda yazılabilir. Yol integralleri, kesikli bir sonlu öklid uzay-zaman örgüsünü kullanarak sayısal olarak ve tamamen pertürbatif olmayan şekilde hesaplanır.

Ağır quark içeren baryonlar, KRD'yi incelemek için heyecan verici bir alan sağladığından ağır çeşnili baryonlar çalışılmıştır. Bunlar yavaş ağır kuarkların rölativistik hafif kuarklar ile kombinasyonlarıdır. Günümüz deneylerinde ulaşılan enerjiler, dedektörler ve parlaklıklar, bir ağır kuarklı ağır baryonların gözlemlenmesini mümkün kılmıştır [7].

Bu çalışmadaki simülasyonlar PACS-CS kolaborasyonu tarafından üretilen pertürbatif olmayan $O(a)$ -geliştirilmiş Wilson kuark eylemi ve Iwasaki ayar eylemi oluşturulmuş, $32^3 \times 64$ büyüklüğünde $2 + 1$ -çeşnili örgülerde yapılmıştır [4]. $\Omega_c \gamma \rightarrow \Omega_c^*$ çalışmasında, magnetic dipol ve elektrik quadropole yapı faktörleri hesaplanmıştır. Manyetik dipole yapı faktörü acayip kuark katkısı tarafından belirlendiği gözlemlenmiştir ve elektrik quadropole yapı faktörü ihmal edilebilecek düzeyde küçük olarak bulunmuştur. Bulunan sonuçlar kuark model ile uyumludur. Aynı zamanda bozunum genişliği ve yaşam süresi hesaplanmıştır.

Ayrıca aynı örgü konfigürasyonları ile $\Xi_c \gamma \rightarrow \Xi_c'$ elektromanyetik geçişleri çalışılmıştır. $\Xi_c - \Xi_c'$ geçiş manyetik momentleri ile Ξ_c' baryonunun bozunum genişliğini verecek olan Sachs ve Pauli yapı faktörleri hesaplanmıştır. $\Xi_c^0 \gamma \rightarrow \Xi_c'^0$ nötral geçişi için sinyal bulunamamıştır, ayrıca bu nötral geçiş U-spin çeşni simetrisi tarafından baskılanmış bir geçiştir. Hesapların yan ürünü olarak Ξ_c ve Ξ_c' baryonlarının manyetik yapı faktörleri ve manyetik momentleri hesaplanmıştır. Bu çalışma, farklı ölçeklerde kütlelere sahip olan u/d , s ve c kuarklarının dinamikleri hakkında bir fikir vermektedir.

Ağır quark içeren baryonların mevcut spektrumlarını incelemek ve yeni durumları tahmin etmek için quark model [8], KRD toplam kuralı [9], ağır quark efektif teori modelleri [10] ve ÖKRD [11] gibi birçok teorik yaklaşım kullanılmıştır. Bu çalışmada bulunan sonuçlar diğer teorik yaklaşımlar ile karşılaştırılmıştır.

Yapılan çalışmalar $\Omega_c \gamma \rightarrow \Omega_c^*$ in Lattice QCD [12] ve $\Xi_c \gamma \rightarrow \Xi_c'$ in Lattice QCD [13], isimleri ile yayınlanmışlardır.

Anahtar Kelimeler: Tılsımlı baryonlar; Elektrik ve manyetik yapı faktörleri; Örgü Kuantum Renk Dinamiği

INTRODUCTION

1.1 Literature Review

The strong, electromagnetic and weak interactions of elementary particles are described by their respective quantum field theories. Quantum Electrodynamics (QED) is the quantum field theory of electrodynamics. It describes the interactions of charged particles with the electromagnetic field. Weak interaction describes the decays of unstable particles. Electromagnetic interactions and weak interactions are unified into a single theory called electroweak interaction. Quantum chromodynamics (QCD) is the fundamental quantum field theory of strong interactions of quarks, anti-quarks and gluons. QCD describes quark and gluon dynamics successfully in large momentum transfer interactions, because in the high energy regime the coupling constant of strong interaction is small and perturbation theory is applicable. On the other hand, in the low energy regime, the strong coupling constant is dominant and perturbative methods cannot be applied. Furthermore, elementary particles of the electromagnetic and weak interactions have been observed directly by high energy experiments, however quarks and gluons, which are the elementary particles of strong interaction, have not been observed as isolated particles. It is believed that the color potential between the quarks and gluons is responsible for such a mechanism that they are confined into the colorless objects called hadrons.

To understand the hadron structure, non-perturbative methods such as QCD Sum Rules [14], Chiral Perturbation theory (χ PT) [15] and Lattice Quantum Chromodynamics (LQCD) [16] have been developed. Each method has its own advantages and disadvantages. Of these non-perturbative methods only LQCD starts directly from the QCD Lagrangian, thus

making it an *ab initio* method. LQCD method has proven itself over years giving precise results for hadron spectroscopy measurements consistent with the experiments [4]. These methods have been applied to light (u, d, s) and heavy (c, b) sectors to understand the non-perturbative structure of QCD. Charm quark sector requires careful treatment in LQCD. The effect of heavy charm quark guides the understanding of heavy QCD dynamics. Furthermore charm physics plays an important role in understanding the quark-gluon plasma.

1.2 Objective of the Thesis

This thesis is focused on radiative decays of Ω_c^* and $\Xi_c^{0,+}$ using LQCD. We perform our simulations using the state of the art $32^3 \times 64$ size unquenched (with sea-quark effects), $2+1$ flavor lattices generated by PACS-CS collaboration [4]. Using these configurations, we inspect radiative transitions of *singly-charmed* baryons. For these baryons the mass differences with respect to the ground states are too small for any strong decay to occur, therefore the radiative channels are the dominant decay modes. In this case, apart from the electromagnetic form factors, the total decay width and the lifetime of the baryon can be calculated directly. Although precise determination of these channels have not been made yet by experiments, the results obtained with LQCD can shed light on the experiments.

The Ω_c^0 baryon are composed of (css) quarks and the quantum numbers are $J^P = \frac{1}{2}^+$. Furthermore, it is the heaviest known single-charmed hadron that decays weakly. Ω_c^0 is on the second layer of mixed $20'$ -plet of SU(4) multiplet. The average mass value of Ω_c reported by Particle Data Group (PDG) is 2695.2(1.7) MeV [17].

Ω_c^* is the excited state of Ω_c^0 . The quantum numbers of Ω_c^* have not been measured yet. However, it is considered that Ω_c^* completes the ground state which has $J^P = \frac{3}{2}^+$ located on the second layer of the 20-plet of SU(4). The average mass value of Ω_c^* reported by PDG is 2765.9(2.0) MeV [17].

The mass difference between Ω_c^* and Ω_c was studied by BaBar and BELLE collaborations [18, 19]. The radiative transition $\Omega_c \gamma \rightarrow \Omega_c^*$ was first observed in the BaBar experiment giving the difference of $\Delta M = 70.8(1.0)(1.1)$ MeV [19]. After that, BELLE mea-

sured the relative mass difference $m_{\Omega_c^*} - m_{\Omega_c} = 70.7(0.9)_{-0.9}^{+0.1}$ MeV in agreement with the BaBar observation [18]. Since the mass differences forbid the strong decay channel, the only decay mode between Ω_c^* and Ω_c is the electromagnetic channel.

The electromagnetic transitions from $J = \frac{1}{2}$ to $J = \frac{3}{2}$ baryons can be explained by three transition form factors, namely magnetic dipole ($M1$), electric quadrupole ($E2$) and electric charge quadrupole ($C2$). These form factors provide useful information about the structure and the shape of these baryons. Earlier studies have focused on the transition moments between spin- $\frac{1}{2}$ (N) to spin- $\frac{3}{2}$ (Δ). Experimentally, pure single spin-flip $M1$ transition has been found to dominate. Small but non zero values of electric quadrupole and electric charge quadrupole moments imply the shapes of N and Δ differing from spherical symmetry [20]. The values of $E2$ and $C2$ are non-zero as observed from experiments [21, 22], and as previously predicted by the quark model [23]. However, this issue is unresolved, because the results from numerous theoretical approaches are not in full agreement with experiment.

Amongst the heavy baryons, Ξ_c and Ξ_c' are particularly interesting since the quarks they are composed of (u , s and c) have different flavors and masses at quite different scales. Therefore, these two baryons provide a good laboratory to study the heavy-quark dynamics.

The neutral $\Xi_c^0(c[sd])$ and the positive state $\Xi_c^+(c[su])$ have the quantum numbers $J^P = \frac{1}{2}^+$ and an anti-symmetric flavor wave function under interchange of light quarks. In group theoretical formalism, they are members of the anti 4-plet ($\bar{4}$) of the SU(4). Ξ_c baryon was first observed in hyperon-beam experiment at CERN [24] and later confirmed by Fermilab [25] and CLEO Collaboration [26]. The average mass reported by PDG is $2470.99_{-0.50}^{+0.30}$ MeV [17].

$\Xi_c'^0(c\{sd\})$ and $\Xi_c'^+(c\{su\})$ have the same quark content and quantum numbers $J^P = \frac{1}{2}^+$ as $\Xi_c^0(c[sd])$ and $\Xi_c^+(c[su])$. They are located on the second layer of the sextet SU(4) multiplet. These two baryons have symmetric flavor wave functions under interchange of light quarks. They were first observed by CLEO Collaboration [27] and confirmed

recently by BaBar [28] and BELLE experiments [29]. The average mass value reported by PDG is 2577.9(2.9) MeV [17].

The mass difference between Ξ'_c and Ξ_c was first reported by CLEO as $\Delta M^+ = 107.8(1.7)(2.5)$ MeV and $\Delta M^0 = 107.0(1.4)(2.5)$ MeV [27] and this difference is too small for any strong decay to occur. Therefore, the electromagnetic $\Xi'_c \rightarrow \Xi_c \gamma$ transition is the dominant decay mode. Studying this electromagnetic transition between different multiplets of SU(4) may shed light on the QCD mechanism governing the charmed baryons.

1.3 Hypothesis

In the limit of heavy quark, *singly-charmed* baryons are especially interesting to study as there appear the effects of heavy quark spin and flavor symmetry. The dynamics within the charmed baryon is governed by two light quarks while the heavy quark acts as a spectator. The electromagnetic transitions of charmed baryons is a good laboratory for understanding the heavy quark effect. Electromagnetic form factors reveal valuable information about the size and the shape of baryons. Determining these form factors is an important achievement to understand the hadron properties in terms of quark-gluon degrees of freedom [30]. In the past years many charmed-baryon states have been discovered by BaBar [31], Belle [32], CLEO [33] and LHCb [34, 35] experiments.

The experimental facilities such as LHCb, PANDA, Belle II, BESIII and J-PARC are expected to give more detailed information about spectroscopy, decays and structure of the charmed baryons. Recent LQCD studies provide a precise determination of their spectroscopy. The ground state charmed baryons have been studied both in quenched [36, 37] and full QCD [38, 39, 5, 40].

There has been intensive effort made from LQCD collaborations to make precise calculations of the light baryon sector. Electromagnetic form factors of light (u and d) baryons [41], moments of parton distributions [42], axial charges [43] have been studied. The results obtained from LQCD have been compared with the experimental results in order to understand the unresolved parts of the strong interaction.

In order to expand our understanding of strong interaction and make a comparison of the LQCD results with chiral perturbation theory, similar studies have been carried out on light mesons by LQCD collaborations. Such as π and ρ -meson form-factors [44], pseudoscalar-meson to octet-baryon coupling constants [45], light meson electromagnetic form factors [46]. Using the information obtained from light hadron calculations, LQCD collaborations have been expanded the research to strange baryons (hyperon). Thus, the effect of strange quark contribution has been examined [47].

As a continuation of previous studies, LQCD collaborations are working to understand hadrons containing heavy quarks. Determination of form factors and mass spectra of the heavy hadrons would reveal valuable information. Comparing the results obtained from LQCD with the experiments will provide an understanding of the heavy quark effect. In the past years comparison was made between strange and charm baryon masses [39]. Precise determination of doubly charmed baryons was made using LQCD [48], electromagnetic form factors [30], and pseudoscalar transitions [49] were studied using LQCD. In the thesis three charmed baryons Ω_c^{*0} , Ξ_c' , and Ξ_c radiative decays will be examined using the LQCD method.

In this thesis we examine the spin-flip effect by studying $\Omega_c^{*0} \rightarrow \Omega_c^0 \gamma$ radiative channel. $\Xi_c' \rightarrow \Xi_c \gamma$ transition is useful to study the effects of the spin-flavor difference moreover this channel gives an insight to the dynamics of light, strange and charm quarks having masses at different scales. Since the transition form factors are calculated separately for each quark contribution we expect to determine the dominant quark while studying the transition form factors. We expect to see the quark contribution decreases as the quark mass increases because of the badly broken SU(4) symmetry. We also expect small decay widths due to small mass splittings.

The thesis is organized as follows. In Chapter 2 Standard model and LQCD are discussed. Chapter 3 is about simulation techniques of LQCD. In Chapter 4 and 5 $\Omega_c^{*0} \rightarrow \Omega_c^0 \gamma$ and $\Xi_c' \rightarrow \Xi_c \gamma$ numerical analyses are given. Discussion of the results is made in Chapter 6.

STANDARD MODEL AND LATTICE QCD

This chapter will provide an overview of Standard Model. Furthermore, LQCD method, which is the key method of this work, will be explained in detail. Moreover discrete symmetries and their connection to lattice action will be explained.

2.1 Introduction

There are four fundamental forces in nature. They are called *strong*, *electromagnetic*, *weak* and *gravitational* forces. Each force has its own specific physical theory and is mediated by particles called gauge bosons. The gauge theories of the four forces and corresponding gauge bosons are listed in Table 2.1. Historically the first formulated force is

Table 2.1 The four fundamental forces [50]

Name	Relative Strength	Boson	Theory
Strong force	1	gluon g	Chromodynamics
Electromagnetic force	10^{-3}	photon γ	Electrodynamics
Weak force	10^{-16}	vector bosons W^\pm and Z	Flavordynamics
Gravitational	10^{-41}	graviton G	Geometroynamics

the gravitational force. Classical theory of gravity was formulated by Newton in 1687 that is called *Newton's law of gravitation*. Its relativistic generalization was made by Einstein in 1915 which is called *general theory of relativity*. Graviton is the force-carrier particle in theory of gravitation. The quantum theory of gravitation has not been developed so far. The quantum effect of gravitation is very small, negligible up to the Planck scale.

The electromagnetic force exists between all particles that are electrically charged. For example, electrons having negative charge are bound with nucleus of an atom, due to the presence of protons having positive charge. The theory of electromagnetic force is called *electrodynamics*. Classical formulation of electrodynamics was culminated in the work of James Clerk Maxwell in the 19th century. He unified the previously developed electric and magnetic theory into a single theory and discovered the electromagnetic nature of light. In classical electromagnetism, the behavior of the electromagnetic field is described by *Maxwell's equations*. Furthermore the electromagnetic force is calculated by *Lorentz's force law*. Quantum theory of electrodynamics – known as Quantum Electrodynamics (QED) – was developed by Feynman, Tomonaga and Schwinger, in 1940s. This theory is one of the most accurate theories where perturbation theory can be applied. Like classical electromagnetism, QED is constructed on U(1) gauge group. *Photon* is the force-carrier particle of QED.

The *strong interaction* is the strongest of the four fundamental forces. It has been known for a long time that the nucleus is composed of protons and neutrons and that protons have positive electric charge, while neutrons are neutral. Normally positive charges would repel one another and the positively charged protons should cause the nucleus to fly apart. Until the 1970s, there was no exact explanation as to how the atomic nuclei are bound together.

In 1934, Yukawa made the first attempt to explain the nuclear force. His theory consisted of massive bosons (mesons) that mediate the interaction between two nucleons. Different theories were introduced until 1960s, but an exact theory could not be found. In 1964 quarks were theorized by Gell-Mann and Zweig. The quark model predicted quark-antiquark (*i.e.* mesons) and three-quark bound states (*i.e.* baryons). There are six different quark types (*flavors*) specifically *u* (up), *d* (down), *s* (strange), *c* (charm), *b* (beauty) and *t* (top). Physicists have been trying to understand the behavior of quarks which cannot be observed in isolation (*color confinement*). In these attempts, the Quantum Chromodynamics was developed describing the strong interactions. *Gluon* is the force-carrier particle of QCD.

The weak forces were first proposed by Enrico Fermi in 1933. He suggested that beta decay could be explained by a four-fermion interaction, involving a contact force with no range. The theory was corrected by Lee and Yang, Feynman and Gell-mann in 1950s. In 1968, Glashow, Salam and Weinberg unified the electromagnetic force and the weak interaction, called as the electro-weak force. There are two gauge bosons mediating weak interaction. They are called W and Z , both of which were experimentally discovered in 1983. Electromagnetic and weak interactions are unified in a theory called Electroweak theory.

Electroweak interaction involves leptons and quarks. There are six different types of leptons: e (electron), μ (muon), τ (tau) and their opposite charged states; neutrinos with the corresponding flavor, namely electron neutrino (ν_e), muon neutrino (ν_μ) and tau neutrino (ν_τ).

The Standard Model is a theory explaining the electroweak and strong interactions, as well as classifying all subatomic particles. It was developed throughout the latter half of the 20th century. The current formulation was finalized in the 1970s upon experimental confirmation of the existence of quarks. Since then, discoveries of the top quark [51] (1995), the tau neutrino [52] (2000), and the Higgs boson [53] (2012) have given further credence to the Standard Model.

In the following subsections, these fundamental interactions will be explained in detail.

2.1.1 Quantum Electrodynamics

QED is a quantum field theory of the electromagnetic force. In other words, it is the quantum field theory of the interactions of electrically charged particles through the electromagnetic field. Mathematically, QED describes the interactions of light with matter, and the interactions of charged particles among each other. The interaction is represented by Feynman diagrams. In this section Tong Lectures notation in Ref. [55] is followed.

We start with the Maxwell's equations which formulate the dynamics of light. Lagrangian

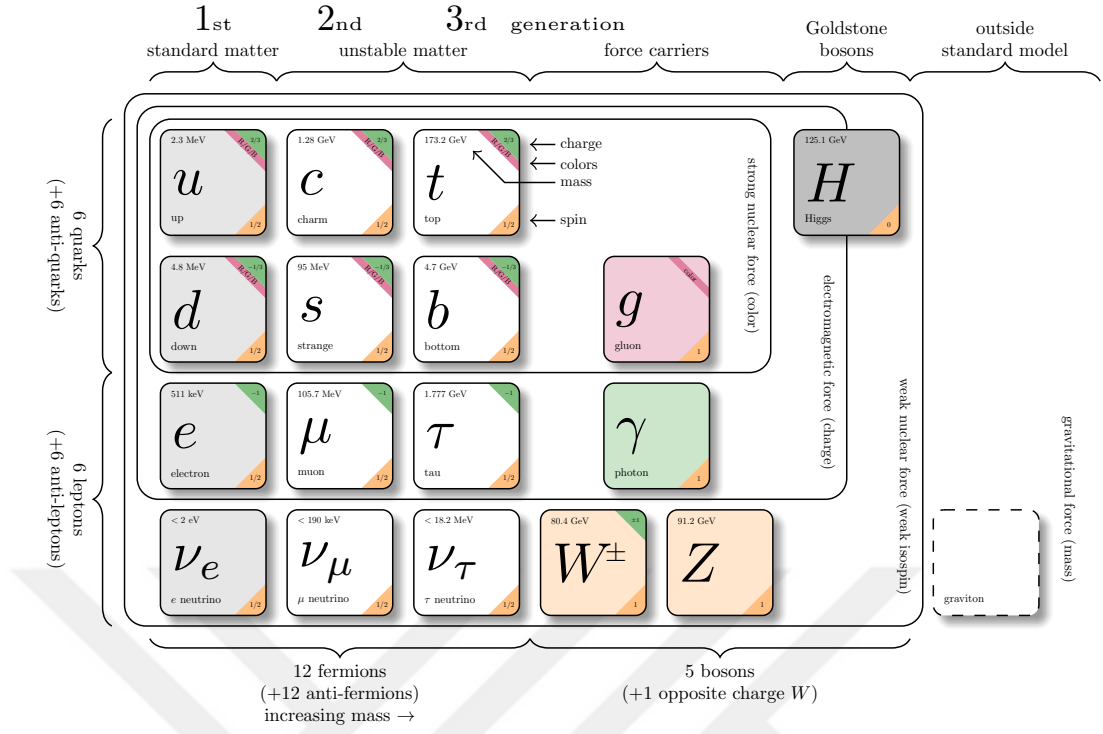


Figure 2.1 The fundamental particles and their interactions [54].

for the Maxwell's equations for the free (absence of source) theory can be written as

$$\mathcal{L} = -\frac{1}{4}F_{\mu\nu}F^{\mu\nu}, \quad (2.1)$$

where, μ is the Lorentz index, $F_{\mu\nu}$ is the field strength tensor defined as

$$F_{\mu\nu} = \partial_\mu A_\nu - \partial_\nu A_\mu, \quad (2.2)$$

which leads to the equations of motion

$$\partial_\mu \frac{\partial \mathcal{L}}{\partial(\partial_\mu A_\nu)} = -\partial_\mu F^{\mu\nu} = 0. \quad (2.3)$$

Results of Eq. (2.3) will be associated with Maxwell's equations. The gauge field A^μ has

four components: $A^\mu = (\phi, \vec{A})$. The field strength tensor can be written as

$$F_{\mu\nu} = \begin{bmatrix} 0 & E_x & E_y & E_z \\ -E_x & 0 & -B_z & B_y \\ -E_y & B_z & 0 & -B_x \\ -E_z & -B_y & B_x & 0 \end{bmatrix}. \quad (2.4)$$

Using the Bianchi identity $\partial_\mu F_{\nu\alpha} + \partial_\alpha F_{\mu\nu} + \partial_\nu F_{\alpha\mu} = 0$, two of the Maxwell's equations can be found. Next step is to write a Lagrangian that couples to a field A_μ , and a matter field j^μ ,

$$\mathcal{L} = -\frac{1}{4}F_{\mu\nu}F^{\mu\nu} - j^\mu A_\mu, \quad (2.5)$$

using the equation of motion

$$\partial_\mu \frac{\partial \mathcal{L}}{\partial(\partial_\mu A_\nu)} = -\partial_\mu F^{\mu\nu} = j^\nu. \quad (2.6)$$

In gauge theories, gauge fields couple to conserved currents. Thus, j^μ must be a conserved current:

$$\partial_\mu j^\mu = 0. \quad (2.7)$$

Substituting the $j^\mu A_\mu$ with a Dirac Lagrangian, the QED Lagrangian becomes

$$\mathcal{L} = -\frac{1}{4}F_{\mu\nu}F^{\mu\nu} - \bar{\psi}(i\mathcal{D} - m)\psi, \quad (2.8)$$

where \mathcal{D} is the covariant derivative

$$\mathcal{D} = \partial_\mu \gamma^\mu + ieA_\mu \gamma^\mu. \quad (2.9)$$

This Lagrangian represents the interaction of an electron or, more generally, interaction of an electrically charged fermion with a photon. The field strength tensor part of the equation gives information about electromagnetism and the remaining part is the Dirac Lagrangian of a massive field, defining fermions. The illustration of a tree-level interaction is given in Fig (3.3).

2.1.2 Weak Interaction

The weak force plays a greater role in decays. There are six different quark flavors and six flavors of leptons. Weak interaction is responsible for the decay of massive quarks and leptons into lighter quarks and leptons. Since the weak interaction changes the flavor of a quark into another, it is also called as *flavordynamics*. Leptons have no color charge so they do not participate in strong interactions. Neutrinos have no electric charge, so they do not experience electromagnetic force. However, they all take part in the weak interactions [50].

The weak interaction is characteristically different from other interactions because

- The weak interaction can change the flavor of quarks.
- It violates P (parity) symmetry also CP (charge-parity) symmetry.
- Its force-carrier particles are massive as explained in the Standard Model by the Higgs mechanism.

Glashow, Salam and Weinberg unified the theory of weak and electromagnetic interaction between elementary particles and they were awarded the Nobel Prize in Physics in 1979. Mathematically, the unification is accomplished under an $SU(2)_L \times U(1)_Y$ gauge group. The gauge bosons are the three W bosons of weak isospin from $SU(2)$, and the B boson of weak hypercharge from $U(1)$.

2.1.3 Quantum Chromodynamics

Quantum Chromodynamics (QCD), is the theory of the strong force. QCD can be constructed in analogy to QED. The fundamental difference between QED and QCD is the gauge group, where QCD is constructed on $SU(3)$ instead of $U(1)$. Thus, QCD has $N^2 - 1 = 3^2 - 1 = 8$ gauge bosons, which are *gluons*.

Due to strong interactions, quarks, anti-quarks and gluons are bound into mesons and baryons. The problem is that, if two quarks are of the same flavor and spatial state, they must have the different spin state. By looking at the $\Omega^-(sss)$, $J = \frac{3}{2}$, it can easily be seen that all quarks are in the same spin states, so the overall wave function is symmetric.

However, this violates the Pauli principle: identical fermions cannot be in the same quantum state. Wave function of fermions must be anti-symmetric. In order to circumvent this problem, a new degree of freedom is defined for quarks and gluons, called *color*.

There are three color states, represented by *red* (r), *green* (g) and *blue* (b). There is direct experimental evidence of color from electron-positron annihilation to hadrons. Quarks carry one color, anti-quarks carry one anti-color and gluons carry one color and one anti-color. Therefore, quarks have three color states and gluons have eight different combination of color states.

Peculiarly, a single quark with a color charge could not be observed. *Color confinement* is the phenomenon proposing that color charged particles cannot be isolated, thus cannot be directly observed. Therefore only colorless (color singlet) particles are observable. The color wave function is the anti-symmetric part of the total wave function. So, the wave function of a baryon can be written as

$$\Psi = \Psi_{space}(r) \Psi_{spin} \Psi_{color}, \quad (2.10)$$

where the color part is anti-symmetric, therefore, the space and spin combination have to be symmetric under quark interchange.

Since gluons couple to color, the strong interaction is independent of flavor. The flavor independence leads to different symmetries like *Isospin*, which assumes u and d quarks to be degenerate. They are different states of one particle and can be written as a doublet $\begin{pmatrix} u \\ d \end{pmatrix}$. The other important result is that gluons are colored bosons. However, theoretically, three or four gluons can be bound into colorless glue-balls and this combination, in principle, can be observed in experiments. However there is no clear experimental evidence for glueballs yet.

The resemblance between QED and QCD leads to the Lagrangian [17],

$$\mathcal{L} = \sum_q \bar{\psi}_{q,a} (i\gamma^\mu \partial_\mu \delta_{ab} - \alpha_s \gamma^\mu t_{ab}^C A_\mu^C - m_q \delta_{a,b}) \psi_{q,b} - \frac{1}{4} F_{\mu\nu}^A F^{A\mu\nu}, \quad (2.11)$$

where ψ_q is the wave function of the quark, a and b are the colors of quarks and γ^μ are

gamma matrices. Here quarks are in the fundamental representation of SU(3) color group and gluons transform under adjoint representation of SU(3), t_{ab}^C are 3×3 matrices and generators of the SU(3) group, α_s is strong coupling constant and $F_{\mu\nu}^A$ is the field strength tensor,

$$F_{\mu\nu}^A = \partial_\mu A_\nu^A - \partial_\nu A_\mu^A - \alpha_s f_{ABC} A_\mu^B A_\nu^C, \quad (2.12)$$

$$[t^A, t^B] = i f_{ABC} t^C.$$

Here, f_{ABC} are the structure constants and the non-zero commutation relation shows the non-abelian nature of the SU(3) color group.

Another interesting feature of QCD is the asymptotic freedom. It can be explained by the behavior of strong coupling constant in Fig (2.2). The strong coupling constant decreases at high energies, so the energetic quarks are nearly free particles. Thus perturbation theory can be applied in the high energy regime. However, as α_s gets larger at low energies, different methods become necessary. Since this energy regime is very complicated, numerical simulations of theory called as Lattice Quantum Chromodynamics can be used to calculate observables in this energy regime.

2.1.4 Non-Perturbative Methods

The strong coupling constant α_s behaves differently than the electromagnetic or weak coupling constants. As shown in Fig (2.2), in the low energy region α_s keeps growing and gets closer to 1, thus perturbation theory breaks down. In order to probe the hadron structure and to calculate the observables theoretically, non-perturbative theories, such as QCD Sum Rule [14] or Chiral Perturbation theory (χ PT) have been developed.

QCD sum rules describe the QCD dynamics in terms of gluon and quark condensates. The method is based on Wilson's operator product expansion (OPE). In the QCD sum rules approach, QCD vacuum is characterized by a sum of condensates: gluon condensate $\langle G_{\mu\nu}^2 \rangle$, the quark condensate $\langle \bar{q}q \rangle$, the mixed condensate $\langle \bar{q}\sigma Gq \rangle$, the four-quark condensate and so on ... These condensate series are asymptotic. QCD sum rules give valuable information about hadronic observables; however, results may have uncontrolled

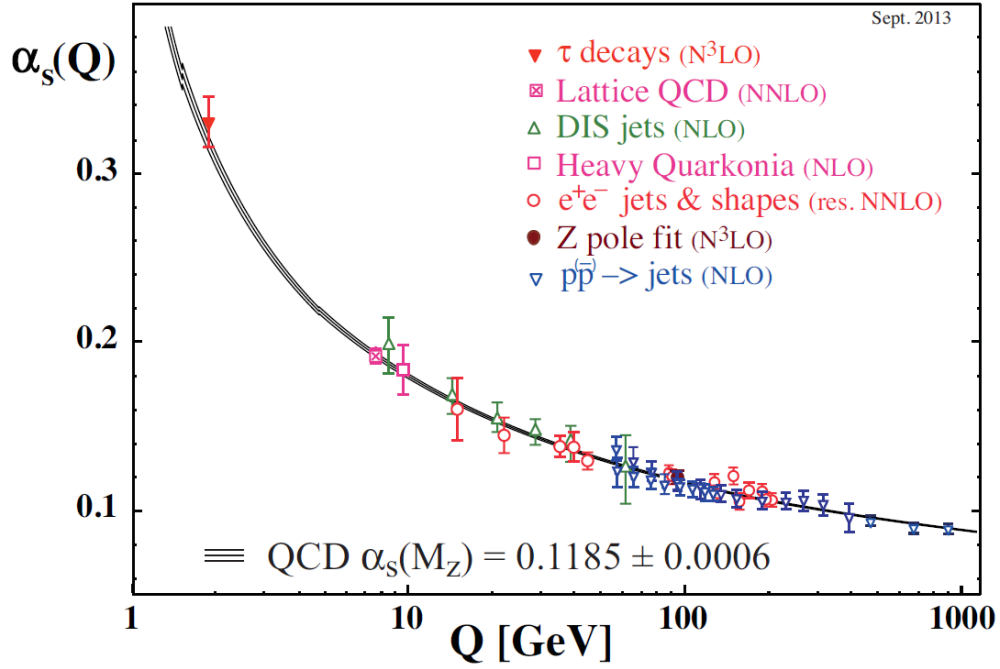


Figure 2.2 Strong Coupling Constant as a function of the energy [17]

uncertainties. The condensates have errors that can introduce some uncertainty.

Chiral perturbation theory [15] is an effective field theory constructed with a Lagrangian consistent with the chiral symmetry of quantum chromodynamics. It is a low-energy effective theory with hadrons as the fundamental degrees of freedom. The theory describes interactions between pions and nucleons schematically. When χ PT is expanded to SU(3), it can also describe interactions of strange mesons and baryons. Since chiral perturbation theory assumes chiral symmetry, quarks have no mass at tree level. The chiral symmetry breaking scale is order of 1 GeV [56].

Another non-perturbative method is LQCD. It is an ab initio method which starts directly from the QCD Lagrangian. LQCD simulates the strong interactions numerically on a discretized Euclidean space-time. In LQCD, quark fields are defined at lattice sites, while the gluon fields are defined on the links connecting these sites. Numerical LQCD calculations using Monte Carlo methods can be computationally intensive, which requires the use of the supercomputers. LQCD method has already proven itself, for instance, the mass of the proton has been determined precisely using LQCD [57] and the prediction for the behavior of the running coupling constant consistent with the experiments [58]. The

following section will present detailed information of LQCD.

2.2 Lattice Quantum Chromodynamics

Lattice Gauge Theory was developed in 1974 by Wilson [16]. Initially, it was studied as an analytic method. In 1979, Creutz, Jacobs, and Rebbi [59] calculated the first numerical solutions using Monte Carlo simulations. Thereafter LQCD was developed both as an analytical and a numerical method to study non-perturbative phenomena. In 1990s, with the development of computer technology, LQCD studies have started to be conducted on supercomputers.

In the LQCD method, Euclidean space-time is discretized. Quark fields are placed on the lattice sites and the gauge fields are defined in terms of *links*, connecting the lattice sites. Lattice spacing, a , acts as a cut-off that regularizes the ultraviolet divergences of the quantum field theory. Continuum results are recovered in the limit $a \rightarrow 0$.

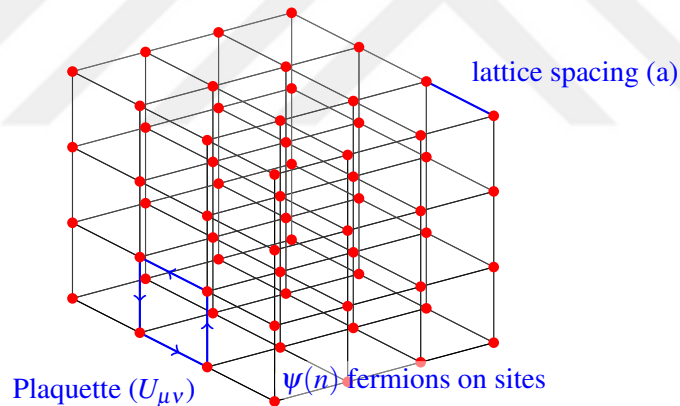


Figure 2.3 Illustration of Lattice, red dots $\psi(n)$ denotes *fermions*, lines that connecting the fermions are *link variables* and the simplest closed loop *plaquette* is illustrated as blue arrows.

In the continuum formulation of a quantum field theory, dimensional regularization is used to regulate the ultraviolet divergences. LQCD is a numerical method, so the results have statistical errors as well as systematical errors stemming from lattice spacing, lattice size, discretization and action [60].

Several theoretical approaches have been used to examine the non-perturbative region, such as quark models [8], QCD sum rules [9], heavy quark effective theory based mod-

els [10] and LQCD [11]. However the LQCD is the only ab initio method which starts directly from the QCD action.

2.2.1 Path Integral in Lattice QCD

LQCD is constructed on the Feynman's path integral approach [61]. To understand the path integration on the lattice, it is better to begin with path integral in quantum mechanics.

In 1948, Feynman developed a new formulation of quantum mechanics, based on discretizing space and time, summing all possible paths between the initial and final points contributing to the propagator. Using the path integral method, propagator can be calculated directly from the Lagrangian. The action is defined as

$$S = \int \mathcal{L} d^4x, \quad (2.13)$$

where the \mathcal{L} denotes the Lagrangian density. The propagator between initial and final quantum states is

$$\langle q_f | e^{-iHT} | q_i \rangle = \int e^{i \int \mathcal{L} d^4x} \mathcal{D}x, \quad (2.14)$$

where $\mathcal{D}x$ is the measure over all paths. In order to derive Eq. (2.14), it is assumed that there is a single particle in the x direction. The Hamiltonian is written as $\hat{H} = \frac{\hat{p}^2}{2m}$, and the Lagrangian is $L = \frac{1}{2}m\dot{q}^2$. When time T in the left-hand side of the Eq. (2.14) is divided into N equal parts, the equation becomes

$$\langle q_f | e^{-iHT} | q_i \rangle = \langle q_f | e^{-iHt} e^{-iHt} \dots e^{-iHt} | q_i \rangle. \quad (2.15)$$

Then, complete set of states are inserted between the exponentials as follows:

$$\begin{aligned} \langle q_f | e^{-iHT} | q_i \rangle &= \left(\prod_{k=1}^{N-1} \int dq_k \right) \langle q_f | e^{-iHt} | q_{N-1} \rangle \langle q_{N-1} | e^{-iHt} | q_{N-2} \rangle \\ &\dots \langle q_1 | e^{-iHt} | q_i \rangle. \end{aligned} \quad (2.16)$$

For a single matrix element, inserting the Hamiltonian and a complete set of states equa-

tion becomes as follows:

$$\langle q_{k+1} | e^{-i\frac{\hat{p}^2}{2m}t} | q_k \rangle = \int \frac{dp}{2\pi} \langle q_{k+1} | e^{-i\frac{\hat{p}^2}{2m}t} | p \rangle \langle p | q_k \rangle, \quad (2.17)$$

where the momentum operator acts as the eigenstate. This can be written as the momentum eigenvalue, in which the other exponential comes from q_{k+1} to q_k :

$$\langle q_{k+1} | e^{-i\frac{\hat{p}^2}{2m}t} | q_k \rangle = \int \frac{dp}{2\pi} e^{-i\frac{p^2}{2m}t} e^{ip(q_{k+1}-q_k)}. \quad (2.18)$$

This is a Gaussian integral which can be easily evaluated to

$$\langle q_{k+1} | e^{-i\frac{\hat{p}^2}{2m}t} | q_k \rangle = \sqrt{\frac{-im}{2\pi t}} e^{it\frac{m}{2}\left(\frac{q_{k+1}-q_k}{t}\right)^2}. \quad (2.19)$$

Inserting Eq. (2.19) in to Eq. (2.16) and solving the N gaussian integrals, Eq. (2.16) reduces to

$$\langle q_f | e^{-i\frac{\hat{p}^2}{2m}t} | q_i \rangle = \left(\sqrt{\frac{-im}{2\pi t}} \right)^N \left(\prod_{j=1}^{N-1} \int dq_j \right) e^{it\frac{m}{2} \sum_{k=0}^{N-1} \left(\frac{q_{k+1}-q_k}{t} \right)^2}. \quad (2.20)$$

In the continuum limit, summations are replaced by integrals and the $\frac{q_{k+1}-q_k}{t}$ term becomes the time derivative of the momentum. Finally by defining the measure

$$\mathcal{D}q = \lim_{N \rightarrow \infty} \left(\sqrt{\frac{-im}{2\pi t}} \right)^N \left(\prod_{j=1}^{N-1} \int dq_j \right), \quad (2.21)$$

path-integral representation is written in a simple form

$$\langle q_f | e^{-iHT} | q_i \rangle = \int \mathcal{D}q e^{i\int_0^T dt \frac{1}{2}m\dot{q}^2}. \quad (2.22)$$

This equation shows that all possible paths contribute to the calculation of the energy operator with their weights. Details of the derivation can be found in Ref. [62].

2.2.2 Discretization of the Gauge Fields

The gauge fields in LQCD are constructed from the link variables. It is crucial to understand the link variable, continuum gauge fields and the relation between them. The link variable connects the n to $n + \hat{\mu}$ lattice points, here $\hat{\mu}$ defines direction on the lattice. In

continuum, such an object is called the gauge transporter,

$$G(x, y) = Pe^{(i \int_{C_{x,y}} A ds)}. \quad (2.23)$$

Analogously, link variables are defined as

$$U_\mu(n) = e^{iaA_\mu(n)}. \quad (2.24)$$

The gauge field ($A_\mu(n)$) obeys Lie Algebra which is $\mathfrak{su}(3)$. The exponential mapping in Eq. (2.24) maps Lie algebra to its Lie group. Thus the link variables are elements of an $SU(3)$ group. $U_\mu(n)$ are traceless and anti-hermitian 3×3 matrices. For small a , link variables can be expanded as

$$\begin{aligned} U_\mu(n) &= \mathbb{1} + iaA_\mu(n) + \mathcal{O}(a^2), \\ U_{-\mu}(n) &= \mathbb{1} - iaA_\mu(n - \hat{\mu}) + \mathcal{O}(a^2), \end{aligned} \quad (2.25)$$

where $-\hat{\mu}$ is the negative direction of $\hat{\mu}$.

It is essential to construct the discrete gluon action using gauge invariant objects to respect the gauge invariance of the action. Consider a path of links that connects n_0 to n_1 ,

$$P[U] = U_{\mu_0}(n_0)U_{\mu_1}(n_0 + \hat{\mu}_0) \dots U_{\mu_{m-1}}(n_1 + \hat{\mu}_{m-1}) \equiv \prod_{(n,\mu) \in P} U_\mu(n), \quad (2.26)$$

which is the lattice version of the gauge transporter given in Eq. (2.23). $P[U]$ transforms as

$$P[U] \rightarrow P[U'] = \Omega(n_0)U_{\mu_0}(n_0)\Omega(n_0 + \hat{\mu}_0)^\dagger \Omega(n_0 + \hat{\mu}_0)U_{\mu_1}(n_0 + \hat{\mu}_0) \dots \\ U_{\mu_{m-1}}(n_1 + \hat{\mu}_{m-1})\Omega(n_1)^\dagger, \quad (2.27)$$

$$P[U'] = \Omega(n_0)P[U]\Omega(n_1)^\dagger, \quad (2.28)$$

and by considering the trace

$$\mathcal{L}[U] = \text{tr} \left[\prod_{(n,\mu) \in \mathcal{L}} U_\mu(n) \right], \quad (2.29)$$

a gauge invariant object is constructed from link variables. The object is gauge invariant

after the trace only if U s in the products start and end at the same point. It can be shown that Eq. (2.29) is a gauge invariant object by inserting the Eq. (2.28). It is useful to build the simplest possible closed loop for the lattice gluon action. Such a variable is called a *plaquette* (see Fig (2.4)). In its simplest form plaquette is defined as a product of four link variables

$$\begin{aligned} U_{\mu\nu}(n) &= U_\mu(n)U_\nu(n + \hat{\mu})U_{-\mu}(n + \hat{\mu} + \hat{\nu})U_{-\nu}(n + \hat{\nu}), \\ U_{\mu\nu}(n) &= U_\mu(n)U_\nu(n + \hat{\mu})U_\mu(n + \hat{\nu})^\dagger U_\nu(n)^\dagger. \end{aligned} \quad (2.30)$$

Inserting Eq. (2.25), the plaquette can be written in terms of the gauge fields,

$$U_{\mu\nu}(n) = e^{iaA_\mu(n)} e^{iaA_\nu(n+\hat{\mu})} e^{-iaA_\mu(n+\hat{\nu})} e^{-iaA_\nu(n)}. \quad (2.31)$$

Using the the Baker-Campbell-Hausdorff [63] formula,

$$e^A e^B = e^{A+B+\frac{1}{2}[A,B]+\dots}, \quad (2.32)$$

the plaquette in Eq. (2.31) becomes

$$\begin{aligned} U_{\mu\nu}(n) &= \exp \left(iaA_\mu(n) + iaA_\nu(n + \hat{\mu}) - \frac{a^2}{2} [A_\mu(n), A_\nu(n + \hat{\mu})] \right. \\ &\quad \left. - iaA_\mu(n + \hat{\mu}) - iaA_\nu(n) - \frac{a^2}{2} [A_\mu(n + \hat{\nu}), A_\nu(n)] \right. \\ &\quad \left. + \frac{a^2}{2} [A_\nu(n + \hat{\mu}), A_\mu(n + \hat{\nu})] + \frac{a^2}{2} [A_\mu(n), A_\nu(n)] \right. \\ &\quad \left. + \frac{a^2}{2} [A_\mu(n), A_\mu(n + \hat{\nu})] + \frac{a^2}{2} [A_\nu(n + \hat{\mu}), A_\nu(n)] + \mathcal{O}(a^3) \right). \end{aligned} \quad (2.33)$$

Replacing the shifted gauge fields by

$$A_\mu(n + \hat{\nu}) = A_\mu(n) + a\partial_\nu A_\mu, \quad (2.34)$$

the plaquette reduces to

$$\begin{aligned} U_{\mu\nu}(n) &= \exp \left(ia^2(\partial_\mu A_\nu(n) - \partial_\nu A_\mu(n) + i[A_\mu(n), A_\nu(n)]) + \mathcal{O}(a^3) \right), \\ U_{\mu\nu}(n) &= \exp \left(ia^2 F_{\mu\nu} + \mathcal{O}(a^3) \right), \\ U_{\mu\nu}(n) &= \mathbb{1} + ia^2 F_{\mu\nu} - \frac{a^4 F_{\mu\nu} F^{\mu\nu}}{2} + \mathcal{O}(a^3). \end{aligned} \quad (2.35)$$

Real part of the expansion gives

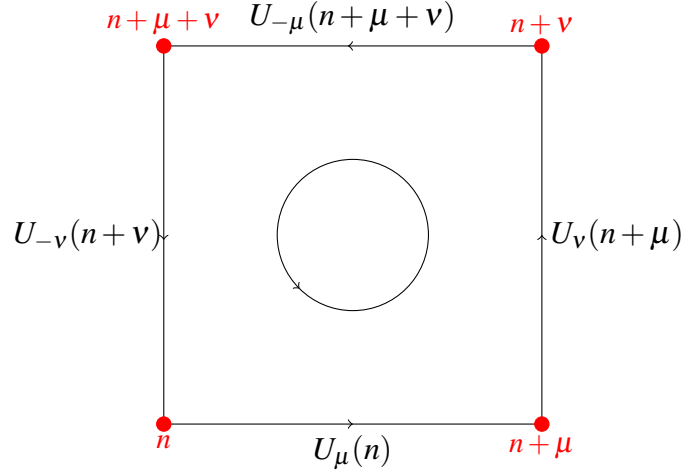


Figure 2.4 1×1 Plaquette $U_{\mu\nu}$

$$\text{Re}[U_{\mu\nu}(n)] = \mathbb{1} - \frac{a^4 F_{\mu\nu} F^{\mu\nu}}{2} + \mathcal{O}(a^3). \quad (2.36)$$

The gauge action in the continuum is defined as

$$S_G = \frac{1}{2g^2} \int d^4x \text{tr}[F_{\mu\nu} F^{\mu\nu}] \xrightarrow{\text{discretization}} \frac{a^4}{2g^2} \sum_{n \in \Lambda} \sum_{\mu < \nu} F_{\mu\nu} F^{\mu\nu}, \quad (2.37)$$

discrete version of which, in terms of the plaquette, is the Wilson's formulation of the gauge action,

$$S_G[U] = \frac{2}{g^2} \sum_{n \in \Lambda} \sum_{\mu < \nu} \text{Re tr}[\mathbb{1} - U_{\mu\nu}(n)]. \quad (2.38)$$

2.2.3 Naive Discretization of Fermions

In order to make calculations on the lattice, it is necessary to discretize the wave functions of fermions. Free Dirac action in continuum is written as

$$S_F^0[\psi, \bar{\psi}] = \int d^4x \bar{\psi}(x) (\gamma_{\mu} \partial_{\mu} + m) \psi(x). \quad (2.39)$$

Space-time is discretized on a 4 dimensional lattice

$$\Lambda = \{n = (n_1, n_2, n_3, n_4) \mid n_1, n_2, n_3 = 0, \dots, N-1; n_4 = 0, \dots, N_T-1\}, \quad (2.40)$$

and the spinors are allowed to live only on the lattice sites. Partial derivative is replaced by its symmetric definition

$$\partial_\mu \psi(x) \rightarrow \frac{\psi(n + \hat{\mu}) - \psi(n - \hat{\mu})}{2a}. \quad (2.41)$$

Therefore the discretized free Dirac action becomes

$$S_F^0[\psi, \bar{\psi}] = a^4 \sum_{n \in \Lambda} \bar{\psi}(n) \left(\sum_{\mu=1}^4 \gamma_\mu \frac{\psi(n + \hat{\mu}) - \psi(n - \hat{\mu})}{2a} + m\psi(n) \right). \quad (2.42)$$

Next step is to focus on the gauge invariance of the discretized fermion action. The *link variables* are used to ensure the gauge invariance. Fermion fields transform as

$$\psi(n) \rightarrow \psi'(n) = \Omega(n)\psi(n), \bar{\psi}(n) \rightarrow \bar{\psi}'(n) = \bar{\psi}(n)\Omega(n)^\dagger. \quad (2.43)$$

Under such transformations, mass term of Eq. (2.42) remains gauge invariant, however, the kinetic part transforms as

$$\begin{aligned} \bar{\psi}'(n)\psi'(n + \hat{\mu}) &= \bar{\psi}(n)\Omega^\dagger(n)\Omega(n + \hat{\mu})\psi(n + \hat{\mu}), \\ \bar{\psi}'(n)\psi'(n - \hat{\mu}) &= \bar{\psi}(n)\Omega^\dagger(n)\Omega(n - \hat{\mu})\psi(n - \hat{\mu}), \end{aligned} \quad (2.44)$$

which is not gauge invariant. To achieve the gauge invariance, two fermion fields are connected with a link variable, U_μ ,

$$\bar{\psi}'(n)U'_\mu(n)\psi'(n + \hat{\mu}) = \bar{\psi}(n)\Omega^\dagger(n)U'_\mu(n)\Omega(n + \hat{\mu})\psi(n + \hat{\mu}), \quad (2.45)$$

where the link variable transforms as

$$U'_\mu(n) = \Omega(n)U_\mu(n)\Omega(n + \hat{\mu})^\dagger. \quad (2.46)$$

In Eq. (2.42) $\psi(n - \hat{\mu})$ transforms as

$$\bar{\psi}'(n)U'_\mu(n)\psi'(n - \hat{\mu}) = \bar{\psi}(n)\Omega^\dagger(n)U'_\mu(n)\Omega(n - \hat{\mu})\psi(n - \hat{\mu}). \quad (2.47)$$

Link variable in Eq. (2.47) points in negative μ direction. Therefore using new notation $U_\mu(n - \hat{\mu})^\dagger \equiv U_{-\mu}(n)$ leads to the transformation of link in negative direction;

$$U'_{-\mu}(n) = \Omega(n)U_{-\mu}(n)\Omega(n - \hat{\mu})^\dagger. \quad (2.48)$$

With these considerations the discretized fermion action becomes



Figure 2.5 Forward and backward link variables.

$$S_F[\psi, \bar{\psi}, U] = a^4 \sum_{n \in \Lambda} \bar{\psi}(n) \left(\sum_{\mu=1}^4 \gamma_\mu \frac{U_\mu(n)\psi(n + \hat{\mu}) - U_{-\mu}(n)\psi(n - \hat{\mu})}{2a} + m\psi(n) \right). \quad (2.49)$$

2.2.4 Fermion Doubling Problem

In this section the fermion doubling problem will be explained which occurs when the action is discretized. The fermion action is bilinear, so it can be written in the form used in Wick's theorem,

$$S_F[\psi, \bar{\psi}, U] = a^4 \sum_{n \in \Lambda} \bar{\psi}(n)_{\alpha a} D(n|m)_{\alpha\beta} \psi(m)_{\beta b}, \quad (2.50)$$

where the Dirac operator is given as

$$D(n|m)_{\alpha\beta} = \sum_{\mu=1}^4 (\gamma_\mu)_{\alpha\beta} \frac{U_\mu(n)_{ab} \delta_{n+\hat{\mu},m} - U_{-\mu}(n)_{ab} \delta_{n-\hat{\mu},m}}{2a} + m\delta_{\alpha\beta} \delta_{ab} \delta_{n,m}. \quad (2.51)$$

In Eq. (2.50) fermion action is rewritten in the form of Wick's theorem in Eq. (A.25) with setting $M = -a^4 D$. The notational difference between Eq. (2.50) and Eq. (A.25) is, in Eq. (A.25) only a single index is used to label the different Grassmann numbers while in Eq. (2.50) is summed over several indices. Before explaining the doubling problem, it is instructive to consider the Fourier transform on the lattice. Fourier transformation in the continuum formalism is basically a mapping of an object between two orthogonal spaces.

For a 1-D variable, it is defined as

$$\tilde{f}(k) = \frac{1}{\sqrt{2\pi}} \int_{-\infty}^{\infty} f(x) e^{-ikx} dx, \quad (2.52)$$

where the object from the x space is mapped to k space. Using the periodic boundary condition

$$f(n + \hat{\mu}N_{\mu}) = e^{i2\pi\theta_{\mu}} f(n), \quad (2.53)$$

momentum space is described as

$$\tilde{\Lambda} = \left\{ p = (p_1, p_2, p_3, p_4) \mid p_{\mu} = \frac{2\pi}{aN_{\mu}}(k_{\mu} + \theta_{\mu}), k_{\mu} = -\frac{N_{\mu}}{2} + 1, \dots, \frac{N_{\mu}}{2} \right\}, \quad (2.54)$$

for a discrete space-time with periodic boundary conditions. The Fourier transformation on the lattice is defined as

$$\tilde{f}(p) = \frac{1}{\sqrt{|\Lambda|}} \sum_{n \in \Lambda} f(n) e^{-ip \cdot na}, \quad (2.55)$$

while the inverse transformation is

$$f(n) = \frac{1}{\sqrt{|\Lambda|}} \sum_{p \in \tilde{\Lambda}} \tilde{f}(p) e^{-ip \cdot na}. \quad (2.56)$$

The Dirac operator in Eq. (2.51), has two space-time arguments (n and m) thus Dirac operator in momentum space is written as

$$\tilde{D}(p|q) = \frac{1}{|\Lambda|} \sum_{n, m \in \Lambda} e^{-ip \cdot na} D(n|m) e^{iq \cdot ma}. \quad (2.57)$$

Expanding the exponentials in Eq. (2.57) and setting the gauge field as $U_{\mu} = \mathbb{1}$ for simplicity, the Eq. (2.57) becomes

$$\begin{aligned} \tilde{D}(p|q) &= \frac{1}{|\Lambda|} \sum_{n \in \Lambda} \left(\sum_{\mu=1}^4 \gamma_{\mu} \frac{e^{-ip \cdot na} e^{iq(n+\hat{\mu})a} - e^{-ip \cdot na} e^{iq(n-\hat{\mu})a}}{2a} + m\mathbb{1} \right), \\ \tilde{D}(p|q) &= \frac{1}{|\Lambda|} \sum_{n \in \Lambda} e^{-i(p-q) \cdot na} \left(\sum_{\mu=1}^4 \gamma_{\mu} \frac{e^{iq_{\mu}a} - e^{-iq_{\mu}a}}{2a} + m\mathbb{1} \right), \\ &\Rightarrow \delta(p-q) \tilde{D}(p). \end{aligned} \quad (2.58)$$

Using the trigonometric identity for the exponentials, the Fourier transformed Dirac operator becomes

$$\tilde{D}(p) = m\mathbb{1} + \frac{i}{a} \sum_{\mu=1}^4 \gamma_{\mu} \sin(p_{\mu}a). \quad (2.59)$$

It is easy to compute the inverse of Dirac operator in momentum space, which is a 4×4 matrix. Eq. (2.59) can be inverted using

$$(a\mathbb{1} + i \sum_{\mu=1}^4 \gamma_{\mu} b_{\mu})^{-1} = \frac{a\mathbb{1} - i \sum_{\mu=1}^4 \gamma_{\mu} b_{\mu}}{a^2 + \sum_{\mu=1}^4 b_{\mu}^2}, \quad (2.60)$$

which can be easily verified by multiplying both sides by $a\mathbb{1} + i \sum_{\mu=1}^4 \gamma_{\mu} b_{\mu}$. Applying Eq. (2.60) inverse of the Dirac matrix is

$$\tilde{D}(p)^{-1} = \frac{m\mathbb{1} - ia^{-1} \sum_{\mu=1}^4 \gamma_{\mu} \sin(p_{\mu}a)}{m^2 + a^{-2} \sum_{\mu=1}^4 \sin(p_{\mu}a)^2}, \quad (2.61)$$

and its inverse Fourier transformation is,

$$D(n|m)^{-1} = \frac{1}{|\Lambda|} \sum_{p \in \tilde{\Lambda}} \tilde{D}(p)^{-1} e^{ip \cdot (n-m)a}, \quad (2.62)$$

which is the quark propagator in Eq. (A.29). Quark propagator, includes all the n point functions. For massless fermions, the lattice propagator becomes

$$\tilde{D}(p)^{-1} \Big|_{m=0} = \frac{-ia^{-1} \sum_{\mu=1}^4 \gamma_{\mu} \sin(p_{\mu}a)}{a^{-2} \sum_{\mu=1}^4 \sin(p_{\mu}a)^2}, \quad (2.63)$$

which, in the continuum limit, reduces to

$$\tilde{D}(p)^{-1} \xrightarrow{a \rightarrow 0} \frac{-i \sum_{\mu} \gamma_{\mu} p_{\mu}}{p^2}. \quad (2.64)$$

In the continuum limit, there is only one pole. On the other hand, Eq. (2.63) has 16 poles. The $p_{\mu}(0,0,0,0)$ corresponds to the continuum but the remaining 15 are called

as doublers $(p_\mu(\frac{\pi}{a}, 0, 0, 0), p_\mu(0, \frac{\pi}{a}, 0, 0), \dots, p_\mu(\frac{\pi}{a}, \frac{\pi}{a}, \frac{\pi}{a}, \frac{\pi}{a}))$. Doublers are not physical, they should be removed. This problem is known as the *fermion doubling*. There are at least two different solutions for this problem, one is Wilson Fermions [16] and the other one is staggered fermions [64].

2.2.5 Wilson's Fermions

Wilson's solution to fermion doubling is to add an extra momentum dependent mass term to fermion action that cancels the unphysical poles. Adding the $\mathbb{1} \frac{1}{a} \sum_{\mu=1}^4 (1 - \cos(p_\mu a))$ term to the action, doubler-free Dirac operator becomes

$$\tilde{D}(p) = m\mathbb{1} + \frac{i}{a} \sum_{\mu=1}^4 \gamma_\mu \sin(p_\mu a) + \mathbb{1} \frac{1}{a} \sum_{\mu=1}^4 (1 - \cos(p_\mu a)). \quad (2.65)$$

The extra term is known as the Wilson term. There is no contribution from this term at the point $p_\mu = 0$, but Wilson's term brings an extra $\frac{2}{a}$ contribution to the unphysical poles. This contribution acts as an additional mass term so that the total mass of the doublers becomes, $m + \frac{2l}{a}$. If the lattice spacing (a) is small enough, doublers become heavy and decouple. Considering the free case, Wilson term in the position space is

$$-a \sum_{\mu=1}^4 \frac{U_\mu(n)_{ab} \delta_{n+\hat{\mu}, m} - 2\delta_{ab} \delta_{n, m} + U_{-\mu} \delta_{n-\hat{\mu}, m}}{2a^2}. \quad (2.66)$$

where the link variables ensure gauge invariance. Eq. (2.66) is nothing but the discrete version of the continuum Laplace operator, ∇^2 . Its proportionality to lattice spacing a ensures that in continuum limit, $a \rightarrow 0$, this part vanishes. The full Dirac operator becomes

$$D^{(f)}(n|m)_{\alpha\beta} = (m^{(f)} + \frac{4}{a}) \delta_{\alpha\beta} \delta_{ab} \delta_{n, m} - \frac{1}{2a} \sum_{\mu=1}^4 (\mathbb{1} - \gamma_\mu)_{\alpha\beta} U_\mu(n)_{ab} \delta_{n+\hat{\mu}, m}. \quad (2.67)$$

The final form of the fermion action is

$$S_F[\psi, \bar{\psi}, U] = \sum_{f=1}^{N_f} a^4 \sum_{n, m \in \Lambda} \bar{\psi}^{(f)}(n) D^{(f)}(n|m) \psi^{(f)}(m). \quad (2.68)$$

2.2.6 Other Lattice Fermion Actions

Eliminating doublers and incorporating the chiral symmetry are issues for which many efforts have been taken to address for years. Therefore, different formulations have been developed. Novel methods and computer technology have made heavy quark calculations possible. This section will give general information about other lattice fermion actions.

2.2.6.1 Staggered Fermions

Staggered Fermions, also called as Kogut-Susskind fermions, are formulated in 1974 by Kogut and Susskind [64]. There are four degenerate states ($4 \times n_f$ quarks) in staggered fermions. Local transformation is

$$\psi_n \rightarrow \Omega_n \psi'_n, \quad \bar{\psi}_n \rightarrow \bar{\psi}'_n \Omega_n^\dagger, \quad \Omega_n = \gamma_0^{n_0} \gamma_1^{n_1} \gamma_2^{n_2} \gamma_3^{n_3}, \quad (2.69)$$

transformation mixes spinor and space-time indices, generating the chiral symmetry, where $n_\mu = (n_1, n_2, n_3, n_4)$ is site index and γ 's are well-known Euclidean gamma matrices. There are sixteen different transformation matrices,

$$\Omega_n^\dagger \gamma_\mu \Omega_{n+\mu} = (-1)^{n_0+n_1+\dots+n_{\mu-1}} = \alpha_\mu(n). \quad (2.70)$$

In terms of the staggered fermion fields, the Wilson fermion action becomes,

$$S_F[\psi', \bar{\psi}'] = a^4 \sum_n \sum_{\epsilon \in \Lambda} \bar{\psi}'(n) \mathbb{1} \left(\sum_{\mu=1}^4 \eta_\mu(x) \frac{\psi'(n+\mu) - \psi'(n-\mu)}{2a} + m \psi'(n) \right), \quad (2.71)$$

where

$$\eta_1(n) = 1, \eta_2(n) = (-1)^{n_1}, \eta_3(n) = (-1)^{n_1+n_2}, \eta_4(n) = (-1)^{n_1+n_2+n_3}, \quad (2.72)$$

are the staggered sign functions. The final action becomes

$$S_F[\chi, \bar{\chi}] = a^4 \sum_n \sum_{\epsilon \in \Lambda} \bar{\chi}(n) \mathbb{1} \left(\sum_{\mu=1}^4 \eta_\mu(x) \chi(n+\mu) \frac{U_\mu(n) - U_\mu^\dagger(n-\mu) \chi(n-\mu)}{2a} + m \chi(n) \right). \quad (2.73)$$

Here $\chi(n)$ s are the Grassmann-valued fields, these fields carry only color indices without Dirac structure. Discarding the three of the four identical copies of $\chi(n)$ only four survives from sixteen d.o.f. With this procedure doublers are eliminated.

2.2.6.2 Twisted Mass Fermions

The formulation of the Twisted Mass fermions dates back to 1999 [65, 66, 67], in which, a so-called chirally twisted mass term

$$D_{twist} = D\mathbb{1}_{2 \times 2} + m\mathbb{1}_{2 \times 2} + i\mu\gamma_5\tau_3, \quad (2.74)$$

is added to the Wilson fermion action. Here, $\tau_3 = \text{diag}(1, -1)$ is the isospin generator and μ is the twisted mass. This term removes doublers from the Dirac operator. This is evident from the following simple arguments:

$$\begin{aligned} \det[D_{twist}] &= \det[D\mathbb{1}_{2 \times 2} + m\mathbb{1}_{2 \times 2} + i\mu\gamma_5\tau_3], \\ &= \det[D + m + i\mu\gamma_5]\det[D + m - i\mu\gamma_5], \\ &= \det[D + m + i\mu\gamma_5]\det[\gamma_5(D + m - i\mu\gamma_5)\gamma_5], \\ &= \det[D + m + i\mu\gamma_5]\det[D^\dagger + m - i\mu\gamma_5], \\ &= \det\left[(D + m + i\mu\gamma_5)(D^\dagger + m - i\mu\gamma_5)\right], \\ &= \det\left[(D + m)(D + m)^\dagger + \mu^2\right] > 0, \mu \neq 0. \end{aligned} \quad (2.75)$$

Since the eigenvalues, $(D + m)(D + m)^\dagger$, are real and must be greater than zero and $\mu^2 > 0$, the Dirac operator must be positive. Hence, Dirac operator can eliminate the doublers.

2.2.6.3 Domain Wall Fermions

Domain wall fermions were introduced by Kaplan in 1992 [68] and then developed by others [69, 70]. This method uses 5-dimensional lattice to create 4-dimensional chiral Dirac's fermions. A 4-dimensional lattice is extended to a 5-dimensional one by adding a fifth dimension, $\Lambda_5 = \Lambda \times Z_{N_5}$. Wilson action is modified accordingly as

$$S_F^{DW}[\psi, \bar{\psi}, U] = \sum_{n,m \in \Lambda} \sum_{r=0}^{N_5-1} \bar{\psi}(n,s) D^{DW}(n,s|m,r) \psi(m,r), \quad (2.76)$$

where the Dirac operator given as

$$D^{DW}(n, s|m, r) = \delta_{s,r}D(n|m) + \delta_{n,m}D_s^{DW}(s|r). \quad (2.77)$$

The spinors are naturally 4-dimensional Dirac spinors ($\psi(n, s)$). The color and Dirac indices in the spinors are in four dimension, however there is an extra term s which behaves like additional fifth dimension. Link variables are the usual 4-dimensional ones. The copies are used for different 4 dimensions; this allows to create 5D lattice with 4D lattice chiral fermions.

2.2.7 Hopping Expansion

In this section notations of Refs. [71] and [72] are used. In LQCD, calculations involving fermions are cumbersome, since fermions obey the Grassmann algebra. Because they have extra variables, it is hard to calculate fermionic path integrals numerically. For example, in pure gauge theory, it is relatively easy to calculate the correlation functions using Monte Carlo methods. To circumvent this issue, fermions must be integrated out first so that the remaining path integral depends only on pure gauge fields, which can be calculated easily.

A direct approach to this calculation does not provide a good perspective to the detailed dynamics. Hopping parameter expansion [73] on the other hand allows to draw the physical picture of hadron propagation on the lattice and reveals the effect of pair production to the observables. Unfortunately, the hopping parameter expansion has its drawbacks. This expansion is applicable to large lattices and large quark masses; so it is not very useful in continuum limit. Despite the limitations of the method, it gives valuable insight about fermions on the lattice.

2.2.7.1 Hopping Expansion of the Quark Propagator

The fermions two point function has an expectation value of fermion and anti-fermion fields. Using the Wick's theorem in Eq. (A.26), the fermion two-point correlation function

can be written as

$$\langle \psi(n) \bar{\psi}(m) \rangle = a^4 D^{-1}(n|m), \quad (2.78)$$

where the $\psi(n)$ ($\bar{\psi}(m)$) is the fermion (anti-fermion) field and D^{-1} is the quark propagator. The propagator is inverse of the Wilson's Dirac operator in Eq. (2.67). For large quark masses, D can be expanded as

$$D = C(\mathbb{1} - \kappa H), \quad \kappa = \frac{1}{2(am + 4)}, \quad C = m + \frac{4}{a}, \quad (2.79)$$

where κ is a real number called Hopping parameter and the C is used to redefine the quark fields like $\psi \rightarrow \sqrt{C}\psi$. The Hopping matrix is

$$H(n|m) = \sum_{\mu=\pm 1}^{\pm 4} (\mathbb{1} - \gamma_{\mu}) U_{\mu}(n) \delta_{n+\hat{\mu}, m}. \quad (2.80)$$

The matrix is a collection of all the nearest-neighbor terms of the Dirac operator. For small κ , the inverse of the Dirac operator can be expanded in a power series as

$$D^{-1}(n|m)_{\alpha\beta} = \sum_{i=0}^{\infty} \kappa^i H^i(n|m)_{\alpha\beta}, \quad (2.81)$$

where H^i means i th power of the Hopping matrix. More information can be found in Refs. [71, 72]. Higher orders of the Hopping matrix can be calculated by inserting Eq. (2.80) iteratively,

$$\begin{aligned} H^0(n|m)_{\alpha\beta} &= \delta_{\alpha\beta} \delta_{ab} \delta_{nm}, \\ H^1(n|m)_{\alpha\beta} &= \sum_{\mu=\pm 1}^{\pm 4} (\mathbb{1} - \gamma_{\mu})_{\alpha\beta} U_{\mu}(n)_{ab} \delta_{n+\hat{\mu}, m}, \\ H^2(n|m)_{\alpha\beta} &= \sum_{k\lambda c} H(n|k)_{\alpha\lambda} H(k|m)_{\lambda\beta}, \\ &= ((\mathbb{1} - \gamma_{\mu})(\mathbb{1} - \gamma_{\nu}))_{\alpha\beta} (U_{\mu}(n) U_{\nu}(n + \hat{\mu}))_{ab} \delta_{n+\hat{\mu}+\hat{\nu}, m}, \\ H^i(n|m)_{\alpha\beta} &= \sum_{\mu_j=\pm 1}^{\pm 4} \left(\prod_{j=1}^i (\mathbb{1} - \gamma_{\mu_j}) \right) P_{\mu_1 \dots \mu_i}(n)_{ab} \delta_{n+\hat{\mu}_1+\dots+\hat{\mu}_i, m}, \end{aligned} \quad (2.82)$$

where $P_{\mu_1 \dots \mu_i}(n)_{ab}$ is a pure gauge object composed of the product of all link variables. The $(\mathbb{1} - \gamma_{\mu_i})$ term, is important and it is related to the link variables. The relation $(\mathbb{1} -$

$\gamma_\nu)(\mathbb{1} + \gamma_\nu) = 0$, ensures that the paths containing back tracks are excluded from the products. The hopping expansion of propagator is written as a sum of forward paths only. It is also clear that the highest contribution comes from the first term, since the contributions of longer paths diminish.

2.2.7.2 Hopping Expansion of the Fermion Determinant

Hopping expansion of the fermion determinant and those of quark propagator are similar. Using Eq. (2.79), fermion determinant can be written as

$$\det[D] = \det[\mathbb{1} - \kappa H]. \quad (2.83)$$

Replacing the determinant by an exponential of trace of the logarithm,

$$\det[\mathbb{1} - \kappa H] = e^{\text{tr}[\ln[\mathbb{1} - \kappa H]]}, \quad (2.84)$$

and expanding the logarithm, it becomes

$$e^{\text{tr}[\ln[\mathbb{1} - \kappa H]]} = e^{(-\sum_{j=1}^{\infty} \frac{1}{j} \kappa^j \text{tr}[H^j])}, \quad (2.85)$$

where the trace acts on the Dirac and the color space. This refers to setting $n = m$, thus, creating closed loops which are *fermion loops*. It is important to stress that they do not correspond to the quark-antiquark loops of the perturbative description.

The insight is obtained from the hopping expansion that the quark propagators are sums over the lines of fermions and the fermion determinant is defined as a sum over the closed fermion loops, which are crucial for incorporating the sea-quark effects into the Monte-Carlo simulations.

2.2.8 Symanzik Improvement of Quark Propagator

Wilson action has $\mathcal{O}(a)$ discretization errors while the plaquette gauge action has $\mathcal{O}(a^2)$. For the charm quark this error corresponds to a relatively high as $aM_Q \approx 1$. There are various ways to reduce this error. The simplest method is changing the derivative operator

as follows:

$$\frac{f(x+a) - f(x-a)}{2a} = \frac{df}{dx} + \mathcal{O}(a^2), \quad (2.86)$$

$$\frac{4}{3} \left[\frac{f(x+a) - f(x-a)}{2a} \frac{f(x+2a) - f(x-2a)}{16a} \right] = \frac{df}{dx} + \mathcal{O}(a^4). \quad (2.87)$$

However, in quantum field theory, complications like operator mixing under renormalization arise and a different solution is needed. Symanzik developed an improvement to the lattice action [74, 75]. The idea is adding a term that cancels the $\mathcal{O}(a)$ and higher order errors. Simply, the derivative can be expanded as,

$$\frac{f(x+a) - f(x-a)}{2a} = f'(x) + a^2 c^{(2)}(x) + a^4 c^{(4)}(x) + \mathcal{O}(a^6), \quad (2.88)$$

where the Taylor expansion has been used,

$$f(x \pm a) = f(x) \pm a f'(x) + \frac{a^2}{2} f''(x) \pm \frac{a^3}{6} f'''(x) + \mathcal{O}(a^4). \quad (2.89)$$

The first higher order term that survives is, $c^{(2)}(x) = \frac{1}{6} f'''(x)$, which is cancelled by adding an extra term to the left hand side of Eq. (2.88):

$$\frac{f(x+a) - f(x-a)}{2a} + ca^2 D^{(3)}(f(x)) = f'(x) + \mathcal{O}(a^4), \quad (2.90)$$

where,

$$D^{(3)}(f(x)) \approx f'''(x) + \mathcal{O}(a^2), \quad (2.91)$$

$$D^{(3)}(f(x)) = \frac{f(x+2a) - 2f(x+a) + 2f(x-a) - f(x-2a)}{2a^3}, c = -\frac{1}{6}.$$

Using the Symanzik improvement, fermion action has an extra term called *Clover term*,

$$S_F^{clover} = S_F^{Wilson} + c_{SW} a^5 \sum_n \sum_{\varepsilon \Lambda \mu < \nu} \bar{\Psi}(n) \frac{1}{2} \sigma_{\mu\nu} \hat{F}_{\mu\nu}(n) \Psi(n), \quad (2.92)$$

where c_{SW} is the Sheikholeslami-Wohlert coefficient and

$$\hat{F}_{\mu\nu} = \frac{-i}{8a^2} (Q_{\mu\nu}(n) - Q_{\nu\mu}(n)). \quad (2.93)$$

$\hat{F}_{\mu\nu}$ is the discretized version of lattice field strength tensor, where $Q_{\mu\nu}(n)$ is defined as the sum of all plaquettes associated with the lattice site n as shown in Fig (2.6). c_{SW} can

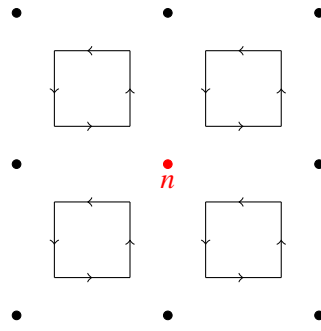


Figure 2.6 Sum of plaquettes in the $\mu - \nu$ plane ($Q_{\mu\nu}$).

be calculated both numerically and perturbatively.



2.3 Discrete Symmetries

Symmetries are essential for particle physics. According to Noether's theorem, symmetries can be associated with conservation laws or the other way around. Symmetries and the corresponding conservation laws are listed in Table (2.2). In the following sections

Table 2.2 Symmetries and conservation laws [50]

Symmetries	\longleftrightarrow	Conservation laws
Transition in time	\longleftrightarrow	Energy
Transition in space	\longleftrightarrow	Momentum
Rotation	\longleftrightarrow	Angular Momentum
Gauge Transformation	\longleftrightarrow	Charge

parity, charge and time-reversal symmetries will be discussed which are using in LQCD calculations.

2.3.1 Parity

Physical processes were assumed to be mirror symmetric until 1957. Wu [76] presented an experiment using the polarized Co^{60} 's β decay showing that the parity is violated in weak interactions. But it is a good symmetry in strong and electromagnetic interactions. Parity in continuum is defined as

$$P : x \rightarrow -x; t \rightarrow t. \quad (2.94)$$

It is a space inversion such that it only changes the sign of the spatial coordinates. While momentum changes angular momentum and spins remain unchanged under parity transformation. (For details see [77, 50].) Discrete parity operation is defined similarly to the continuum case. Parity operator changes the spatial coordinates, leaving the temporal

coordinate intact,

$$\begin{aligned}
\psi(n, n_4) &\xrightarrow{\mathcal{P}} \gamma_4 \psi(-n, n_4), \\
\bar{\psi}(n, n_4) &\xrightarrow{\mathcal{P}} \bar{\psi}(-n, n_4) \gamma_4, \\
U_i(n, n_4) &\xrightarrow{\mathcal{P}} U_{-i}(-n, n_4)^\dagger, \\
U_4(n, n_4) &\xrightarrow{\mathcal{P}} U_4(-n, n_4).
\end{aligned} \tag{2.95}$$

The hopping part of the Wilson action remains invariant under parity transformation. Details of the calculation can be found at Appendix D.1.

2.3.2 Charge Conjugation

The operator that changes the sign of the charge is called *charge conjugation*. This operator converts the particle into its anti-particle and it is defined as,

$$C |p\rangle \rightarrow |\bar{p}\rangle. \tag{2.96}$$

Basically, it changes the sign of all internal quantum numbers, such as charge, baryon number, quark contents of the particle while its mass, energy, momentum and spin remain the same. Discrete charge conjugation operator is defined as

$$\begin{aligned}
\psi(n) &\xrightarrow{C} \psi(n)^C = C^{-1} \bar{\psi}(n)^T, \\
\bar{\psi}(n) &\xrightarrow{C} \bar{\psi}(n)^C = -\psi(n)^T C,
\end{aligned} \tag{2.97}$$

where the charge conjugation matrix acts on the Dirac space only and is defined as a combination of gamma matrices $C = \gamma_2 \gamma_4$. Charge conjugation of link variable is

$$e^{iaA_\mu(n)} \xrightarrow{C} e^{iaA_\mu(n)^C} \rightarrow e^{iaA_\mu(n)^*} \rightarrow e^{-iaA_\mu(n)^T}, \tag{2.98}$$

where the transformation, $A_\mu(n) \rightarrow -A_\mu(n)^T$ shows that the corresponding antiparticle has the opposite charge of the particle.

The Wilson action given in Eq. (2.67) remains invariant under charge conjugation. The mass term is

$$\bar{\psi}^C(n) \psi^C(n) = -\psi^T(n) C C^{-1} \bar{\psi}^T(n) = \bar{\psi}(n) \psi(n), \tag{2.99}$$

and the hopping part of the Wilson action shown to be invariant in Appendix D.2.

2.3.3 Time-Reversal and γ_5 -hermicity

Time-reversal symmetry replaces a forward propagating particle with its anti-particle, propagating backwards in time direction. Time-reversal operator, \mathcal{T} , is anti-linear and it cannot be matched to any observable. It does not correspond to a quantum number. Furthermore, it is not an exact symmetry.

In lattice formulation, it is associated with γ_5 hermicity. Most of the Dirac operators are γ_5 hermitian, so they obey the relation,

$$D^\dagger = (\gamma_5 D \gamma_5). \quad (2.100)$$

Mass term of the Wilson action is invariant and the hopping part can be found in Appendix D.3.

The γ_5 hermicity is extensively used in quark propagator and correlator calculations. Eq. (D.17) also shows that the fermion determinant is real. All of the discrete symmetry operators of the lattice formulation are listed in Table 2.3.

Table 2.3 Table of discrete symmetry operators on Lattice [78].

Variables	\mathcal{P}	\mathcal{C}	\mathcal{T}
$U_4(n, n_4)$	$U_4(-n, n_4)$	$U_4^*(n, n_4)$	$U_{-4}(n, -n_4)$
$U_i(x, n_4)$	$U_{-i}(-n, n_4)^\dagger$	$U_i^*(x, \mathcal{T})$	$U_i(x, -\mathcal{T})$
$\psi(x, \mathcal{T})$	$\gamma_4 \psi(-x, \mathcal{T})$	$\gamma_4 \gamma_2 \psi^T(x, \mathcal{T})$	$\gamma_4 \gamma_5 \psi(x, -\mathcal{T})$
$\bar{\psi}(x, \mathcal{T})$	$\bar{\psi}(-x, \mathcal{T}) \gamma_4$	$-\bar{\psi}^T(x, \mathcal{T}) \gamma_2 \gamma_4$	$\bar{\psi}(x, -\mathcal{T}) \gamma_5 \gamma_4$

Discrete symmetries are crucial in defining the interpolating fields that will be described in the next chapter.

TECHNICALITIES

In this chapter we will describe how to perform numerical calculations in LQCD. In section 3.1, correlators in LQCD will be explained and two-point correlators will be defined. In section 3.2 the information will be given about baryon spectroscopy in LQCD. Effective mass and matrix elements will be defined and the analysis steps will be explained through sample analyses. Finally baryons in LQCD will be discussed.

3.1 Correlators in Lattice QCD

In this section, interpolating fields will be defined by using the discrete symmetry operators that have been introduced in section 2.3. Later the two-point correlators will be explained and a convention for performing Wick contractions will be introduced. Finally explicit spectral forms of two-point correlators for spin- $\frac{1}{2}$ and spin- $\frac{3}{2}$ fields will be calculated.

3.1.1 Interpolating Fields

Discrete symmetries help to build interpolators and to classify the hadrons. In simplest interpretation, baryons are composed of three valence quarks. Baryon interpolator can be written by taking into account the quantum numbers describing that particular baryon. As an example, quantum numbers of the proton are $I = \frac{1}{2}, Q = 1, P = +1$. It consists of two u and one d quarks. Commonly used interpolating operator for the proton is

$$O_N = \epsilon_{abc} [u(n)_b^T C \gamma_5 d(n)_c] u(n)_a, \quad (3.1)$$

where $u(n)$ and $d(n)$ are Dirac 4-spinors, T is the transpose and a, b, c are the color indices. Anti-symmetric tensor, ϵ_{abc} , makes the interpolator color singlet. The term in parentheses is defined as a diquark which has two quark spinors. The diquark part is $I = 0$ and $J = 0$ due to $C\gamma_5$ term.

The parity of proton is $P = +1$. In order to project the desired parity, *parity projection operator*, P_{\pm} , is defined. The proton interpolator is

$$O_{N_{\pm}} = \epsilon_{abc} P_{\pm} (u(n)_b^T C \gamma_5 d(n)_c) u(n)_a, \quad (3.2)$$

where $P_{\pm} = \frac{1}{2}(1 \pm \gamma_4)$. Interpolators for other octet baryons are given in Table 3.1.

Table 3.1 Interpolating fields of spin- $\frac{1}{2}$ baryons.

$O_{N_{\pm}} = \epsilon_{abc} P_{\pm} \Gamma^A u_a [u_b^T \Gamma^B d_c]$
$O_{\Sigma_{\pm}} = \epsilon_{abc} P_{\pm} \Gamma^A u_a [u_b^T \Gamma^B s_c]$
$O_{\Xi_{\pm}} = \epsilon_{abc} P_{\pm} \Gamma^A s_a [s_b^T \Gamma^B u_c]$
$O_{\Lambda_{\pm}} = \epsilon_{abc} P_{\pm} \Gamma^A ((2s_a [u_b^T \Gamma^B d_c]) + (d_a [u_b^T \Gamma^B s_c]) - (u_a [d_b^T \Gamma^B s_c]))$

For the spin $J = \frac{3}{2}$ baryons, the corresponding gamma matrices are $\Gamma_A, \Gamma_B = (1, C\gamma_j)$. The spatial gamma matrix, which makes the diquark $J = 1$ and together with the quark spinor outside the diquark structure, the interpolator defines a $J = \frac{3}{2}$ baryon. There is also an admixture of $J = \frac{1}{2}$ components.

The hadron interpolator has to be projected to a definite momentum via the Fourier transformation

$$\tilde{O}(\mathbf{p}, n_t) = \frac{1}{\sqrt{|\Lambda_s|}} \sum_{\mathbf{n} \in \Lambda_s} O(\mathbf{n}, n_t) e^{-i\mathbf{a}\mathbf{n}\mathbf{p}}, \quad (3.3)$$

where Λ_s is the spatial part of the lattice and \mathbf{p} is the spatial momenta. In continuum, QCD observables are defined using angular momentum and parity J^P which lead to rotation group $\mathcal{O}(3)$. However, the continuous rotational symmetry is broken on the lattice since we are using discrete space and time. Fortunately there is a relevant symmetry group which is cubic point group \mathcal{O}_h hence the lattice states are classified by these irreducible representations Λ^P rather than J^P [79].

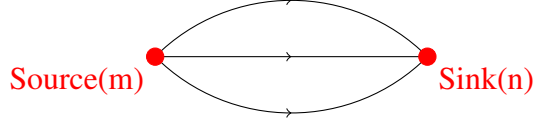


Figure 3.1 Illustration of a two-point function: Arrows are the quark propagators. Node (m) is the source point and node (n) is the sink point

3.1.2 Two-Point Correlators

A two-point *correlator* is defined as the product of two interpolating fields as, $\langle O_B(n)_\alpha \bar{O}_B(m)_\alpha \rangle$.

It has the physical meaning that one interpolator creates a baryon at one point and the other annihilates the baryon at another point.

To illustrate, consider the calculation of proton's two-point correlator. Replacing $O_B(n)_\alpha$, by the proton interpolator given in Eq. (3.1), since the interpolators are Grassmann valued fields, there must be a minus sign when the fields are interchanged:

$$\begin{aligned} \langle O_B(n)_\alpha \bar{O}_B(m)_\alpha \rangle &= -\langle \bar{O}_B(m)_\alpha O_B(n)_\alpha \rangle, \\ -\langle \bar{O}_B(m)_\alpha O_B(n)_\alpha \rangle &= -\langle \varepsilon_{abc} \varepsilon_{d'b'c'} (\bar{u}(n)_a C \gamma_5 \bar{d}(n)_b^T) \bar{u}(n)_c P_\pm \\ &\quad P_\pm u(m)_{c'} (u(m)_{d'}^T C \gamma_5 d(m)_{b'}) \rangle. \end{aligned} \quad (3.4)$$

The identity $P_\pm^2 = P_\pm$ is useful in this case. Keeping in mind that the contraction of two quark fields reduces to the propagator $D_{\alpha\alpha'}^{-1(q)} = q_\alpha \bar{q}_{\alpha'}$. Correlation function in terms of propagators is written as

$$\begin{aligned} \langle O_B(n)_\alpha \bar{O}_B(m)_\alpha \rangle &= \varepsilon_{abc} \varepsilon_{d'b'c'} (C \gamma_5)_{\alpha'\beta'} (C \gamma_5)_{\alpha\beta} (P_\pm)_{\gamma\gamma'} \left[(D_{\beta'\beta}^{-1(d)} D_{\alpha'\alpha}^{-1(u)} \right. \\ &\quad \left. D_{\gamma'\gamma}^{-1(u)} - (D_{\beta'\beta}^{-1(d)} D_{\alpha'\gamma}^{-1(u)} D_{\gamma'\alpha}^{-1(u)}) \right], \end{aligned} \quad (3.5)$$

$$\begin{aligned} &= \varepsilon_{abc} \varepsilon_{d'b'c'} \text{tr} [D_{c'c}^{-1(u)} (P_\pm)] \text{tr} [(C \gamma_5) D_{b'b}^{-1(d)} (C \gamma_5) D_{a'a}^{-1(u)}] \\ &\quad + \text{tr} [D_{d'c}^{-1(u)} (P_\pm) D_{b'b}^{-1(u)} (C \gamma_5) D_{c'a}^{-1(d)} (C \gamma_5)]. \end{aligned} \quad (3.6)$$

The two-point correlators can be used to calculate the masses of hadrons. The contraction of two- and three-point functions can be calculated much more easily with a different convention. In CHROMA's [1] convention, the correlation functions for interpolating fields are generically labelled as B . For baryon contraction, in general, there appear two

types of traces:

$$\text{tr}[D_{c'c}^{-1(3)}] \text{tr}[D_{b'b}^{-1(2)} D_{a'a}^{-1(1)}], \quad (3.7)$$

$$\text{tr}[D_{a'c}^{-1(1)} D_{b'b}^{-1(2)} D_{c'a}^{-1(3)}]. \quad (3.8)$$

In CHROMA's convention, the fields are defined as

$$\begin{aligned} \left\langle B_\gamma^{123}(x) \bar{B}_{\bar{\gamma}}^{123}(0) \right\rangle &= -\varepsilon^{abc} \varepsilon^{a'b'c'} \left\langle \left(q_{1,\alpha}^{Ta} (C\gamma_5)_{\alpha\beta} q_{2,\beta}^b \right) q_{3,\gamma}^c(x) \right. \\ &\quad \left. \left(\bar{q}_{1,\bar{\alpha}}^{T a'} (C\gamma_5)_{\bar{\alpha}\bar{\beta}} \bar{q}_{2,\bar{\beta}}^b \right) \bar{q}_{3,\gamma}^{c'}(0) \right\rangle, \\ &= \varepsilon^{abc} \varepsilon^{a'b'c'} (C\gamma_5)_{\alpha\beta} (C\gamma_5)_{\bar{\alpha}\bar{\beta}} D^{-1(1)}(x,0)_{\alpha\bar{\alpha}}^{aa'} \\ &\quad D^{-1(2)}(x,0)_{\beta\bar{\beta}}^{bb'} D^{-1(3)}(x,0)_{\gamma\bar{\gamma}}^{c'c}, \end{aligned} \quad (3.9)$$

$$\begin{aligned} \left\langle B_\gamma^{123}(x) \bar{B}_{\bar{\gamma}}^{132}(0) \right\rangle &= -\varepsilon^{abc} \varepsilon^{a'b'c'} \left\langle \left(q_{1,\alpha}^{Ta} (C\gamma_5)_{\alpha\beta} q_{2,\beta}^b \right) q_{3,\gamma}^c(t) \right. \\ &\quad \left. \left(\bar{q}_{1,\bar{\alpha}}^{T a'} (C\gamma_5)_{\bar{\alpha}\bar{\beta}} \bar{q}_{3,\bar{\beta}}^b \right) \bar{q}_{2,\gamma}^{c'}(0) \right\rangle, \\ &= -\varepsilon^{abc} \varepsilon^{a'b'c'} (C\gamma_5)_{\alpha\beta} (C\gamma_5)_{\bar{\alpha}\bar{\beta}} D^{-1(1)}(x,0)_{\alpha\bar{\alpha}}^{aa'} \\ &\quad D^{-1(2)}(x,0)_{\beta\bar{\gamma}}^{bc'} D^{-1(3)}(x,0)_{\gamma\bar{\beta}}^{c'b'}, \end{aligned} \quad (3.10)$$

The traces are written as

$$\text{tr}[D_{\gamma\gamma'}^{-1(3)}] \text{tr}[(D_{\alpha\alpha'}^{-1(1)} D_{\beta\beta'}^{-1(2)})] = \langle B_\gamma^{123} \bar{B}_{\gamma'}^{123} \rangle, \quad (3.11)$$

$$\text{tr}[(D_{\beta\beta'}^{-1(2)} D_{\alpha\alpha'}^{-1(1)} D_{\gamma\gamma'}^{-1(3)})] = \langle B_\gamma^{123} \bar{B}_{\gamma'}^{132} \rangle. \quad (3.12)$$

As an example the proton's interpolating field is defined as

$$O_N = \varepsilon_{abc} (u(n)_b^T C\gamma_5 d(n)_c) u(n)_a \rightarrow B^{udu}. \quad (3.13)$$

The contraction for two-point function can easily be stated with

$$\langle B_\gamma^{udu} \bar{B}_{\gamma'}^{udu} \rangle. \quad (3.14)$$

It is important to note that the first quark flavors are the same for traces in Eqs. (3.11) and (3.12). An interchange can be made to make the first quark flavors the same. However, interchange for octet baryons brings minus sign, $B_\gamma^{123} = -B_\gamma^{213}$. The two-point correlator

reduces to

$$\langle B_\gamma^{u_1 du_2} \bar{B}_\gamma^{u_1 du_2} \rangle + \langle B_\gamma^{u_1 du_2} \bar{B}_\gamma^{u_2 du_1} \rangle,$$

$$\langle B_\gamma^{u_1 du_2} \bar{B}_\gamma^{u_1 du_2} \rangle + \langle B_\gamma^{du_1 u_2} \bar{B}_\gamma^{du_2 u_1} \rangle,$$

$$\langle B_\gamma^{123} \bar{B}_\gamma^{123} \rangle_{1=u_1, 2=d, 3=u_2} + \langle B_\gamma^{123} \bar{B}_\gamma^{132} \rangle_{1=d, 2=u_1, 3=u_2}. \quad (3.15)$$

$$(3.16)$$

Quarks are labeled because there are two quarks with the same flavor in proton's interpolating field.

In order to extract form factors properly the coefficients in front of the two-point correlators must be carefully treated. Consider the two-point correlation function projected to a definite momentum:

$$\langle F^{NN}(t; p; \Gamma) \rangle = \sum_x e^{i\vec{p}'x} \Gamma^{\beta\alpha} \langle \Omega | T(\chi^\alpha(x) \bar{\chi}^\beta(0)) | \Omega \rangle. \quad (3.17)$$

Inserting complete set of states between χ 's, we obtain

$$\langle F^{NN}(t; p; \Gamma) \rangle = \sum_x \sum_{N, p, s} e^{i\vec{p}'x} \Gamma^{\beta\alpha} \langle \Omega | T(\chi^\alpha(x) |N(\vec{p}, s)\rangle \langle N(\vec{p}, s) | \bar{\chi}^\beta(0)) | \Omega \rangle, \quad (3.18)$$

where $|N(\vec{p}, s)\rangle \langle N(\vec{p}, s)| = \mathbb{1}$. Baryon to vacuum transition matrix element is defined as

$$\langle \Omega | \chi^\alpha(x) | N(\vec{p}, s) \rangle = Z_B \sqrt{\frac{M}{E_p}} u(\vec{p}, s). \quad (3.19)$$

Here Z_B is coupling strength and $E_p = \sqrt{\vec{p}^2 + M^2}$. The free spinor sum is

$$\sum_s u(\vec{p}, s) \bar{u}(\vec{p}, s) = \frac{i\not{p} + M}{2M}. \quad (3.20)$$

The $\chi^\alpha(x)$ in Eq. 3.18 can be written as evaluation operator

$$\langle F^{NN}(t; p; \Gamma) \rangle = \sum_x \sum_{N, p, s} e^{i\vec{p}'x} \Gamma^{\beta\alpha} \langle \Omega | T(\chi^\alpha(0) e^{ipx} |N(\vec{p}, s)\rangle \langle N(\vec{p}, s) | \bar{\chi}^\beta(0)) | \Omega \rangle. \quad (3.21)$$

Exponential in bracket is four vector, it can be split in energy and spatial parts

$$\langle F^{NN}(t; p; \Gamma) \rangle = \sum_x \sum_{N, p, s} e^{i(\vec{p}' - \vec{p})x} \Gamma^{\beta\alpha} \langle \Omega | T(\chi^\alpha(0) | N(\vec{p}, s)) \rangle e^{-E_p t} \langle N(\vec{p}, s) | \bar{\chi}^\beta(0) | \Omega \rangle. \quad (3.22)$$

The exponential of $(\vec{p}' - \vec{p})$ gives the dirac delta in three dimensions

$$\langle F^{NN}(t; p; \Gamma) \rangle = \sum_{N, s} \delta_{\vec{p}', \vec{p}}^{(3)} \Gamma^{\beta\alpha} \langle \Omega | T(\chi^\alpha(0) | N(\vec{p}, s)) \rangle e^{-E_p t} \langle N(\vec{p}, s) | \bar{\chi}^\beta(0) | \Omega \rangle. \quad (3.23)$$

Using Eq. (3.19), the two-point function becomes

$$\langle F^{NN}(t; p; \Gamma) \rangle = \sum_{N, s} e^{-E_p t} \Gamma^{\beta\alpha} Z_B \sqrt{\frac{M}{E_p}} u^\alpha(p, s) Z_B \sqrt{\frac{M}{E_p}} \bar{u}^\beta(p, s). \quad (3.24)$$

Using Eq. (3.20), we get

$$\langle F^{NN}(t; p; \Gamma) \rangle = \sum_N e^{-E_p t} \Gamma^{\beta\alpha} Z_B \sqrt{\frac{M}{E_p}} Z_B \sqrt{\frac{M}{E_p}} \left[\frac{i\not{p} + M}{2M} \right]^{\alpha\beta}. \quad (3.25)$$

Collecting all variables, Γ and $\frac{i\not{p} + M}{2M}$ becomes trace. Hence, the two-point function is

$$\langle F^{NN}(t; p; \Gamma) \rangle = \sum_N e^{-E_p t} \frac{Z_B^2}{2E_p} \text{tr} \left[\Gamma i\not{p} + M \right]. \quad (3.26)$$

We can follow a similar procedure for spin- $\frac{3}{2}$ particles. Spin- $\frac{3}{2}$ particles are represented by the Rarita-Schwinger Lagrangian [80]. Accordingly, interpolating fields acquire an extra index and the two-point function can be written as

$$\langle F_{\sigma\tau}^{\Delta\Delta}(t; p; \Gamma) \rangle = \sum_x e^{i\vec{p}'x} \Gamma^{\beta\alpha} \langle \Omega | T(\chi_\sigma^\alpha(x) \bar{\chi}_\tau^\beta(0)) | \Omega \rangle. \quad (3.27)$$

Following steps similar to the spin-1/2 case, $\chi^\alpha(x)$ is written as evaluation operator by separating the energy (temporal) and spatial parts. Thus the two-point function becomes

$$\langle F_{\sigma\tau}^{\Delta\Delta}(t; p; \Gamma) \rangle = \sum_{N, s} e^{-E_p t} \Gamma^{\beta\alpha} Z_B \sqrt{\frac{M}{E_p}} u_\sigma^\alpha(p, s) Z_B \sqrt{\frac{M}{E_p}} \bar{u}_\tau^\beta(p, s), \quad (3.28)$$

Using the Rarita-Schwinger spin sum in Euclidean space we get,

$$\sum_s u_\sigma^\alpha(p, s) \bar{u}_\tau^\beta(p, s) = \frac{-i\not{p} + M}{2M} \left[g_{\sigma\tau} - \frac{1}{3} \gamma_\sigma \gamma_\tau + \frac{2p_\sigma p_\tau}{3M^2} - i \frac{p_\sigma \gamma_\tau - p_\tau \gamma_\sigma}{3M} \right], \quad (3.29)$$

where σ and τ are Lorentz indices and when taken as, $\sigma = \tau$ with the choice of Γ_4 for the projection operator. Finally the two-point correlator for spin- $\frac{3}{2}$ particles becomes

$$\langle F_{\sigma\sigma}^{\Delta\Delta}(t; p; \Gamma_4) \rangle = \frac{2}{3} \left(1 + \frac{p_\sigma^2}{M^2} \right) \left(\frac{E_p + M}{2E_p} \right) e^{-E_p t}. \quad (3.30)$$

3.2 Lattice Simulations

In this section baryon spectroscopy of LQCD will be discussed. Before calculating the observables, gauge configurations and individual quark propagators on each gauge configuration have to be generated. Generating the gauge configurations is a very costly procedure, since huge computational resources are needed. In our work we are using $32^3 \times 64$ size lattices generated by PACS-CS collaboration [4], the configuration generation does not to be discussed in detail but we briefly outline the method. Detailed information about lattice generation can be found in the Refs. [11, 72].

A typical measurement on the Lattice is generally summarized in three steps,

1. Generating Configurations (Monte Carlo, Metropolis algorithms etc...).
2. Computing quark propagators and the correlation functions.
3. Data analysis (extracting the physics).

First step is calculating the path integral using Monte Carlo methods, in which the Boltzmann factor, e^{-S} , must be taken into account. Different paths of the action S have different weights, so they give different field configurations. The integral can be approximated by using the Importance Sampling Monte Carlo method. Expectation value of a function $f(x)$, is given in the form

$$\langle f(x) \rangle_\rho = \frac{\int_a^b dx \rho(x) f(x)}{\int_a^b dx \rho(x)}, \quad (3.31)$$

where $\rho(x)$ is the probability distribution density. The function, $f(x)$, can be calculated using the Importance Sampling Monte Carlo integration,

$$\langle f(x) \rangle_\rho = \lim_{N \rightarrow \infty} \frac{1}{N} \sum_{n=1}^N f(x_n), \quad (3.32)$$

where the x_n is randomly sampled value with the probability density

$$dP(x) = \frac{\rho(x) dx}{\int_a^b dx \rho(x)}. \quad (3.33)$$

The QCD action is not a simple function and it contains gauge fields (*link variables*). The expectation value of an hadronic observable is written as,

$$\langle O \rangle_\rho = \lim_{N \rightarrow \infty} \frac{1}{N} \sum_{n=1}^N O[U_n], \quad (3.34)$$

with the probability density,

$$dP(U) = \frac{e^{-S[U]} \mathcal{D}[U]}{\int \mathcal{D}[U] e^{-S[U]}}, \quad (3.35)$$

where the measure $\mathcal{D}[U]$ is defined over link variables. SU(3) adaptation is required for the Markov Chains and Metropolis algorithms [81]. After the adaptation, Metropolis algorithm for Wilson's gauge action can be written, so that the gauge configurations can be created.

Next step is to compute the quark propagators on individual gauge configurations for each flavor. Propagators should be specifically calculated for each configuration because every gauge configuration has different sea-quark weights. The propagator matrix consists of $\mathcal{O}(10^{12})$ complex numbers. Each entry connects the source point to the sink point. These entries are highly correlated, which means that the entries contain very little information. Therefore, calculating the whole propagator is unnecessary. In order to ease the computation, a common practice is to choose a source point and calculate the propagator originating from that point only. In this work point source, shell source and wall source are used. Therefore; detailed information will be given about these type of sources.

3.2.1 Quark Sources

Propagator is obtained by inverting the Dirac matrix, $D^{-1}(n|m)_{ba}^{\beta\alpha}$, which connects source point, n , to the sink point, m , for all Dirac (β, α) and color (a, b) components.

If the source of the propagator is fixed to a site m_0 , the propagator with a specific Dirac,

α_0 , and color, a_0 , component is written as

$$D^{-1}(n|m_0)_{b a_0}^{\beta \alpha_0} = \sum_{m, \alpha, a} D^{-1}(n|m)_{b a}^{\beta \alpha} \delta(m - m_0) \delta_{\alpha \alpha_0} \delta_{a a_0}, \quad (3.36)$$

where

$$S_{point}^{m_0, \alpha_0, a_0} = \delta(m - m_0) \delta_{\alpha \alpha_0} \delta_{a a_0}, \quad (3.37)$$

is defined as the point source. Eq. (3.36) has to be calculated for each Dirac and color index in order to compute the full propagator. Point-source technique, however, does not reflect the relevant physics. In order to achieve the ground-state dominance, interpolating fields must be optimized and wave functions must be improved. In order to achieve this, smeared sources are used for improvement. The basic idea is writing the new wave functions with smeared fermion fields,

$$\tilde{\Psi}(n_0, n_t)_{\alpha_0 a_0} = \sum_{n_1} S_{smear}^{m_0, \alpha_0, a_0}(n_1)_{\alpha_1 a_1} \Psi(n_1, n_t)_{\alpha_1 a_1}. \quad (3.38)$$

Similar to Eq. (3.36), the propagator, with a smeared source is written as

$$[1]D^{-1}(n|m_0)_{b a_0}^{\beta \alpha_0} = \sum_{m, \alpha, a} D^{-1}(n|m)_{b a}^{\beta \alpha} S^{(m_0, \alpha_0, a_0)}(m)_{\alpha, a}, \quad (3.39)$$

here $S(m)$ is the smeared source defined by a Gaussian smearing procedure [82],

$$S_{smeared}^{m_0, \alpha_0, a_0} = S_{point}^{m_0, \alpha_0, a_0} \sum_{i=0}^N \sigma^i H^i, \quad (3.40)$$

$$H(n, m) = \sum_{j=1}^3 (U_j(n, n_t) \delta(n + \hat{j}, m) + U_j(n - \hat{j}, n_t)^\dagger \delta(n - \hat{j}, m)). \quad (3.41)$$

Here H is spatial part of the hopping matrix in Eq. (2.82) (fixed time at n_t), N is the number of smearing steps and σ is the dimensionless parameter tuned to reproduce a hadron's average root mean square radius. It is obvious that the $\sum_{i=0}^N \sigma^i H^i$ part in smeared source definition is expansion of an exponential.

3.2.1.1 Wall Smearing

Wall smearing corresponds to setting, $\sigma = 0$, in Eq. (3.40), which means assigning a Dirac delta function to all spatial lattice sites,

$$S_{wall}^{m_0, \alpha_0, a_0} = \delta(m - m_0). \quad (3.42)$$

This method comes with large statistical errors. An advantage of wall smearing method can be seen from a three-point function perspective. Fast-forwarding, in Eq. (3.81), before doing the propagator inversion, summation over the spatial sites at the sink point, x_2 , is made. Instead of the hadron state, the propagator gets projected on to a definite momentum. The advantage of the wall smearing is computing the shell (Gaussian smeared) and wall propagators and then contracting these in order to obtain the three-point correlator, avoiding any sequential inversions [83].

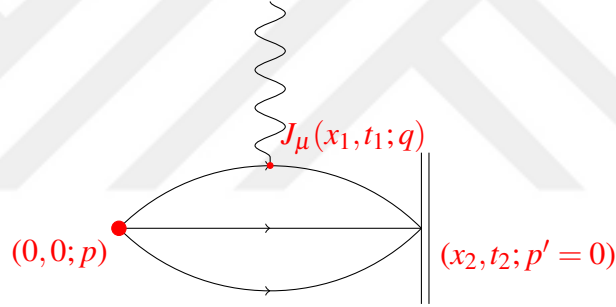


Figure 3.2 Illustration of wall smeared three-point function. J_μ is the inserted current, x_1 and t_1 is spatial and temporal points respectively.

The Fig. (3.2) illustrates the wall smearing method. The propagators without the current insertion are shell source-wall sink smeared propagators. Propagator that the external current is inserted is the combination of shell source $S_{smear}(0, 0)$, point sink $S_{point}(x_1, t_1)$ propagator, and point source $S_{point}(x_1, t_1)$, wall sink $S_{wall}(x_2, t_2)$ propagator. The momentum is carried by the $D^{-1}(x_1, t_1 | 0, 0)$ shell-wall propagator.

3.2.2 CHROMA Software

In order to tackle the immense LQCD calculations introduced in the previous chapter, several LQCD software packages developed such as fermiQCD [84], Colombia Physics System (CPS) [85], MILC [86] and CHROMA [1]. We performed our computations

using a modified version of CHROMA software system [1] on CPU clusters and with QUDA [2, 3] for propagator inversion on GPUs.

The CHROMA software is a collection of LQCD applications that supports parallel programming constructs for LQCD. Program uses SciDAC, QDP++, QMP programs which are written in C++. It contains rich library for gauge actions, fermion actions, gauge observables, and quark sources.

With the recent advances in technology, using the GPUs in graphics card have become very efficient method in numerical calculations. The USQCD Collaboration also have worked on this area and developed a subroutine for CHROMA called QUDA [3], which uses NVIDIA's CUDA platform. In this work, the propagators are calculated using QUDA and the correlation functions are calculated by conventional CPUs.

3.3 Baryon Spectroscopy and Form Factors

In LQCD, calculating baryon masses from two-point correlation functions is a straightforward procedure. First, quark propagators are numerically calculated. Then, the two-point correlator is calculated as in Eq.(3.6). Following these steps, the two-point function is numerically estimated and the mass is extracted in a way that is explained below. Derivation of form factors follows that discussion.

3.3.1 Effective Mass

Operator in quantum mechanics in the Heisenberg picture is defined as

$$\hat{O}(t) = e^{it\hat{H}/\hbar}\hat{O}e^{-it\hat{H}/\hbar}, \quad (3.43)$$

in Minkowski metric. To work in Euclidean metric, Wick rotation, $t \rightarrow it$, is applied.

With this transformation operator in Euclidean metric becomes

$$\hat{O}(t) = e^{-t\hat{H}}\hat{O}e^{t\hat{H}}. \quad (3.44)$$

A two-point correlator in the Euclidean metric is defined as

$$\langle O_2(t)|O_1(0)\rangle_T = \frac{\text{tr}\left[e^{-(T-t)\hat{H}} \hat{O}_2 e^{-t\hat{H}} \hat{O}_1\right]}{\text{tr}\left[e^{-T\hat{H}}\right]}. \quad (3.45)$$

The denominator is the partition function of the system, t is the actual time, T is the maximal distance of time taken to infinity, \hat{H} is the Hamiltonian of the system and the exponential terms in the numerator are time evolution operators. When the trace operator is written in basis form, the partition function becomes

$$\text{tr}[e^{-TH}] = \langle n|e^{-T\hat{H}}|n\rangle = \sum_n e^{-TE_n}, \quad (3.46)$$

and via the same procedure, the numerator becomes

$$\begin{aligned} \text{tr}[e^{-(T-t)\hat{H}} \hat{O}_2 e^{-t\hat{H}} \hat{O}_1] &= \sum_m \langle m|e^{-(T-t)\hat{H}} \hat{O}_2 e^{-t\hat{H}} \hat{O}_1|m\rangle, \\ &= \sum_{n,m} \langle m|e^{-(T-t)\hat{H}} \hat{O}_2 |n\rangle \langle n| e^{-t\hat{H}} \hat{O}_1|m\rangle, \\ &= \sum_{n,m} e^{-(T-t)E_m} \langle m|\hat{O}_2|n\rangle e^{-tE_n} \langle n|\hat{O}_1|m\rangle. \end{aligned} \quad (3.47)$$

On the second step the unit operator is inserted as a complete set of states $\sum_n |n\rangle \langle n| = \mathbb{1}$ and on the last step the eigenvalues of the time evolution operators are used. Combining Eq. (3.46) and Eq. (3.47), factoring out the energy of the ground state, the spectral decomposition of the two-point correlation function is written as

$$\langle O_2(t)|O_1(0)\rangle_T = \frac{\sum_{n,m} \left(\langle m|\hat{O}_2|n\rangle \langle n|\hat{O}_1|m\rangle e^{-(T-t)\Delta E_m} e^{-t\Delta E_n} \right) e^{-TE_0}}{(1 + e^{-T\Delta E_1} + e^{-T\Delta E_2} + \dots) e^{-TE_0}}, \quad (3.48)$$

where, $\delta E_{m,n} = E_{m,n} - E_0$ is the energy difference between the ground state and the m^{th} (n^{th}) excited state. In the limit $T \rightarrow \infty$, excited states do not contribute so that only the ground state remains. There is no contribution from $e^{-(T-t)\Delta E_m} \xrightarrow{T \rightarrow \infty} 0$ term also so that Eq. (3.47) reduces to,

$$\lim_{T \rightarrow \infty} \langle O_2(t)|O_1(0)\rangle_T = \sum_n \langle 0|\hat{O}_2|n\rangle \langle n|\hat{O}_1|0\rangle e^{-t\Delta E_n}. \quad (3.49)$$

The effective masses are computed using two-point correlation function in Eq. (3.49). It is obvious that the two-point correlation functions are the sum of eigenstates of the baryon. The correlation function at zero momentum is written as

$$\langle O(0, n_t) | \bar{O}(0, 0) \rangle = \sum_n \langle 0 | \hat{O} | n \rangle \langle n | \hat{O} | 0 \rangle e^{-n_t E_n}. \quad (3.50)$$

If the operator couples to more than one mass eigenstates (i.e. excited states of particle). The two-point correlator can be written as sum of exponentials

$$C(n_t) = A_0 e^{-n_t E_0} + A_1 e^{-n_t E_1} + A_2 e^{-n_t E_2} \dots \quad (3.51)$$

In the limit of $n_t \rightarrow \infty$, the excited states decay and only the ground state remains. The effective mass of the ground state can be written as

$$m_{eff}(n_t + 1/2) = \ln \frac{C(n_t)}{C(n_t + 1)}. \quad (3.52)$$

The leading term of the Eq. (3.51) gives $E_0 = m_{eff}$.

The propagation of n_t and $N_t - n_t$ differ with a minus sign. Correlator function of ground state can be written as hyperbolic trigonometric functions as well;

$$A_0 e^{-n_t E_0} \pm A_0 e^{-(N_t - n_t) E_0} = \begin{cases} 2A_0 e^{-N_t E_0/2} \cosh((N_t/2 - n_t) E_0) \\ 2A_0 e^{-N_t E_0/2} \sinh((N_t/2 - n_t) E_0). \end{cases} \quad (3.53)$$

However this is a assumption of a special case. Specifically after the parity projection, the interpolator projects to definite parity. The baryon propagates in n_t , and in $N_t - n_t$ negative parity partner of baryon projected. If there is mass difference between the hadrons of opposite parities, propagator is not symmetric. Hence besides trigonometric functions, the exponential form of propagator must be used for fitting the function.

3.3.2 Form Factors

High energetic electron beams have been used to understand the structure inside the baryon. The high energetic electrons scatter with the baryon nucleus, while creating the interaction inside the baryon with (virtual) photon exchange. The wavelength of photon

becomes smaller than the size of the nucleus (See Fig 3.3). The dynamics inside the nucleus can be probed at this energy scale. [87]. This interaction is called as *Deep Inelastic Scattering* [88]. Using the information obtained from experiments the observables such as the spatial charge distribution, spins, magnetic moments, decay constants can be obtained.

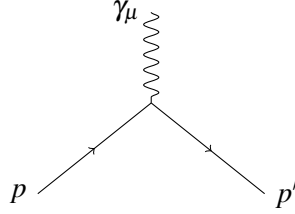


Figure 3.3 Illustration of vertex function at tree level.

The hadron structure is examined theoretically by using the matrix elements, basically written as, $\langle B | J_\mu | B \rangle$ where J_μ is the current. The vector current leads to electromagnetic form factors; and the axial vector current leads to weak form factors. To begin with consider an electron elastically interacting with photon. The electron vertex function at tree level is defined as

$$iM_0^\mu = -ie\bar{u}(p')\gamma^\mu u(p), \quad (3.54)$$

where u it is spinor of electron. The photon momentum is $q^\mu = p'^\mu - p^\mu$. The vertex function can be written using sigma tensor and Gordon identity as

$$-ie\bar{u}(p')\gamma^\mu u(p) = -ie\bar{u}(p') \left[\frac{(p' + p)^\mu}{2m} \right] u(p) - \frac{ie}{2m} [\sigma^{\mu\nu} (q^\nu)] u(p), \quad (3.55)$$

where the first term in right hand side of the equation is like scalar QED interaction. The second term is spin-dependent part and gives the anomalous magnetic moment. Loops at all order contribute the vertex function like in Fig. (3.4). The calculation of vertex function can be found in Appendix E.1.

The vertex function in Fig. (3.4) is formulated as

$$-ie\bar{u}(p')\Gamma^\mu u(p) = -ie\bar{u}(p')[-ie\gamma^\mu + ie\Gamma_\mu^2 + \dots]u(p). \quad (3.56)$$

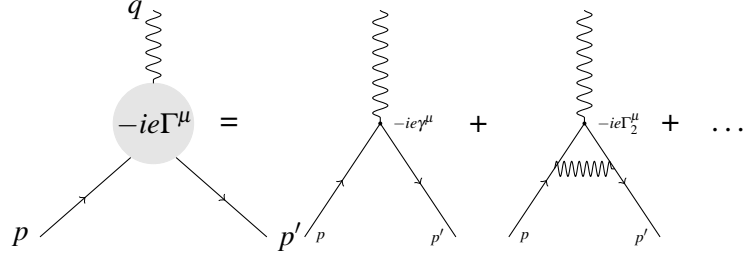


Figure 3.4 Illustration of vertex function as sum of all contributions.

The Eq. (3.56) can be parametrized for general and any-loop order [89],

$$-ie\bar{u}(p')\Gamma^\mu u(p) = \bar{u}(p')(f_1\gamma^\mu + f_2q^\mu + f_3p'^\mu + f_4p^\mu)u(p), \quad (3.57)$$

where f_i are constants. From the conservation of momentum $q^\mu = p'^\mu - p^\mu$, f_2 is found as 0. Using the Ward identity,

$$0 = q_\mu\bar{u}(p')(f_1\gamma^\mu + f_3p'^\mu + f_4p^\mu)u(p), \quad (3.58)$$

$$0 = f_1\bar{u}(p')\not{q}u(p) + (q \cdot p')f_3\bar{u}(p')u(p) + (q \cdot p)f_4\bar{u}(p')u(p),$$

f_1 part can be re-written from Gordon identity in Eq. (E.3). Using the relation $q \cdot p' = p' \cdot p - m^2 = -q \cdot p$, it is seen that $f_3 = f_4$. Therefore the vertex function can be written as,

$$iM^\mu = (-ie)\bar{u}(p') \left[F_1(q^2)\gamma^\mu + i\frac{\sigma^{\mu\nu}q_\nu}{2m}F_2(q^2) \right] u(p). \quad (3.59)$$

This parametrization contains all orders and $F_1(q^2)$ and $F_2(q^2)$ are called as form factors. At the tree level $F_1 = 1$ and $F_2 = 0$; while one must take into account higher loop contributions. $F_1(q^2)$ part gives the renormalized electric charge, the $F_2(q^2)$ part gives the magnetic moment.

In deep inelastic scattering baryon breaks up into its constituent quarks at high momentum transfer. The hadronic part describes the inelastic interaction of baryon in terms of structure functions W_1 and W_2 . The simplest inelastic cross section to measure is the inclusive cross section, for which only the final electron is observed. Summing all of the hadronic final states gives the cross section [77]. The process is visualized in Fig. (3.5). The leptonic part of the interaction can be written in terms of incoming and outgoing

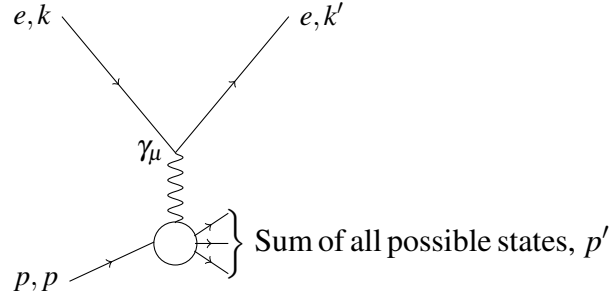


Figure 3.5 Electron proton scattering, a virtual photon exchange approximation, k is momentum of incoming electron, k' is momentum of outgoing electron.

momenta and metric tensor,

$$L_{\mu\nu} = 2[k'_\mu k_\nu + k'_\nu k_\mu + (q^2/2)g_{\mu\nu}]. \quad (3.60)$$

Hadronic part of the interaction can be written as a sum over all spin states and all possible hadronic states,

$$W^{\mu\nu} = \frac{1}{4\pi M} \frac{1}{2} \sum_s \sum_X \langle p : p, s | j^\mu(0) | X; p' \rangle \langle X; p' | j^\nu(0) | p : p, s \rangle \times (2\pi)^4 \delta^4(p + q - p'), \quad (3.61)$$

$$W^{\mu\nu} = (-g^{\mu\nu} + \frac{q^\mu q^\nu}{q^2}) W_1(Q^2, \nu) + [p^\mu - (p \cdot \frac{q}{q^2}) q^\mu][p^\nu - (p \cdot \frac{q}{q^2}) q^\nu] M^{-2} W_2(Q^2, \nu). \quad (3.62)$$

The cross section is obtained by contracting the leptonic and hadronic vertices given in Eq. (3.60) and Eq. (3.61) respectively,

$$d\sigma \approx L_{\mu\nu} W^{\mu\nu}(q, p). \quad (3.63)$$

This interaction can be parametrized as $F_1(x)$ and $F_2(x)$ for spin 1/2 particles. Note that these are not the same as $F_1(q^2)$ and $F_2(q^2)$ in elastic scattering!

$$F_1(x) \rightarrow m_b W_1(\nu, Q^2), \quad (3.64)$$

$$F_2(x) \rightarrow \nu W_2(\nu, Q^2), \quad (3.65)$$

where Q^2 is four momentum transfer ν is inelasticity and x is fraction of the baryon energy

$x = \frac{Q^2}{2m_b v}$. In this work, we calculate elastic interactions.

Considering the elastic case, both electric and magnetic part contribute to cross section. There is a different convention, $F_1(q^2)$ and $F_2(q^2)$ can be written in terms of Sachs [90] form factors $G_E(q^2)$ and $G_M(q^2)$. G_E and G_M give directly the Rosenbluth formula for the cross section;

$$\left(\frac{d\sigma}{d\Omega}\right)_{lab} = \left(\frac{d\sigma}{d\Omega}\right)_{point} \left[\frac{G_E^2(q^2) + G_M^2(q^2)}{1 + \xi} + 2\xi G_M^2(q^2) \tan^2 \frac{\theta}{2} \right], \quad (3.66)$$

where ξ is defined as

$$\xi = \left(\frac{q}{2m}\right)^2. \quad (3.67)$$

The Sachs form factors can be written in terms of Dirac ($F_1(q^2)$) and Pauli ($F_2(q^2)$) form factors as

$$\begin{aligned} G_E(q^2) &= F_1(q^2) - \xi F_2(q^2), \\ G_M(q^2) &= F_1(q^2) + F_2(q^2). \end{aligned} \quad (3.68)$$

The Sachs form factors give following observables at zero momentum,

$$G_E(0) \Rightarrow \text{Charge}, \quad (3.69)$$

$$G_M(0) \Rightarrow \text{Magnetic Dipole Moment}.$$

The primary difference between these form factors is that $F_1(q^2)$ and $F_2(q^2)$ are categorized according to the helicity. $F_1(q^2)$ represents helicity-preserving part and $F_2(q^2)$ represents helicity-flipping part of the scattering [87]. It is also essential to examine the asymptotic form of form factors. Experiments reveal that in the limit of large momentum transfer, proton form factors and the magnetic form factor of a neutron are identical to each other except for a scale factor, which is defined as magnetic moment (μ_B),

$$G_E^p(q^2) = \frac{G_M^p}{\mu_p} = \frac{G_M^n}{\mu_n} = G(q^2). \quad (3.70)$$

The function can be generalized as dipole form

$$G(q^2) = \frac{G_{E,M}(0)}{\left(1 + \left(\frac{Q}{\lambda_{E,M}}\right)^2\right)^2}, \quad (3.71)$$

where the parameter λ is an empirical value that comes from the fit results. Using the dipole form, charge radius of the baryon can be found [87],

$$\langle r^2 \rangle = \frac{\int_0^\infty r^4 \rho_0 e^{-\lambda r} dr}{\int_0^\infty \rho_0 e^{-\lambda r} r^2 dr} = \frac{12}{\lambda}. \quad (3.72)$$

where ρ is spatial charge distribution. We note that the high momentum cross section is dominated by $G_M(q^2)$, which can be easily seen by inspecting Eq. (3.66).

For spin $\frac{1}{2} \gamma \rightarrow \frac{3}{2}$ transitions, there are three transition form factors, namely, the magnetic dipole ($M1$), the electric quadrupole ($E2$) and the electric charge quadrupole ($C2$). Spin $\frac{3}{2}$ particles are represented by Rarita-Schwinger Lagrangian [80] and for this representation every spinor gains an extra index. The matrix element is written as

$$\langle \chi^*(p', s') | J_\mu | \chi(p, s) \rangle = i\sqrt{2/3} \left(\frac{m_* m}{E_*(p') E(p)} \right) \bar{u}_\tau(p', s') \mathcal{O}^{\tau\mu} u(p, s), \quad (3.73)$$

where the vertex tensor $\mathcal{O}^{\tau\mu}$ is written in terms of Sachs form factors [91],

$$\mathcal{O}^{\tau\mu} = G_{M1}(q^2) K_{M1}^{\tau\mu} + G_{E2}(q^2) K_{E2}^{\tau\mu} + G_{C2}(q^2) K_{C2}^{\tau\mu}. \quad (3.74)$$

where

$$K_{M1}^{\tau\mu} = -\frac{3}{(m_* + m)^2 + q^2} \frac{(m_* + m)}{2m} i \varepsilon^{\tau\mu\alpha\beta} P_\alpha q_\beta, \quad (3.75)$$

$$K_{E2}^{\tau\mu} = -K_{M1}^{\tau\mu} + 6\Omega^{-1}(q^2) \frac{(m_* + m)}{2m} i \gamma_5 \varepsilon^{\tau\lambda\alpha\beta} P_\alpha q_\beta \varepsilon^{\mu\lambda\gamma\delta} (2P_\gamma + q_\gamma) q_\delta, \quad (3.76)$$

$$K_{C2}^{\tau\mu} = -6\Omega^{-1}(q^2) \frac{(m_* + m)}{2m} i \gamma_5 q_\tau (q^2 P_\mu - q \cdot P q_\mu). \quad (3.77)$$

3.3.2.1 Form Factors in Lattice QCD

In LQCD the three-point correlators are written as

$$\langle F^{NJ_\mu N}(t_2, t_1; p', p; \Gamma) \rangle = \sum_{x_1, x_2} e^{-i\vec{p}'x_2} e^{i(\vec{p}' - \vec{p})x_1} \Gamma^{\beta\alpha} \langle \Omega | T(\chi^\alpha(x_2) J_\mu(x_1) \bar{\chi}^\beta(0)) | \Omega \rangle. \quad (3.78)$$

Here t_2 is the sink time, t_1 is the current insertion time, x_2 is the sink point, x_1 is the current insertion point, p' is the final momentum of the baryon, p is the initial momentum of the baryon, α and β are Dirac indices. The matrix element is defined like continuum,

$$\langle \chi(p', s') | J_\mu | \chi(p, s) \rangle = \bar{u}(p') \left[F_1(q^2) \gamma_\mu + i \frac{\sigma_{\mu\nu} q^\nu}{2m} F_2(q^2) \right] u(p). \quad (3.79)$$

The three point correlator is visualized in Fig. (3.6).

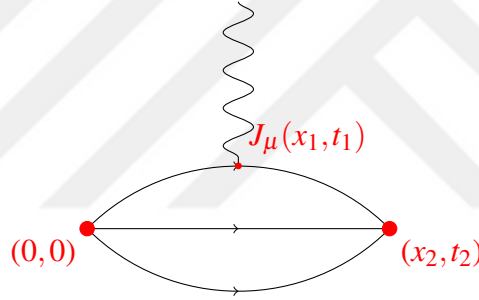


Figure 3.6 Illustration of three-point function. J_μ is the inserted current, x_1 and t_1 is spatial and temporal points respectively.

χ denotes the interpolating fields, similarly to two-point function. However the inserted current J_μ changes the propagators as $D^{-1(f)} = q_f \tilde{D}^{-1(f)}$, where q_f is the charge of the quark propagator [92]. To illustrate the current insertion, consider the proton interpolating field,

$$\begin{aligned} \langle \chi(p', s') | J_\mu | \chi(p, s) \rangle &= \sum_{x_2} e^{-i\vec{p}'x_2} \varepsilon_{abc} \varepsilon_{a'b'c'} (\text{tr}[q_u \tilde{D}_{c'c}^{-1(u)}] \text{tr}[D_{b'b}^{-1(d)} D_{a'a}^{-1(u)}] \\ &+ \text{tr}[D_{c'c}^{-1(u)}] \text{tr}[q_d \tilde{D}_{b'b}^{-1(d)} D_{a'a}^{-1(u)}] + \text{tr}[D_{c'c}^{-1(u)}] \text{tr}[D_{b'b}^{-1(d)} q_u \tilde{D}_{a'a}^{-1(u)}] \\ &+ \text{tr}[q_u \tilde{D}_{a'c}^{-1(u)} D_{b'b}^{-1(d)} D_{c'a}^{-1(u)}] + \text{tr}[D_{a'c}^{-1(u)} q_d \tilde{D}_{b'b}^{-1(d)} D_{c'a}^{-1(u)}] \\ &+ \text{tr}[D_{a'c}^{-1(u)} D_{b'b}^{-1(d)} q_u \tilde{D}_{c'a}^{-1(u)}]). \end{aligned} \quad (3.80)$$

The quark propagator coupled with electromagnetic current is written as [92]

$$\begin{aligned} \tilde{D}^{-1}(x_2, 0; t_1, q, \mu) \equiv & \kappa \sum_{x_1} e^{i(\vec{p}' - \vec{p})x_1} \left[D^{-1}(x_2, x_1 + a_\mu)(1 + \gamma_\mu)U_\mu^\dagger(x_1)D^{-1}(x_1, 0) \right. \\ & \left. - D^{-1}(x_2, x_1)(1 - \gamma_\mu)U_\mu D^{-1}(x_1 + a_\mu, 0) \right]. \end{aligned} \quad (3.81)$$

The current insertion procedure is illustrated in Fig. (3.7).

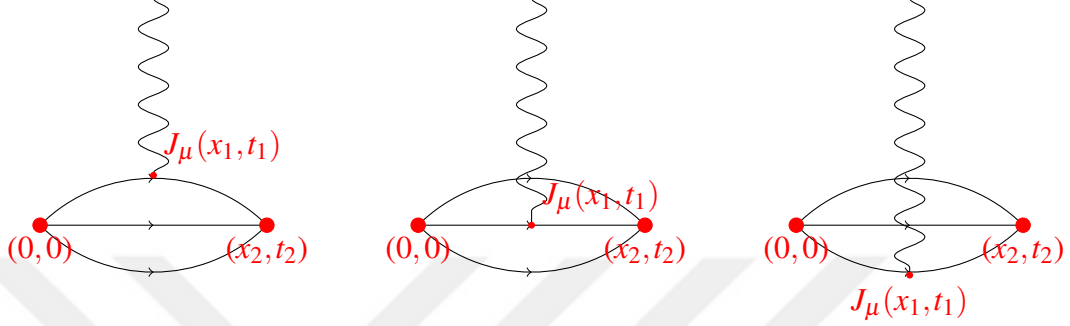


Figure 3.7 Illustration of current insertion to the propagators one by one.

The coefficients in matrix elements are crucial for calculating the ratio and finding the form factors of the transition. The two-point correlator can be written as

$$\begin{aligned} \langle F^{NJ_\mu N}(t_2, t_1; p', p; \Gamma) \rangle = & \sum_{x_1, x_2} e^{-i\vec{p}'x_2} e^{i(\vec{p}' - \vec{p})x_1} \Gamma^{\beta\alpha} \\ & \langle \Omega | T(\chi^\alpha(x_2) J_\mu(x_1) \bar{\chi}^\beta(0)) | \Omega \rangle. \end{aligned} \quad (3.82)$$

Inserting complete set of states both sides of $J_\mu(x_1)$ the three-point function becomes

$$\begin{aligned} \langle F^{NJ_\mu N}(t_2, t_1; p', p; \Gamma) \rangle = & \sum_{x_1, x_2} \sum_{m, n, s, s', k, k'} e^{-i\vec{p}'x_2} e^{i(\vec{p}' - \vec{p})x_1} \Gamma^{\beta\alpha} \langle \Omega | \chi^\alpha(x_2) | n(\vec{k}', s') \rangle \\ & \langle n(\vec{k}', s') | J_\mu(x_1) | m(\vec{k}, s) \rangle \langle m(\vec{k}, s) | \bar{\chi}^\beta(0) | \Omega \rangle. \end{aligned} \quad (3.83)$$

The calculation is similar to two-point function, the only difference is all operators must be written in terms of x_1

$$\begin{aligned} \langle F^{NJ_\mu N}(t_2, t_1; p', p; \Gamma) \rangle = & \sum_{x_1, x_2} \sum_{m, n, s, s', k, k'} e^{-i\vec{p}'x_2} e^{i(\vec{p}' - \vec{p})x_1} \Gamma^{\beta\alpha} \langle \Omega | \chi^\alpha(x_1) e^{ik'(x_2 - x_1)} | n(\vec{k}', s') \rangle \\ & \langle n(\vec{k}', s') | J_\mu(x_1) | m(\vec{k}, s) \rangle \langle m(\vec{k}, s) | e^{ik(x_1)} \bar{\chi}^\beta(x_1) | \Omega \rangle. \end{aligned} \quad (3.84)$$

After separating the temporal and spatial parts, the three point function reduces to

$$\begin{aligned} \langle F^{NJ_\mu N}(t_2, t_1; p', p; \Gamma) \rangle &= \sum_{x_1, x_2} \sum_{m, n, s, s', k, k'} e^{-i\vec{p}'x_2} e^{i(\vec{p}'-\vec{p})x_1} e^{i\vec{k}'(x_2-x_1)} e^{i\vec{k}(x_1)} \Gamma^{\beta\alpha} \\ &\langle \Omega | \chi^\alpha(x_1) | n(\vec{k}', s') \rangle e^{-E_{k'}(t_2-t_1)} \langle n(\vec{k}', s') | J_\mu(x_1) | m(\vec{k}, s) \rangle e^{-E_k(t_1)} \\ &\langle m(\vec{k}, s) | \bar{\chi}^\beta(x_1) | \Omega \rangle, \end{aligned} \quad (3.85)$$

$$\begin{aligned} &= \sum_{x_1, x_2} \sum_{m, n, s, s', k, k'} e^{-i(\vec{p}'-\vec{k}')x_2} e^{i(\vec{p}'-\vec{k}')x_1} e^{-i(\vec{p}-\vec{k})x_1} \Gamma^{\beta\alpha} \langle \Omega | \chi^\alpha(x_1) | n(\vec{k}', s') \rangle \\ &\langle n(\vec{k}', s') | J_\mu(x_1) | m(\vec{k}, s) \rangle \langle m(\vec{k}, s) | \bar{\chi}^\beta(x_1) | \Omega \rangle e^{-E_{k'}(t_2-t_1)} e^{-E_k(t_1)}. \end{aligned} \quad (3.86)$$

Using the definition of Dirac delta, $\sum_{x_2} e^{-i(\vec{p}'-\vec{k}')x_2} = \delta_{\vec{p}', \vec{k}'}^{(3)}$, the equation becomes

$$\begin{aligned} \langle F^{NJ_\mu N}(t_2, t_1; p', p; \Gamma) \rangle &= \sum_{m, n, s, s'} \delta_{\vec{p}', \vec{k}'}^{(3)} \delta_{\vec{p}, \vec{k}}^{(3)} \Gamma^{\beta\alpha} \langle \Omega | \chi^\alpha(x_1) | n(\vec{k}', s') \rangle \\ &\langle n(\vec{k}', s') | J_\mu(x_1) | m(\vec{k}, s) \rangle \langle m(\vec{k}, s) | \bar{\chi}^\beta(x_1) | \Omega \rangle e^{-E_{k'}(t_2-t_1)} e^{-E_k(t_1)}. \end{aligned} \quad (3.87)$$

We finally obtain the following three-point function

$$\begin{aligned} \langle F^{NJ_\mu N}(t_2, t_1; p', p; \Gamma) \rangle &= \sum_{m, n, s, s'} \frac{m_m m_n}{E_m(\vec{p}') E_n(\vec{p})} e^{-E_{p'}(t_2-t_1)} e^{-E_p(t_1)} \Gamma^{\beta\alpha} \\ &\langle \Omega | \chi^\alpha(x_1) | n(\vec{p}', s') \rangle \langle n(\vec{p}', s') | J_\mu(x_1) | m(\vec{p}, s) \rangle \langle m(\vec{p}, s) | \bar{\chi}^\beta(x_1) | \Omega \rangle. \end{aligned} \quad (3.88)$$

Spin $\frac{1}{2} \rightarrow \frac{3}{2}$ ($N \rightarrow \Delta$) transition is similar to the spin $\frac{1}{2} \rightarrow \frac{1}{2}$ three-point correlators, apart from some notational differences

$$\langle F^{NJ_\mu \Delta}(t_2, t_1; p', p; \Gamma) \rangle = \sum_{x_1, x_2} e^{-i\vec{p}'x_2} e^{i(\vec{p}'-\vec{p})x_1} \Gamma^{\beta\alpha} \langle \Omega | T(\chi_\Delta^\alpha(x_2) J_\mu(x_1) \bar{\chi}_N^\beta(0)) | \Omega \rangle. \quad (3.89)$$

Two identity operators can be put between $\chi_\Delta^\alpha(x_2)$ and $\bar{\chi}_N^\beta(0)$,

$$\begin{aligned} \langle F^{NJ_\mu \Delta}(t_2, t_1; p', p; \Gamma) \rangle &= \sum_{x_1, x_2} \sum_{\Delta, N, s', s} e^{-i\vec{p}'x_2} e^{i(\vec{p}'-\vec{p})x_1} \Gamma^{\beta\alpha} \langle \Omega | \chi_\Delta^\alpha(x_2) | \Delta(\vec{p}', s') \rangle \\ &\frac{m_\Delta}{E_\Delta(\vec{p}')} \langle \Delta(\vec{p}', s') | J_\mu(x_1) | N(\vec{p}, s) \rangle \frac{m_N}{E_N(\vec{p})} \langle N(\vec{p}, s) | \bar{\chi}_N^\beta(0) | \Omega \rangle. \end{aligned} \quad (3.90)$$

Following similar procedure as in $\frac{1}{2}$ calculation, the three-point function becomes

$$\langle F^{NJ\mu\Delta}(t_2, t_1; p', p; \Gamma) \rangle = \sum_{s, s'} \frac{m_\Delta m_N}{E_\Delta(\vec{p}') E_N(\vec{p})} e^{-E_\Delta(\vec{p}')(t_2 - t_1)} e^{-E_N(\vec{p})(t_1)} \Gamma^\beta \alpha_{u\sigma}(\vec{p}', s') \langle \Delta(\vec{p}', s') | J_\mu(x_1) | N(\vec{p}, s) \rangle \bar{u}(\vec{p}, s). \quad (3.91)$$

We construct proper ratios using two- and three-point functions so as to eliminate time dependent exponential terms. This will be explained in detail in following chapters.

3.3.3 Baryons in Lattice QCD

The mass spectrum of light baryons has been the focus of LQCD Collaborations. The detailed research has been made over the last several years [93]. The baryon spectrum obtained by numerical calculations has been compared to experimental results. Theoretical results obtained for the light baryon spectroscopy will shed light on our understanding of strong interaction.

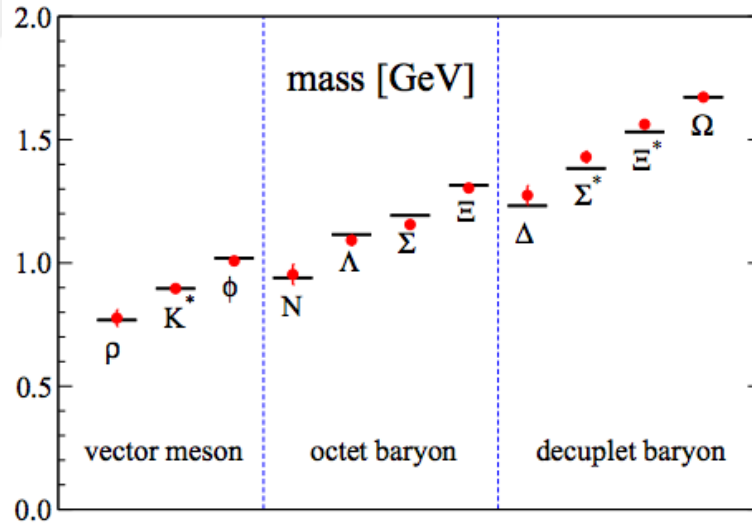


Figure 3.8 Light hadron spectrum extrapolated to the physical point (red circles) calculated by PACS-CS Collaboration [93] in comparison with the experimental values (black bars).

A comparison has been made of LQCD results with the experimental values in Fig. (3.8). For light baryons there is remarkable agreement. Furthermore several LQCD collaborations are running simulations such as magnetic moment, form factors, lifetimes.

Baryons can be grouped according to their flavors and spins $SU(3)_f$ group generated with u , d and s quarks. Spin $\frac{1}{2}$ states form an octet $8 \oplus 1$ which is shown in Fig. (3.9). While spin $\frac{3}{2}$ states form a decuplet (see Fig (3.10)).

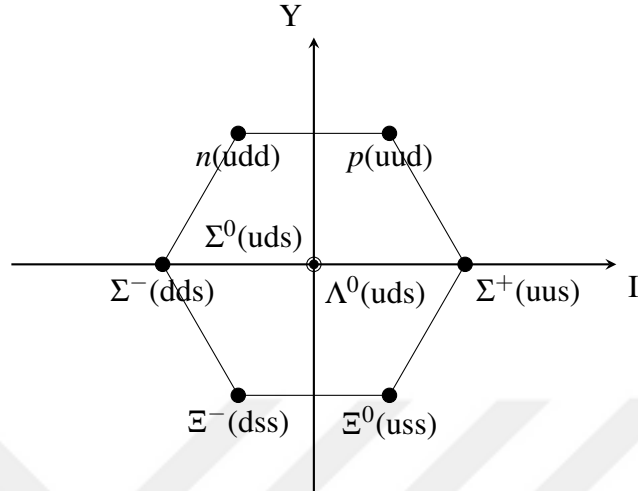


Figure 3.9 Octet baryons.

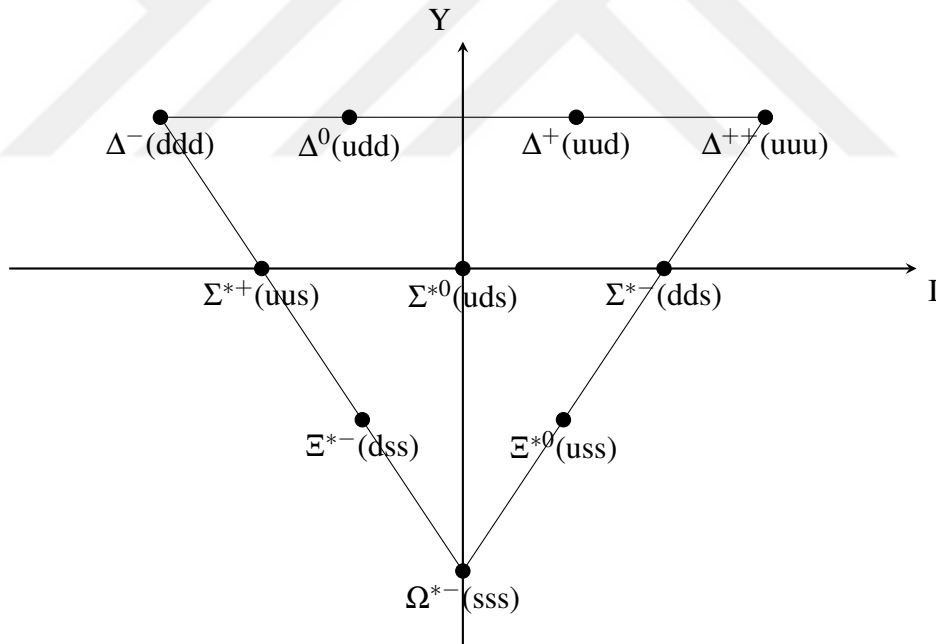


Figure 3.10 Decuplet baryons.

3.3.3.1 Charmed Baryons

The charmed baryon spectroscopy is an excellent laboratory to understand the dynamics of heavy quarks, heavy quark symmetry and chiral symmetry. In the past years many charmed baryon states were discovered by BaBar [94], BELLE [94], CLEO [95] and

LHCb [96] Collaborations. This will have interesting implications for the low-energy dynamics of heavy baryons interacting with the Goldstone bosons [97]. Eighteen of the charmed baryons have been observed so far and four of them have not been confirmed yet.

The first observed baryon that consists of charm quark was the Λ_c^+ (udc) in 1975 [98]. Mass of Λ_c^+ was measured as 2286.46(14) MeV by BABAR experiment [99]. The Λ_c^+ has been produced and studied in different experiments, like fixed-target experiments such as FOCUS [100] and SELEX [101] and $e^-e^+ \rightarrow B$ experiments such as ARGUS [102], CLEO [103], BABAR [104], and BELLE [105].

Σ_c particles have the same quark content as Λ_c , but its flavor wave function is different. Moreover, Σ_c particles have isospin 1 which means that there are three Σ_c charged states. The first observed Σ_c is the doubly charged one [106]. In 1987 to 1989, various experiments such as E-400 [107], ARGUS [102] and CLEO [103] tried to confirm Σ_c with much larger statistics and found clear evidence for both the doubly charged and neutral states. The singly-charged state was difficult to detect because the resolution of the detector needed to be very good. The singly charged Σ_c was observed by CLEO in 1993 [108].

Ξ_c^+ has $c[su]$ quark combination and the Ξ_c^0 has $c[sd]$ quark combination. The first observed Ξ_c was charged particle in 1983 by WA62 [24]. Ξ_c^+ was later confirmed by six other experiments including CLEO [109], ARGUS [110], BELLE and CDF [95]. The average mass of Ξ_c^+ reported by PDG is 2467.9(4) MeV. The neutral state of Ξ_c baryon was first observed by CLEO [95] in 1988. The average mass reported by PDG is $m_{\Xi_c^0} = 2470.99_{-0.50}^{+0.30}$ MeV [17]. The two other baryons with the same quark content and quantum numbers, $J^P = \frac{1}{2}^+$, are $\Xi_c^{\prime 0}$ ($c\{sd\}$) and $\Xi_c^{\prime +}$ ($c\{su\}$), which are located on the second layer of the sextet SU(4) multiplet. They were first observed by CLEO Collaboration [27] and confirmed recently by BABAR [28] and BELLE experiments [29]. The average mass reported by PDG is $m_{\Xi_c^{\prime 0}} = 2577.9(2.9)$ MeV [17].

The Ω_c^0 baryon observed in 1984 by CERN SPS hyperon beam experiment [111], is

composed of two strange and one charm quark (ssc). Later CLEO, ARGUS [112], E-687 [113] and BELLE [114] experiments measured the Ω_c^0 mass the average value reported by PDG is $m_{\Omega_c^0} = 2695.2^{+1.8}_{-1.6}$ MeV. The excited Ω_c^* (css) baryon was first observed by BABAR [19]. It was later confirmed by BELLE experiment [18]. The average mass value is $m_{\Omega_c^*} = 2765.9(2.0)$ MeV [17]. All eighteen of charmed baryons with their decay channels are listed in Fig. (3.11).

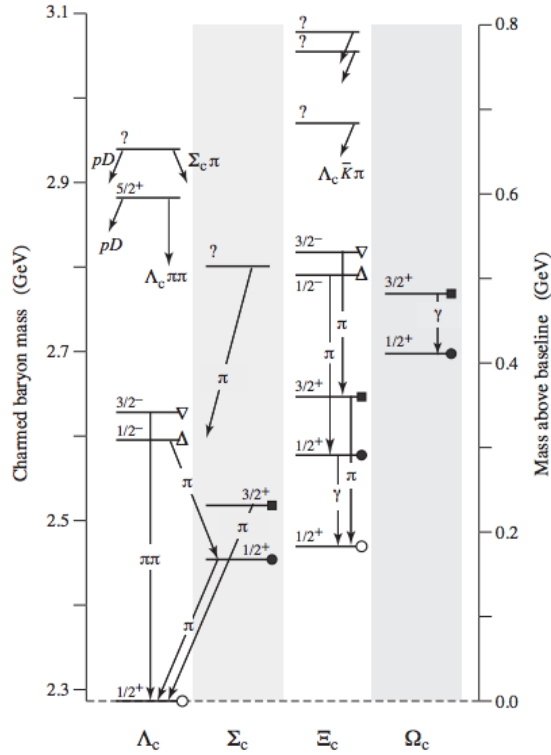


Figure 3.11 Experimentally observed charmed baryons and their decay channels [17].

There is intensive effort from LQCD collaborations to determine the spectrum of charmed baryons. To this end a comparison was made with LQCD results in Fig. (3.12).

Similar to the light baryons the charmed baryons can be grouped according to their flavors and spins. The charmed baryon multiplets are called as SU(4) multiplets. The $20'$ -plet bottom layer is an SU(3) octet having spin- $\frac{1}{2}$ baryons in the multiplet Fig. (3.13a), the $\bar{4}$ is an inverted tetrahedron, also having spin- $\frac{1}{2}$ baryons (Λ_c^0 at the bottom) Fig. (3.13b) but different spin/flavor wave functions. The 20-plet bottom layer is an SU(3) decuplet, having spin- $\frac{3}{2}$ baryons in Fig. (3.14).

In the charmed baryon sector only three electromagnetic transitions of singly charmed

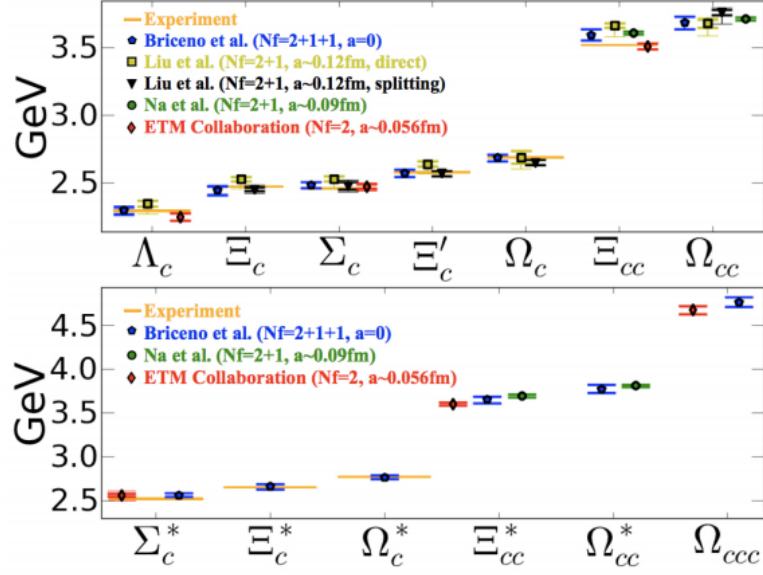
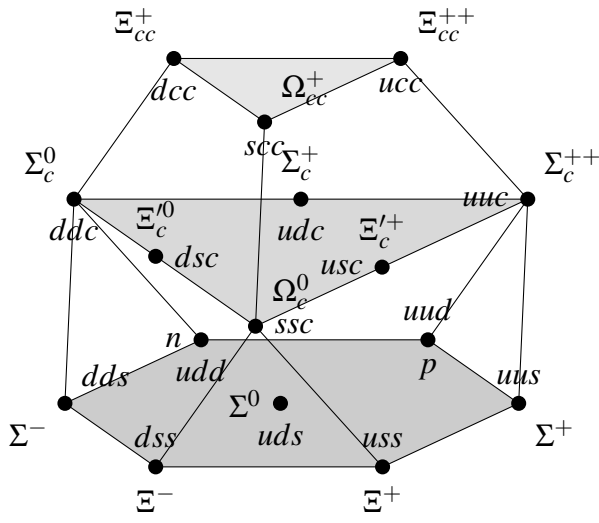


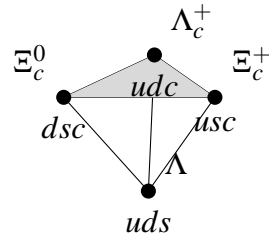
Figure 3.12 Charmed baryon spectrum comparison with LQCD results [40].

baryons have been observed, which are $\Xi_c^{\prime 0} \rightarrow \Xi_c^0 \gamma$, $\Xi_c^{\prime +} \rightarrow \Xi_c^+ \gamma$, and $\Omega_c^{*0} \rightarrow \Omega_c^0 \gamma$.

For $\Xi_c^{\prime 0} \rightarrow \Xi_c^0 \gamma$, $\Xi_c^{\prime +} \rightarrow \Xi_c^+ \gamma$, and $\Omega_c^{*0} \rightarrow \Omega_c^0 \gamma$ precise measurements have not done experimentally yet due to their small decay widths [97]. In the next two chapters, radiative transitions of Ξ_c , Ω_c^{*0} , Ξ_c^{\prime} will be studied in LQCD.



(a) 20-plet of SU(4) for spin- $\frac{1}{2}$



(b) $\bar{4}$ plet of SU(4) for spin- $\frac{1}{2}$

Figure 3.13 SU(4) multiplets of spin- $\frac{1}{2}$

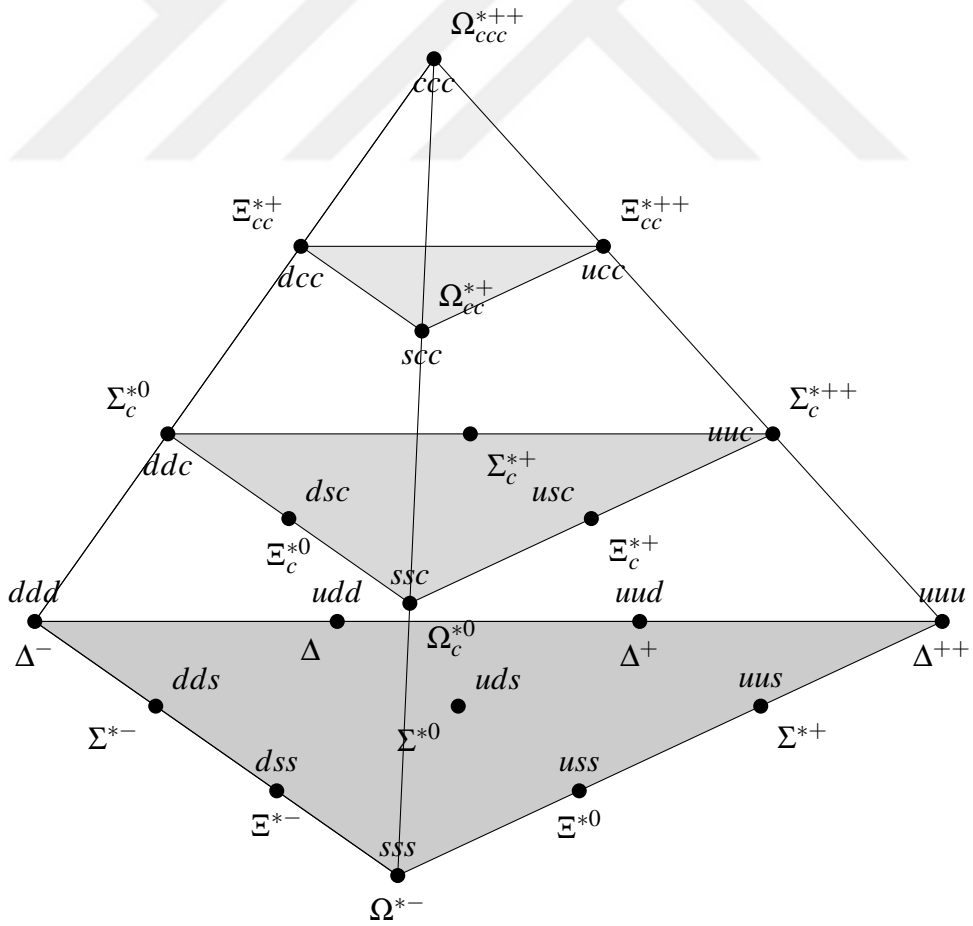


Figure 3.14 20-plet of SU(4) for spin- $\frac{3}{2}$

$\Omega_c \gamma \rightarrow \Omega_c^*$ TRANSITION IN LATTICE QCD

In the previous chapters the method of LQCD was discussed. Moreover baryon spectroscopy in LQCD was explained and form factors were introduced. In this chapter, using the information given in Chapters 2 and 3, radiative transition of Ω_c to Ω_c^* baryon will be explained. The $\Omega_c \gamma \rightarrow \Omega_c^*$ is spin- $\frac{1}{2} \rightarrow \frac{3}{2}$ transition which gives rise to three transition form factors, namely, the magnetic dipole ($M1$), the electric quadrupole ($E2$) and the electric charge quadrupole ($C2$). In this work $M1$ and $E2$ transition form factors as well as the helicity amplitudes, the decay width and the lifetime will be calculated in LQCD. Calculations are made using near physical 2+1-flavor lattices which correspond to a pion mass of approximately $m_\pi \approx 156$ MeV. The results of this chapter have been previously published in [12].

4.1 Lattice Formulation

Electromagnetic transition form factors of $\Omega_c \gamma \rightarrow \Omega_c^*$ can be calculated by considering the baryon matrix element. The electromagnetic vector current is defined as

$$J_\mu = \sum_q C_q \bar{q}(x) \gamma_\mu q(x), \quad (4.1)$$

where C_q is the charge of the quark and γ_μ are the gamma matrices. Both Ω_c and Ω_c^* have the same quark content (css). Therefore the vector current reduces to

$$J_\mu = \frac{2}{3} \bar{c}(x) \gamma_\mu c(x) - \frac{1}{3} \bar{s}(x) \gamma_\mu s(x). \quad (4.2)$$

The matrix element can be written in the following form

$$\langle \chi^*(p', s') | J_\mu | \chi(p, s) \rangle = i\sqrt{2/3} \left(\frac{m_* m}{E_*(p') E(p)} \right) \bar{u}_\tau(p', s') \mathcal{O}^{\tau\mu} u(p, s). \quad (4.3)$$

The star denotes Ω_c^* and others denote Ω_c . The $\Omega_c \gamma \rightarrow \Omega_c^*$ electromagnetic transition gives rise to three form factors since the spin- $\frac{3}{2}$ particles have an extra index. Using the current conservation, $q_\tau \mathcal{O}^{\tau\mu} = 0$ for $q^2 \neq 0$, vertex is restricted to combination of three covariants

$$\begin{aligned} K_1^{\tau\mu} &= (q^\tau \gamma^\mu - q \cdot \gamma g^{\tau\mu}) \gamma^5, \\ K_2^{\tau\mu} &= (q^\tau P^\mu - q \cdot P g^{\tau\mu}) \gamma^5, \\ K_3^{\tau\mu} &= (q^\tau q^\mu - q^2 g^{\tau\mu}) \gamma^5. \end{aligned} \quad (4.4)$$

Here p and p' denote the incoming and the outgoing momenta, respectively, $q = p' - p$ is the transferred four-momentum and $P^\mu = (p'^\mu + p^\mu)/2$. The three covariants correspond to three form factors. The vertex tensor $\mathcal{O}^{\tau\mu}$ can be written in terms of Sachs [90] form factors [91] in the following form:

$$\mathcal{O}^{\tau\mu} = G_{M1}(q^2) K_{M1}^{\tau\mu} + G_{E2}(q^2) K_{E2}^{\tau\mu} + G_{C2}(q^2) K_{C2}^{\tau\mu}. \quad (4.5)$$

$K_{M1}^{\tau\mu}$, $K_{E2}^{\tau\mu}$ and $K_{C2}^{\tau\mu}$ are called as magnetic dipole, electric quadrupole and Coulomb quadrupole respectively and they are defined as

$$K_{M1}^{\tau\mu} = -\frac{3}{(m_* + m)^2 + q^2} \frac{(m_* + m)}{2m} i \varepsilon^{\tau\mu\alpha\beta} P_\alpha q_\beta, \quad (4.6)$$

$$K_{E2}^{\tau\mu} = -K_{M1}^{\tau\mu} + 6\Omega^{-1}(q^2) \frac{(m_* + m)}{2m} i \gamma_5 \varepsilon^{\tau\lambda\alpha\beta} P_\alpha q_\beta \varepsilon^{\mu\lambda\gamma\delta} (2P_\gamma + q_\gamma) q_\delta, \quad (4.7)$$

$$K_{C2}^{\tau\mu} = -6\Omega^{-1}(q^2) \frac{(m_* + m)}{2m} i \gamma_5 q_\tau (q^2 P_\mu - q \cdot P q_\mu), \quad (4.8)$$

where

$$\Omega(q^2) = [(m_* + m)^2 + q^2] [(m_* - m)^2 + q^2]. \quad (4.9)$$

The spins are denoted by s and s' , whereas $u(p, s)$ is the Dirac spinor $u_\tau(p, s)$ is the Rarita-Schwinger spin vector. For real photons $G_{C2}(0)$ does not play any role as it is

proportional to the longitudinal helicity amplitude. The Rarita-Schwinger spin sum is given in Eq. (3.29) as

$$\sum_s u_\sigma(p, s) \bar{u}_\tau(p, s) = \frac{-i\not{p} + M}{2M} \left[g_{\sigma\tau} - \frac{1}{3} \gamma_\sigma \gamma_\tau + \frac{2p_\sigma p_\tau}{3M^2} - i \frac{p_\sigma \gamma_\tau - p_\tau \gamma_\sigma}{3M} \right], \quad (4.10)$$

and the Dirac spin spin sum is given in Eq. (3.20) as

$$\sum_s u(\vec{p}, s) \bar{u}(\vec{p}, s) = \frac{i\not{p} + M}{2M}. \quad (4.11)$$

The detailed calculations of form factors can be found in Appendix E.3. To extract the form factors, a ratio which consists of two-point and three-point functions should be defined. The two- and three-point functions are

$$\langle F_{\sigma\tau}^{\Omega_c^* \Omega_c^*}(t; p; \Gamma_4) \rangle = \sum_x e^{-i\vec{p}\cdot x} \Gamma_4^{\beta\alpha} \langle vac | T[\chi_\sigma^\beta(x) \bar{\chi}_\tau^\alpha(0)] | vac \rangle, \quad (4.12)$$

$$\langle F^{\Omega_c \Omega_c}(t; p; \Gamma_4) \rangle = \sum_x e^{-i\vec{p}\cdot x} \Gamma_4^{\beta\alpha} \langle vac | T[\chi^\beta(x) \bar{\chi}^\alpha(0)] | vac \rangle, \quad (4.13)$$

$$\langle F^{\Omega_c^* J_\mu \Omega_c}(t_2, t_1; p', p; \Gamma) \rangle = -i \sum_{x_1, x_2} e^{-i\vec{p}\cdot x_2} e^{i\vec{q}\cdot x_1} \Gamma_4^{\beta\alpha} \langle vac | T[\chi^\beta(x_2) J_\mu(x_1) \bar{\chi}^\alpha(0)] | vac \rangle. \quad (4.14)$$

Here, α, β are the Dirac indices, σ and τ are the Lorentz indices of the spin- $\frac{3}{2}$ interpolating field. The spin projection matrices are defined as

$$\Gamma_i = \frac{1}{2} \begin{bmatrix} \sigma_i & 0 \\ 0 & 0 \end{bmatrix}, \quad \Gamma_4 = \frac{1}{2} \begin{bmatrix} I & 0 \\ 0 & 0 \end{bmatrix}, \quad (4.15)$$

and σ_i are the Pauli spin matrices.

An initial Ω_c state is created at time zero and interacts with the external electromagnetic field at time t_1 . At time t_2 , the final Ω_c^* state is annihilated. The baryon interpolating fields are chosen as

$$\chi_\mu^*(x) = \frac{1}{\sqrt{3}} \epsilon^{ijk} [2[s^{Ti}(x)(C\gamma_\mu)c^j(x)]s^k(x) + [s^{Ti}(x)(C\gamma_\mu)s^j(x)]c^k(x)], \quad (4.16)$$

$$\chi(x) = \epsilon^{ijk} [s^{Ti}(x)(C\gamma_5)c^j(x)]s^k(x), \quad (4.17)$$

where i, j, k denote the color indices and C is the charge conjugation matrix defined as $C = \gamma_4 \gamma_2$. It has been shown in Ref. [5] that the interpolating field of Ω_c^* has minimal overlap with spin-1/2 states, hence, it does not need any spin-3/2 projection. Using the convention explained in Section 3.1.2, the interpolating fields of Ω_c and Ω_c^* are picked as $\chi_\gamma = B_\gamma^{css}$, where $B_\gamma^{123} = -B_\gamma^{213}$ and $\chi_{k,\gamma}^* = 2B_{k,\gamma}^{css} + B_{k,\gamma}^{ssc}$, where $B_{k,\gamma}^{213} = B_{k,\gamma}^{123}$.

The two-point function for Ω_c^* and Ω_c can be written as

$$\begin{aligned} \langle \chi_{k,\gamma}^*(x) \bar{\chi}_{\bar{k},\bar{\gamma}}^*(0) \rangle &= 4 \langle B_{k,\gamma}^{123}(x) \bar{B}_{\bar{k},\bar{\gamma}}^{123}(0) \rangle_{\substack{1=c \\ 2,3=s}} + 2 \langle B_{k,\gamma}^{123}(x) \bar{B}_{\bar{k},\bar{\gamma}}^{123}(0) \rangle_{\substack{1,2=s \\ 3=c}} \\ &\quad + 4 \langle B_{k,\gamma}^{123}(x) \bar{B}_{\bar{k},\bar{\gamma}}^{132}(0) \rangle_{\substack{1=c \\ 2,3=s}} + 4 \langle B_{k,\gamma}^{123}(x) \bar{B}_{\bar{k},\bar{\gamma}}^{132}(0) \rangle_{\substack{1,3=s \\ 2=c}} \\ &\quad + 4 \langle B_{k,\gamma}^{123}(x) \bar{B}_{\bar{k},\bar{\gamma}}^{132}(0) \rangle_{\substack{1,2=s \\ 3=c}}, \end{aligned} \quad (4.18)$$

$$\langle \chi_\gamma(x) \bar{\chi}_{\bar{\gamma}}(0) \rangle = \langle B_\gamma^{123}(x) \bar{B}_{\bar{\gamma}}^{123}(0) \rangle_{\substack{1=c \\ 2,3=s}} + \langle B_\gamma^{123}(x) \bar{B}_{\bar{\gamma}}^{132}(0) \rangle_{\substack{1=c \\ 2,3=s}}. \quad (4.19)$$

The three-point function of $\Omega_c \gamma \rightarrow \Omega_c^*$ can be written as

$$\begin{aligned} \langle \chi_{k,\gamma}^*(x) \bar{\chi}_{\bar{\gamma}}(0) \rangle &= 2 \langle B_{k,\gamma}^{cs_1s_2}(x) \bar{B}_{\bar{\gamma}}^{cs_1s_2}(0) \rangle + 2 \langle B_{k,\gamma}^{cs_1s_2}(x) \bar{B}_{\bar{\gamma}}^{cs_2s_1}(0) \rangle \\ &\quad + \langle B_{k,\gamma}^{s_1s_2c}(x) \bar{B}_{\bar{\gamma}}^{cs_1s_2}(0) \rangle + \langle B_{k,\gamma}^{s_1s_2c}(x) \bar{B}_{\bar{\gamma}}^{cs_2s_1}(0) \rangle, \\ &= 2 \langle B_{k,\gamma}^{123}(x) \bar{B}_{\bar{\gamma}}^{123}(0) \rangle_{1=c,2=s_1,3=s_2} + 2 \langle B_{k,\gamma}^{123}(x) \bar{B}_{\bar{\gamma}}^{132}(0) \rangle_{1=c,2=s_1,3=s_2} \\ &\quad - \langle B_{k,\gamma}^{123}(x) \bar{B}_{\bar{\gamma}}^{132}(0) \rangle_{1=s_1,2=s_2,3=c} - \langle B_{k,\gamma}^{123}(x) \bar{B}_{\bar{\gamma}}^{132}(0) \rangle_{1=s_2,2=s_1,3=c}. \end{aligned} \quad (4.20)$$

To extract the form factors, a ratio of two- and three-point functions is defined:

$$R_\sigma(t_2, t_1, p', p, \Gamma, \mu) = \frac{\langle F_\sigma^{\Omega_c^* J \mu \Omega_c}(t_2, t_1; p', p; \Gamma) \rangle}{\langle \delta_{ij} F_{ij}^{\Omega_c^* \Omega_c^*}(t_2; p'; \Gamma_4) \rangle} \left[\frac{\langle \delta_{ij} F_{ij}^{\Omega_c^* \Omega_c^*}(2t_1; p'; \Gamma_4) \rangle}{\langle F^{\Omega_c \Omega_c}(2t_1; p; \Gamma_4) \rangle} \right]^{\frac{1}{2}}. \quad (4.21)$$

In the large time limit, $t_2 - t_1 \gg a$ and $t_1 \gg a$, the time dependence of the correlators is eliminated and the ratio reduces to the desired form:

$$R(t_2, t_1; p', p; \Gamma; \mu) \xrightarrow[t_1 \gg a]{t_2 - t_1 \gg a} \Pi(p', p; \Gamma; \mu). \quad (4.22)$$

The plateau region must be carefully determined to extract the form factors. The ratio in Eq. (4.21) has been selected among several other alternatives [6, 115], owing to the quality of the signal and the good plateau regions. Sachs form factors are singled out by

choosing appropriate combinations of Lorentz direction μ and projection matrices. When Ω_c is produced at rest and momentum is inserted in one spatial direction, the form factors are

$$G_{C2}(q^2) = C(q^2) \frac{2m_*}{q^2} \Pi_j(q, 0, i\Gamma_j; 4), \quad (4.23)$$

$$G_{M1}(q^2) = C(q^2) \frac{1}{|q|} \left[\Pi_k(q_j, 0, \Gamma_j; k) - \frac{m_*}{E_*} \Pi_k(q_k, 0, \Gamma_j; j) \right], \quad (4.24)$$

$$G_{E2}(q^2) = C(q^2) \frac{1}{|q|} \left[\Pi_k(q_j, 0, \Gamma_j; k) + \frac{m_*}{E_*} \Pi_k(q_k, 0, \Gamma_j; j) \right], \quad (4.25)$$

where

$$C(q^2) = 2\sqrt{6} \frac{E_* m_*}{m + m_*} \sqrt{1 + \frac{m_*}{E_*}} \sqrt{1 + \frac{q^2}{3m_*^2}}, \quad (4.26)$$

j and k are two distinct indices running from 1 to 3. When Ω_c^* is produced at rest, $m_* = E_*$ in Eqs. (4.23 - 4.25) and $C(q^2)$ becomes

$$C(q^2) = 2\sqrt{6} \frac{Em}{m + m_*} \sqrt{1 + \frac{m}{E}} \sqrt{1 + \frac{q^2}{3m_*^2}}. \quad (4.27)$$

The gauge configurations we are employing have been generated by PACS-CS [4] collaboration with the $\mathcal{O}(a)$ -improved Wilson quark action and the Iwasaki gauge action. The simulations are carried out with near physical u, d sea quarks of hopping parameter $\kappa_\ell = 0.13781$, which corresponds to a pion mass of approximately 156 MeV [4]. The hopping parameter for the sea s quark was fixed to $\kappa_s^{sea} = 0.13640$ and for the consistency of the simulations the hopping parameter of the valence s quark is taken to be the same.

As we carry out the simulations at only near-physical quark mass, a chiral extrapolation cannot be applied. However, an estimation of an uncertainty can be made from such an extrapolation, using our previous results of elastic form factors [30]. We have performed the chiral extrapolations for electric/magnetic charge radii and the magnetic moment of Ω_c baryon in Ref. [30] again, including the data at $m_\pi \approx 156$ MeV. We tested constant, linear and quadratic fit functions. For all cases, the chiral-extrapolated values and those at $m_\pi \approx 156$ MeV are in very good agreement within their error bars. Different fit forms

Table 4.1 The details of the gauge configurations used in the analysis [4]. N_s and N_t are the spatial and temporal sizes of the lattice, respectively, N_f is the number of flavors, a is the lattice spacing, L is the volume of the lattice, β is the inverse gauge coupling, c_{sw} is the Clover coefficient, κ_{sea}^f is the hopping parameter of the quark with flavor f and m_π is the pion mass.

$N_s \times N_t$	N_f	a (fm)	L (fm)	β
$32^3 \times 64$	2+1	0.0907(13)	2.90	1.90
c_{sw}	κ_{sea}^l	κ_{sea}^s	# of conf	m_π [MeV]
1.715	0.13781	0.13640	194	156(7)(2)

we use refer a systematic error of less than 1%. Hence, we assume to have a similarly negligible error from such an extrapolation of $M1$ and $E2$ form factors.

The hopping parameters of light and strange quarks were fixed by PACS-CS [4] collaboration. However, for the charm quarks, hopping parameter has to be tuned. In order to be consistent with the dynamical quarks, Clover action is employed. Although, the Clover action has $\mathcal{O}(a)$ discretization errors, those effects must be accounted for since the charm quark's larger mass would enhance the discretization error for heavy quarks frequently used Fermilab action [116]:

$$\begin{aligned}
S = & \sum_n \bar{\psi}_n \psi_n - \kappa \sum_n [\bar{\psi}_n (1 - \gamma_4) U_{n,4} \psi_{n+\hat{4}} + \bar{\psi}_{n+\hat{4}} (1 - \gamma_4) U_{n,4}^\dagger \psi_n] \\
& - \kappa \xi \sum_{n,i} [\bar{\psi}_n (r_s - \gamma_i) U_{n,i} \psi_{n+\hat{i}} + \bar{\psi}_{n+\hat{i}} (r_s - \gamma_i) U_{n,i}^\dagger \psi_n] \\
& - c_B \kappa \xi \sum_n \bar{\psi}_n i \Sigma \cdot B_n \psi_n - c_E \kappa \xi \sum_{n,i} \bar{\psi}_n \alpha \cdot E_n \psi_n,
\end{aligned} \tag{4.28}$$

where U denotes the gluon field and ψ denotes the fermion fields. The Clover definitions of the chromomagnetic and chromoelectric fields B and E can be found at Ref. [116]. The action reduces to the Wilson action when $\xi = r_s = 1$ and $c_B = c_E = 0$ [117]. Sheikholeslami-Wohlert action is obtained when $\xi = r_s = 1$ and $c_B = c_E = c_{sw}$ [118]. In this simplest form of the Fermilab method, the Clover coefficients are set to the tadpole-improved value $\frac{1}{u_0^3}$, where u_0 is the average link. Following the approach in Ref. [119], u_0 was estimated as the fourth root of the average plaquette. The charm-quark hopping parameter κ_c is deter-

mined nonperturbatively. We determine κ_c by measuring spin-averaged static masses of charmonium and heavy-light mesons and tuning accordingly to the experimental results, which yields $\kappa_c = 0.1246$ [30].

The simulations are made with the lowest allowed lattice momentum transfer $q = \frac{2\pi}{N_s a}$. Here N_s is the spatial dimension of the lattice and a is the lattice spacing. This corresponds to three-momentum squared value of $q^2 = 0.183 \text{ GeV}^2$. In order to make contact the values of the form factors at $Q^2 = 0$, the procedure in Ref. [6] is applied and assumed that the momentum-transfer dependence of the transition form factors is the same with that of the momentum dependence of the Ω_c^* baryon charge form factor. Such a scaling was also suggested by the experimentally measured proton form factors and it was used in Ref. [6]. The scaling technique provides a precise determination of the form-factor values at zero momentum transfer. On the other hand, extrapolations in finite momentum have to rely on a functional form, that suffer from large statistical errors. In the analysis, s and c quark sectors are calculated separately as their contributions to the charge form factors scale differently. For example, the scaling of G_{M1} is

$$G_M^{s,c}(0) = G_M^{s,c}(q^2) \frac{G_E^{s,c}(0)}{G_E^{s,c}(q^2)}. \quad (4.29)$$

The form factors are extracted in two kinematically different cases. In the first case, the Ω_c^* is produced at rest and the Ω_c has momentum $-q$. In the second case, the Ω_c is at rest and Ω_c^* carries momentum q .

Positive and negative momenta are inserted in spatial directions to increase the statistics and a simultaneous fit is made over all available data. The source-sink time separation is fixed to 1.09 fm ($t_2 = 12a$), that is shown to be sufficient to avoid excited state contaminations for electromagnetic form factors [30]. Using translational symmetry multiple source-sink pairs are employed by shifting them 12 lattice units in the temporal direction. All statistical errors are estimated by the single-elimination Jackknife analysis. Point-split lattice vector current is considered

$$j_\mu = \frac{1}{2} [\bar{q}(x+\mu)U_\mu^\dagger(1+\gamma_\mu)q(x) - \bar{q}(x)U_\mu(1-\gamma_\mu)q(x+\mu)], \quad (4.30)$$

which is a conserved current by Wilson fermions.

Here we used wall-source/sink method [83]. This method provides a simultaneous extraction of all spin, momentum and projection components of the correlators. On the other hand, the wall-source/sink is a gauge-dependent object which requires fixing the gauge. The gauge is fixed to Coulomb, which gives a better coupling to the ground state as compared to Landau. The Ω_c^* operator is smeared over the three spatial dimensions using a Gaussian form. In the case of s quark, the smearing parameters are chosen, in order to give a root-mean-square radius of $\langle r_\ell \rangle \sim 0.5$ fm. As for the charm quark, the smearing parameters are adjusted to obtain $\langle r_c \rangle = \frac{\langle r_\ell \rangle}{3}$.

4.2 Numerical Results

Ω_c^* and Ω_c masses are extracted by using the two-point correlators in Eqs. (4.13) and (4.14). In the analysis, shell smeared source and point sink (shpt) two-point correlation functions are used for clean signal. In the limit of $n_t \rightarrow \infty$, the excited states are eliminated and only the ground state remains so that the effective mass can be written as Eq. (3.52). In order to avoid correlation there must be a large spacing between the source (t_1) and sink (t_2) time points. Since the data may still have been correlated, a resampling method (Jackknife, bootstrap etc. . .) have to be used. In this analysis Jackknife resampling method is used. Details of Jackknife method is given in Appendix A.3. The obtained results are in lattice units and must be multiplied with inverse lattice spacing a^{-1} for the physical results.

The results for the Ω_c^* and Ω_c masses are given in Table 4.2, together with the experimental values and those obtained by other lattice collaborations. While there are a few percent discrepancy between the results obtained at a pion mass of $m_\pi = 156$ MeV and those from PACS-CS obtained at the physical point, the mass splitting $\Delta m = m_* - m$ is produced in agreement with experiment.

We define the sum of all correlation-function ratios as

$$\Pi_1 = \frac{C(q^2)}{|q|} \frac{1}{6} \sum_{k,l} \Pi_l(q_k, 0; \Gamma_k; l), \quad \Pi_2 = \frac{C(q^2)}{|q|} \frac{1}{6} \sum_{k,l} \Pi_k(q_k, 0; \Gamma_l; l). \quad (4.31)$$

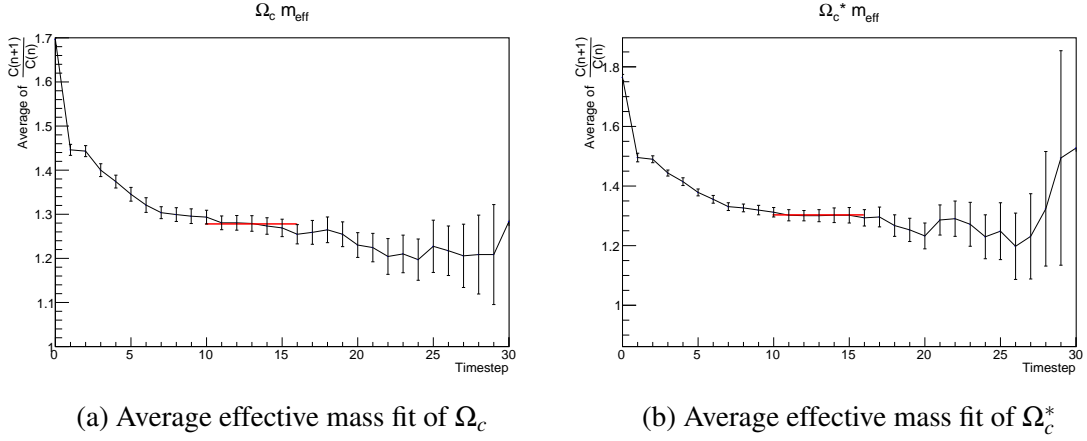


Figure 4.1 Two-point functions of Ω_c and Ω_c^* , red horizontal line indicates the fit region.

Table 4.2 The Ω_c and Ω_c^* masses at $m_\pi = 156$ MeV.

	This work [12]	PACS-CS [38]	ETMC [5]	Briceno et al. [40]	Experiment [17]
m GeV	2.750(15)	2.673(17)	2.629(22)	2.681(48)	2.695(2)
m_* GeV	2.828(15)	2.738(17)	2.709(26)	2.764(49)	2.766(2)

The Eq. (4.24) and Eq. (4.25) becomes

$$G_{M1} = \Pi_1 - \frac{m_*}{E_*} \Pi_2, \quad (4.32)$$

$$G_{E2} = \Pi_1 + \frac{m_*}{E_*} \Pi_2. \quad (4.33)$$

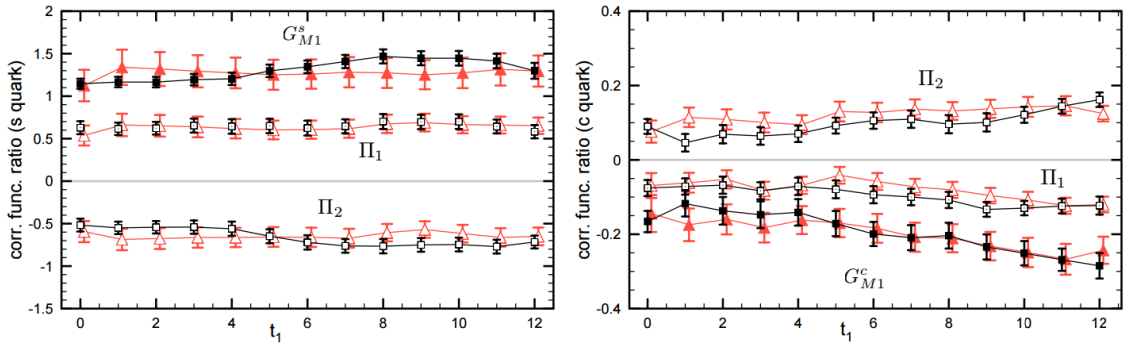


Figure 4.2 The correlation function ratios Π_1 and Π_2 as functions of the current insertion time. $G_{M1}^{s,c}$ were obtained. The squares denote the kinematical case when Ω_c^* at rest and triangles denote the kinematical case when Ω_c at rest

The two ratios (Π_1 and Π_2) have opposite sign and they add constructively when they are subtracted. The form factors are extracted by fitting the correlation-function ratios by

a constant parameter where a plateau develops. Both kinematical cases give consistent results within their error bars. There is a clear plateau region in both kinematical cases. However when Ω_c is produced at rest, plateau region is more flat. The correlation function ratios are fit in the range $t_1 = [3, 6]$. The statistical errors are smaller when Ω_c^* is at rest. The values of the form factors from the two kinematical cases are consistent with each other.

After the construction of G_{M1} , construction of G_{E2} is straightforward. The correlation functions have opposite signs and are of similar magnitudes, which result in a vanishing value for G_{E2} when they are added. This procedure gives consistent results with fitting the sum of the correlation ratios.

The numerical results are reported in Table 4.3. The values of G_{M1} and G_{E2} form factors are given at both the lowest allowed momentum transfer and at zero momentum transfer for the two kinematical cases as explained above. The quark sector contributions to each form factor are given separately. The form factors of individual quark contributions are

$$G_{M1}(Q^2) = \frac{2}{3}G_{M1}^c(Q^2) - \frac{1}{3}G_{M1}^s(Q^2), \quad (4.34)$$

$$G_{E2}(Q^2) = \frac{2}{3}G_{E2}^c(Q^2) - \frac{1}{3}G_{E2}^s(Q^2). \quad (4.35)$$

Their values at $Q^2 = 0$ are extracted using the scaling assumption.

$M1$ is dominantly determined by the contribution of the s quark, which is approximately one order of magnitude larger than that of the c quark. The results are consistent with hyperon transition form factors [6]. The heavier quark contribution is systematically smaller than the light quarks. From the quark-model perspective, the coupling of the photon to the light quarks dominate in the heavy-quark limit and the heavy quark acts as a spectator. In this limit, only $M1$ transition is allowed, because the transition occurs dominantly through the spin flip of the light d.o.f. Only mass effects of the heavy quark might lead to a nonzero value of $E2$ form factor. The results show that the two quark sectors contribute with opposite signs and produce a value with a statistical error of approximately 5% when combined. However, the values of G_{E2} at finite and zero momentum transfer are small

Table 4.3 The results for form factors at the lowest allowed four momentum transfer and zero momentum transfer for the two kinematical cases [12].

$Q^2 \text{GeV}^2$	$G_{M1}^s(Q^2)$	$G_{M1}^c(Q^2)$	$G_{M1}(Q^2)$	
Ω_c^* at rest	0.180	1.257(67)	-0.167(33)	-0.530(28)
	0	1.622(87)	-0.175(34)	-0.657(33)
Ω_c at rest	0.168	1.269(177)	-0.174(37)	-0.539(78)
	0	1.637(229)	-0.183(39)	-0.667(96)

$Q^2 \text{GeV}^2$	$G_{E2}^s(Q^2)$	$G_{E2}^c(Q^2)$	$G_{E2}(Q^2)$	
Ω_c^* at rest	0.180	0.041(132)	0.008(26)	-0.008(50)
	0	0.052(171)	0.009(27)	-0.012(62)
Ω_c at rest	0.168	-0.035(124)	0.061(25)	0.052(48)
	0	-0.045(160)	0.064(27)	0.058(60)

and consistent with zero.

A comparison between G_{M1} and G_{E2} show that the transition is fully determined by $M1$ transition. Quark model prediction of the quadrupole transition moments arises from the tensor-induced D-state admixtures of the single-quark wave functions [120] and the two-quark exchange currents [121, 122]. In the first, the spins of the quarks remain the same but an S-state quark is changed into a D-state. This change can be interpreted as the spin flip of a diquark inside the baryon. Given the dependence of the tensor force on the inverse quark mass, one would expect to obtain a smaller G_{E2} value for heavy baryons as compared to that in the light-baryon sector, which is consistent with the results. The $E2$ form factor smallness can also be explained as a chiral suppression. The $E2$ amplitude is dominated by pion loops and the leading contribution is coming from chiral logs that can be computed in heavy-baryon chiral perturbation theory [123, 124].

The Sachs form factors can be related to phenomenological observables. The relation between the Sachs form factors to transition amplitudes in standard definitions f_{M1} and

f_{E2} in the rest frame of Ω_c^* is given by [125, 126]

$$\begin{aligned} f_{M1}(q^2) &= \frac{\sqrt{4\pi\alpha}}{2m} \sqrt{\frac{|q|m_*}{m}} \frac{G_{M1}(q^2)}{\sqrt{1 - \frac{q^2}{(m+m_*)^2}}}, \\ f_{E2}(q^2) &= \frac{\sqrt{4\pi\alpha}}{2m} \sqrt{\frac{|q|m_*}{m}} \frac{G_{E2}(q^2)}{\sqrt{1 - \frac{q^2}{(m+m_*)^2}}}, \end{aligned} \quad (4.36)$$

where fine structure constant $\alpha = \frac{1}{137}$. The helicity amplitudes can be found from the transition amplitudes,

$$A_{1/2}(q^2) = -\frac{1}{2}[f_{M1}(q^2) + 3f_{E2}(q^2)], \quad (4.37)$$

$$A_{3/2}(q^2) = -\frac{\sqrt{3}}{2}[f_{M1}(q^2) - f_{E2}(q^2)]. \quad (4.38)$$

The decay width is

$$\Gamma = \frac{m_*m}{8\pi} \left(1 - \frac{m^2}{m_*^2}\right)^2 [|A_{1/2}(0)|^2 + |A_{3/2}(0)|^2], \quad (4.39)$$

where the constraint $q = (m_*^2 - m^2)/2m_*$ is used at $q^2 = 0$. The decay width can be found using the Sachs form factors:

$$\Gamma = \frac{\alpha}{16} \frac{(m_*^2 - m^2)^3}{m_*^3 m^2} [3|G_{E2}(0)|^2 + |G_{M1}(0)|^2]. \quad (4.40)$$

Table 4.4 The results for helicity amplitudes in the rest frame of Ω_c^* [12].

Q^2 GeV ²	$f_{M1} 10^{-2}$ GeV ^{-1/2}	$f_{E2} 10^{-2}$ GeV ^{-1/2}
0.180	-0.795(42)	-0.012(75)
0	-0.988(50)	-0.018(93)
Q^2 GeV ²	$f_{M1} 10^{-2}$ GeV ^{-1/2}	$f_{E2} 10^{-2}$ GeV ^{-1/2}
0.180	0.416(116)	0.678(71)
0	0.521(145)	0.840(88)

Since the formulas in Eqs. (4.37-4.40) are continuum relations, experimental values of the Ω_c and Ω_c^* masses are used in calculating the helicity amplitudes and the decay width.

The numerical results for the helicity amplitudes in the rest frame of Ω_c^* and the decay width are given at finite and zero momentum transfer, in Table (4.4). A comparison to the $N \rightarrow \Delta$ transition [17] shows that, the helicity amplitudes are suppressed roughly by five orders of magnitude due to decreasing contribution of the heavy quark, the overall reduction in the transition form factors and the larger baryon masses.

The mass splitting between Ω_c^* and Ω_c forbids the strong decay channel, so the total decay width of Ω_c^* can be calculated from electromagnetic channel. The Ω_c^* decay is suppressed, this suppression of decay width can be ascribed to small mass splitting. Suppressed value of the Ω_c^* baryon decay width makes Ω_c^* one of the longest living spin-3/2 charmed hadrons. The decay width is found as $\Gamma = 0.074(8)$ KeV which is translated into lifetime $\tau = \frac{1}{\Gamma} = 8.901(913) \times 10^{-18}$ sec.

Non-relativistic quark model prediction for Ω_c^* decay width [127] is one order of magnitude larger than this work's result. Considering the mass splitting, such a large width would require a G_{M1} value as large as $N \rightarrow \Delta$ transition. This cannot be justified as the heavy-quark contribution diminishes and there was no indication that the light quark contribution is enhanced. $\Omega_c \gamma \rightarrow \Omega_c^*$ transition is in the interest of LHCb, PANDA, Belle II, BESIII and J-PARC experiments. These experimental facilities are expected to measure electromagnetic decay widths of charmed baryons with higher precision.

$\Xi_c \gamma \rightarrow \Xi'_c$ TRANSITION IN LATTICE QCD

In this chapter, the $\Xi_c \gamma \rightarrow \Xi'_c$ transition will be evaluated in 2+1-flavor LQCD. As a by-product the electromagnetic form factors of Ξ_c and Ξ'_c baryons will be computed. Simulations will be made with near physical light-quark masses which gives a pion mass of ~ 156 MeV. Using an appropriate ratio of two- and three-point correlation functions, the electric and magnetic form factors will be extracted which gave the decay rate of Ξ'_c and the magnetic moments of Ξ_c and Ξ'_c . The results of this chapter have been previously published in [13].

5.1 Lattice Formulation

The calculation of $\Xi_c \gamma \rightarrow \Xi'_c$ transition begins with defining the matrix element. Afterwards, electromagnetic current is used to study the electromagnetic and transition form factors of Ξ_c and Ξ'_c baryons:

$$J_\mu = \frac{2}{3} \bar{c}(x) \gamma_\mu c(x) - \frac{1}{3} \bar{s}(x) \gamma_\mu s(x) + c_\ell \bar{\ell}(x) \gamma_\mu \ell(x), \quad (5.1)$$

where ℓ denotes the flavor of the light quark (u and d) and c_ℓ is its charge ($\frac{2}{3}$ or $-\frac{1}{3}$). Using the definition of the vector current, the current is coupled to each quark one by one and the electromagnetic transition form factors are computed. The form factors are described by the matrix element

$$\langle B'(p', s') | J_\mu(x_1) | B(p, s) \rangle = \bar{u}(p', s') \left[\gamma_\mu F_1(q^2) - \frac{\sigma_{\mu\nu} q_\nu}{m_B + m_{B'}} F_2(q^2) \right] u(p, s). \quad (5.2)$$

Here $F_1(q^2), F_2(q^2)$ are the Dirac and Pauli form factors respectively. $u(p', s')$ and $u(p, s)$ are the Dirac spinor of the outgoing and incoming baryons with masses $m_{B'}$ and m_B .

$q_\mu = p'_\mu - p_\mu$ is the transferred four momentum with the momentum of the incoming (outgoing) baryon p (p').

The electric and magnetic Sachs form factors are defined in terms of Dirac and Pauli form factors as follows:

$$G_E(q^2) = F_1(q^2) - \frac{q^2}{(m_B + m_{B'})^2} F_2(q^2), \quad (5.3)$$

$$G_M(q^2) = F_1(q^2) + F_2(q^2). \quad (5.4)$$

The form factors are extracted considering the following two-point correlation functions

$$\langle F^{BB}(t; p; \Gamma_4) \rangle = \sum_x e^{ip'x} \Gamma_4^{\beta\alpha} \langle \Omega | T(\chi_B^\beta(x) \bar{\chi}_B^\alpha(0)) | \Omega \rangle, \quad (5.5)$$

and the following three-point correlation functions

$$\langle F^{B'J_\mu B}(t_2, t_1; p', p; \Gamma) \rangle = -i \sum_{x_1, x_2} e^{-ip'x_2} e^{iqx_1} \Gamma^{\beta\alpha} \langle \Omega | T(\chi_{B'}^\beta(x_2) J_\mu(x_1) \bar{\chi}_B^\alpha(0)) | \Omega \rangle, \quad (5.6)$$

with B denotes Ξ_c and B' denotes Ξ'_c . Here t_1 is the time when the electromagnetic current is inserted, t_2 is the time when the final baryon is annihilated and $\Gamma_4 = \frac{1}{2} \begin{bmatrix} 1 & 0 \\ 0 & 0 \end{bmatrix}$ with

$$\Gamma_i = \frac{1}{2} \begin{bmatrix} \sigma_i & 0 \\ 0 & 0 \end{bmatrix}.$$

The baryon interpolating fields are chosen as

$$\chi_{\Xi'_c} = \frac{1}{\sqrt{2}} \varepsilon_{abc} [(\ell_a^T (C\gamma_5) c_b) s_c + (s_a^T (C\gamma_5) c_b) \ell_c], \quad (5.7)$$

$$\chi_{\Xi_c} = \frac{1}{\sqrt{6}} \varepsilon_{abc} [2(s_a^T (C\gamma_5) \ell_b) c_c + (s_a^T (C\gamma_5) c_b) \ell_c - (\ell_a^T (C\gamma_5) c_b) s_c], \quad (5.8)$$

where $\ell = u$ for the charged states Ξ_c^+ , Ξ'_c^+ , and $\ell = d$ for the neutral states Ξ_c^0 , Ξ'_c^0 .

The indices a, b, c denote color and the charge conjugation matrix is defined as $C = \gamma_4 \gamma_2$.

Using the convention explained in Section 3.1.2, the interpolating fields of Ξ_c and Ξ'_c are picked as $\Xi_c = 2B_\gamma^{s\ell c} + B_\gamma^{s\ell c} + B_\gamma^{c\ell s}$ and $\Xi'_c = (B_\gamma^{\ell c s} + B_\gamma^{s\ell c})$, where $B_\gamma^{123} = -B_\gamma^{213}$.

The two-point function for Ξ'_c and Ξ_c can be written as

$$\langle \Xi'_c(x) \bar{\Xi}'_c(0) \rangle = \left(B_\gamma^{\ell cs}(x) + B_\gamma^{scl}(x) \right) \left(\bar{B}_{\gamma'}^{\ell cs}(0) + \bar{B}_{\gamma'}^{scl}(0) \right) \quad (5.9)$$

$$\begin{aligned} &= \langle B_\gamma^{\ell cs}(x) \bar{B}_{\gamma'}^{\ell cs}(0) \rangle + \langle B_\gamma^{scl}(x) \bar{B}_{\gamma'}^{scl}(0) \rangle + \langle B_\gamma^{\ell cs}(x) \bar{B}_{\gamma'}^{scl}(0) \rangle \\ &+ \langle B_\gamma^{scl}(x) \bar{B}_{\gamma'}^{\ell cs}(0) \rangle \\ &= \langle B_\gamma^{\ell cs}(x) \bar{B}_{\gamma'}^{\ell cs}(0) \rangle + \langle B_\gamma^{scl}(x) \bar{B}_{\gamma'}^{scl}(0) \rangle + \langle B_\gamma^{cls}(x) \bar{B}_{\gamma'}^{cls}(0) \rangle \\ &+ \langle B_\gamma^{csl}(x) \bar{B}_{\gamma'}^{csl}(0) \rangle \\ &= \langle B_\gamma^{123}(x) \bar{B}_{\gamma'}^{123}(0) \rangle_{1=\ell, 2=c, 3=s} + \langle B_\gamma^{123}(x) \bar{B}_{\gamma'}^{123}(0) \rangle_{1=s, 2=c, 3=\ell} \\ &+ \langle B_\gamma^{123}(x) \bar{B}_{\gamma'}^{132}(0) \rangle_{1=c, 2=\ell, 3=s} + \langle B_\gamma^{123}(x) \bar{B}_{\gamma'}^{132}(0) \rangle_{1=c, 2=s, 3=\ell}, \end{aligned} \quad (5.10)$$

$$\langle \Xi_c(x) \bar{\Xi}_c(0) \rangle = \left(2B_\gamma^{slc}(x) + B_\gamma^{scl}(x) + B_\gamma^{cls}(x) \right) \left(2\bar{B}_{\gamma'}^{slc}(0) + \bar{B}_{\gamma'}^{scl}(0) + \bar{B}_{\gamma'}^{cls}(0) \right) \quad (5.11)$$

$$\begin{aligned} &= 4\langle B_\gamma^{slc}(x) \bar{B}_{\gamma'}^{slc}(0) \rangle + \langle B_\gamma^{cls}(x) \bar{B}_{\gamma'}^{cls}(0) \rangle + \langle B_\gamma^{scl}(x) \bar{B}_{\gamma'}^{scl}(0) \rangle \\ &+ 2\langle B_\gamma^{slc}(x) \bar{B}_{\gamma'}^{scl}(0) \rangle + 2\langle B_\gamma^{scl}(x) \bar{B}_{\gamma'}^{cls}(0) \rangle + 2\langle B_\gamma^{cls}(x) \bar{B}_{\gamma'}^{slc}(0) \rangle \\ &+ 2\langle B_\gamma^{scl}(x) \bar{B}_{\gamma'}^{slc}(0) \rangle + \langle B_\gamma^{scl}(x) \bar{B}_{\gamma'}^{cls}(0) \rangle + \langle B_\gamma^{cls}(x) \bar{B}_{\gamma'}^{scl}(0) \rangle \\ &= 4\langle B_\gamma^{slc}(x) \bar{B}_{\gamma'}^{slc}(0) \rangle + \langle B_\gamma^{cls}(x) \bar{B}_{\gamma'}^{cls}(0) \rangle + \langle B_\gamma^{scl}(x) \bar{B}_{\gamma'}^{scl}(0) \rangle \\ &+ 2\langle B_\gamma^{slc}(x) \bar{B}_{\gamma'}^{scl}(0) \rangle + 2\langle B_\gamma^{lsc}(x) \bar{B}_{\gamma'}^{\ell cs}(0) \rangle + 2\langle B_\gamma^{\ell cs}(x) \bar{B}_{\gamma'}^{\ell sc}(0) \rangle \\ &+ 2\langle B_\gamma^{scl}(x) \bar{B}_{\gamma'}^{slc}(0) \rangle + \langle B_\gamma^{csd}(x) \bar{B}_{\gamma'}^{cls}(0) \rangle + \langle B_\gamma^{cls}(x) \bar{B}_{\gamma'}^{csd}(0), \rangle \\ &= 4\langle B_\gamma^{123}(x) \bar{B}_{\gamma'}^{123}(0) \rangle_{1=s, 2=\ell, 3=c} + \langle B_\gamma^{123}(x) \bar{B}_{\gamma'}^{123}(0) \rangle_{1=c, 2=\ell, 3=s} \\ &+ \langle B_\gamma^{123}(x) \bar{B}_{\gamma'}^{123}(0) \rangle_{1=s, 2=c, 3=\ell} + 2\langle B_\gamma^{123}(x) \bar{B}_{\gamma'}^{132}(0) \rangle_{1=s, 2=\ell, 3=c} \\ &+ 2\langle B_\gamma^{123}(x) \bar{B}_{\gamma'}^{132}(0) \rangle_{1=\ell, 2=s, 3=c} + 2\langle B_\gamma^{123}(x) \bar{B}_{\gamma'}^{132}(0) \rangle_{1=\ell, 2=c, 3=s} \\ &+ 2\langle B_\gamma^{123}(x) \bar{B}_{\gamma'}^{132}(0) \rangle_{1=s, 2=c, 3=\ell} - \langle B_\gamma^{123}(x) \bar{B}_{\gamma'}^{132}(0) \rangle_{1=c, 2=s, 3=\ell} \\ &- \langle B_\gamma^{123}(x) \bar{B}_{\gamma'}^{132}(0) \rangle_{1=c, 2=\ell, 3=s}. \end{aligned} \quad (5.12)$$

The three-point function of $\Xi_c \gamma \rightarrow \Xi'_c$ can be written as

$$\langle \Xi_c(x) \bar{\Xi}'_c(0) \rangle = (2B_\gamma^{slc}(x) + B_\gamma^{scl}(x) + B_\gamma^{cls}(x)) (\bar{B}_\gamma^{\ellcs}(0) + \bar{B}_\gamma^{scl}(0)) \quad (5.13)$$

$$\begin{aligned} &= 2\langle B_\gamma^{slc}(x) \bar{B}_\gamma^{\ellcs}(0) \rangle + 2\langle B_\gamma^{slc}(x) \bar{B}_\gamma^{scl}(0) \rangle + \langle B_\gamma^{cls}(x) \bar{B}_\gamma^{\ellcs}(0) \rangle \\ &+ \langle B_\gamma^{cls}(x) \bar{B}_\gamma^{scl}(0) \rangle + \langle B_\gamma^{scl}(x) \bar{B}_\gamma^{\ellcs}(0) \rangle + \langle B_\gamma^{scl}(x) \bar{B}_\gamma^{scl}(0) \rangle \\ &= -2\langle B_\gamma^{\ellsc}(x) \bar{B}_\gamma^{\ellcs}(0) \rangle + 2\langle B_\gamma^{slc}(x) \bar{B}_\gamma^{scl}(0) \rangle - \langle B_\gamma^{cls}(x) \bar{B}_\gamma^{\ellcs}(0) \rangle \\ &- \langle B_\gamma^{cls}(x) \bar{B}_\gamma^{scl}(0) \rangle + \langle B_\gamma^{csl}(x) \bar{B}_\gamma^{\ellcs}(0) \rangle + \langle B_\gamma^{scl}(x) \bar{B}_\gamma^{scl}(0) \rangle \\ &= -2\langle B_\gamma^{123}(x) \bar{B}_\gamma^{132}(0) \rangle_{1=\ell, 2=s, 3=c} + 2\langle B_\gamma^{123}(x) \bar{B}_\gamma^{132}(0) \rangle_{1=s, 2=\ell, 3=c} \\ &- \langle B_\gamma^{123}(x) \bar{B}_\gamma^{123}(0) \rangle_{1=c, 2=\ell, 3=s} - \langle B_\gamma^{123}(x) \bar{B}_\gamma^{132}(0) \rangle_{1=c, 2=\ell, 3=s} \\ &+ \langle B_\gamma^{123}(x) \bar{B}_\gamma^{132}(0) \rangle_{1=c, 2=s, 3=\ell} + \langle B_\gamma^{123}(x) \bar{B}_\gamma^{123}(0) \rangle_{1=s, 2=c, 3=\ell}. \end{aligned} \quad (5.14)$$

The following ratio is used to eliminate the normalization factors and to extract the baryon electromagnetic form factors:

$$\begin{aligned} R(t_2, t_1, p', p, \Gamma', \Gamma, \mu) &= \frac{\langle F^{B'J_\mu B}(t_2, t_1; p', p; \Gamma') \rangle}{\langle F_{shwl}^{B'B'}(t_2; p'; \Gamma_4) \rangle} \times \left[\frac{\langle F_{shsh}^{BB}(t_2 - t_1; p; \Gamma_4) \rangle}{\langle F_{shsh}^{B'B'}(t_2 - t_1; p'; \Gamma_4) \rangle} \right. \\ &\left. \frac{\langle F_{shsh}^{B'B'}(t_1; p'; \Gamma_4) \rangle \langle F_{shsh}^{B'B'}(t_2; p'; \Gamma_4) \rangle}{\langle F_{shsh}^{BB}(t_1; p; \Gamma_4) \rangle \langle F_{shsh}^{BB}(t_2; p; \Gamma_4) \rangle} \right]^{\frac{1}{2}}. \end{aligned} \quad (5.15)$$

where the subscripts of the correlators indicate smearing at the source and sink points. The correlator which is shell smeared both in the source and sink points, is labelled as shsh. Besides the correlator which is shell smeared at source point and wall smeared at sink point, is labelled as shwl. Using the definition of two- and three-point functions the ratio becomes

$$\begin{aligned} \frac{\langle F_{shwl}^{NJ_\mu N'}(t_2, t_1; p', p; \Gamma) \rangle}{\langle F_{shwl}^{NN}(t_2; p'; \Gamma_4) \rangle} &= \frac{\frac{Z_v |Z_b|^2}{4E_N(\vec{p}')^2 E_N(\vec{p})} e^{-E_N \vec{p} t_1} e^{-E_N \vec{p}' (t_2 - t_1)}}{\frac{|Z_b|^2}{2E_N(\vec{p}')} e^{-E_N \vec{p}' t_2}} \\ &= \frac{Z_v}{2E_N(\vec{p})} e^{-t_1 (E_N(\vec{p}) - E_N(\vec{p}'))}. \end{aligned} \quad (5.16)$$

The square root part is

$$\begin{aligned}\sqrt{A} &= \left[\frac{\frac{|Z_b|^2}{2E_N(\vec{p}')} e^{-E_N \vec{p}' t_1} \frac{|Z_b|^2}{2E_N(\vec{p}')} e^{-E_N \vec{p}' t_2} \frac{|Z_b|^2}{2E_N(\vec{p})} e^{-E_N \vec{p} (t_2 - t_1)}}{\frac{|Z_b|^2}{2E_N(\vec{p})} e^{-E_N \vec{p} t_1} \frac{|Z_b|^2}{2E_N(\vec{p})} e^{-E_N \vec{p} t_2} \frac{|Z_b|^2}{2E_N(\vec{p}')} e^{-E_N \vec{p}' (t_2 - t_1)}} \right]^{\frac{1}{2}}, \\ &= \left[\frac{E_N(\vec{p}) e^{-E_N \vec{p}' (t_1 + t_2)} e^{-E_N \vec{p} (t_2 - t_1)}}{E_N(\vec{p}') e^{-E_N \vec{p} (t_1 + t_2)} e^{-E_N \vec{p}' (t_2 - t_1)}} \right]^{\frac{1}{2}} = \left[\frac{E_N(\vec{p})}{E_N(\vec{p}')} e^{2t_1 (E_N(\vec{p}) - E_N(\vec{p}'))} \right]^{\frac{1}{2}}.\end{aligned}\quad (5.17)$$

Collecting the two parts, final definition of ratio becomes

$$\begin{aligned}R(t_2, t_1, p', p, \Gamma, \mu) &= \frac{Z_v}{2E_N(\vec{p})} e^{-t_1 (E_N(\vec{p}) - E_N(\vec{p}'))} \left[\frac{E_N(\vec{p})}{E_N(\vec{p}')} e^{2t_1 (E_N(\vec{p}) - E_N(\vec{p}'))} \right]^{\frac{1}{2}} \\ &\quad \langle \Omega | T [\chi_N^\alpha(x_2) J_\mu(x_1) \bar{\chi}_N^{\alpha'}(0)] | \Omega \rangle\end{aligned}\quad (5.18)$$

$$R(t_2, t_1, p', p, \Gamma, \mu) = \frac{Z_v}{2\sqrt{m_N E_N(\vec{p})}} \langle \Omega | T [\chi_N^\alpha(x_2) J_\mu(x_1) \bar{\chi}_N^{\alpha'}(0)] | \Omega \rangle. \quad (5.19)$$

In the large time limit, $t_2 - t_1 \gg a$ and $t_1 \gg a$, the time dependence of the correlators are eliminated and the ratio in Eq. (5.19) reduces to

$$R(t_2, t_1; p', p; \Gamma', \Gamma; \mu) \xrightarrow[t_1 \gg a]{t_2 - t_1 \gg a} \Pi(p', p; \Gamma', \Gamma; \mu). \quad (5.20)$$

The Sachs form factors can be extracted from the ratio by choosing particular combinations of the projection matrices Γ, Γ' and the Lorentz index μ ,

$$\Pi(p', p; \Gamma_4, \Gamma_4; \mu = 4) = \frac{1}{2} \sqrt{\frac{(E_{B'} + m_{B'})(E_B + m_B)}{E_B E_{B'}}} G_E(q^2), \quad (5.21)$$

$$\Pi(p', p; \Gamma_j, \Gamma_4; \mu = i) = \sqrt{\frac{(E_B + m_B)}{E_B E_{B'} (E_{B'} + m_{B'})}} G_M(q^2). \quad (5.22)$$

It should be noted that, when the incoming and the outgoing baryon states are identical, *i.e.* $B' = B$, the electric form factor $G_E(q^2 = 0)$ gives the electric charge of the baryon. As for the magnetic form factor, $G_M(q^2 = 0)$ gives the magnetic moment of the baryon when $B' = B$ and it gives the transition magnetic moment when $B' \neq B$. The details of calculations are explained in Appendix E.2.

In the broken flavor SU(3) symmetry, there is a mixing between Ξ_c and Ξ'_c baryons. Such mixing have been discussed to be negligibly small [128, 129], which was also confirmed by LQCD simulations [130]. The approximate SU(3) flavor symmetry and the heavy-

quark spin symmetry are the reasons for small $\Xi_c - \Xi'_c$ mixing. Therefore, in the calculations the small mixing effects are neglected.

5.1.1 Lattice Setup

We used the same Lattice setup in Chapter 4. Since the Ξ_c and Ξ'_c baryons have both light and strange quarks we have to generate both light and strange valance quarks. The hopping parameters are selected as $\kappa_{\text{val}}^{\ell} = \kappa_{\text{sea}}^{\ell} = 0.13781$ and $\kappa_{\text{val}}^s = \kappa_{\text{sea}}^s = 0.13640$ in order to be consistent with PACS-CS. Clover action is used for the calculating both valence quarks. Computations are performed using a modified version of CHROMA software system [1] on CPU clusters and with QUDA [2, 3] for propagator inversion on GPUs.

Table 5.1 The details of the gauge configurations used in the analysis [4]. N_s and N_t are the spatial and temporal sizes of the lattice, respectively, N_f is the number of flavors, a is the lattice spacing, L is the volume of the lattice, β is the inverse gauge coupling, c_{sw} is the Clover coefficient, κ_{sea}^f is the hopping parameter of the quark with flavor f and m_{π} is the pion mass.

$N_s \times N_t$	N_f	a (fm)	L (fm)	β
$32^3 \times 64$	2+1	0.0907(13)	2.90	1.90
c_{sw}	$\kappa_{\text{sea}}^{\ell}$	κ_{sea}^s	# of conf	m_{π} [MeV]
1.715	0.13781	0.13640	163	156(7)(2)

Positive and negative momenta in all spatial directions are inserted in order to increase statistics and to make a simultaneous fit over all data. Current is inserted along all spatial directions. The source-sink time separation is fixed to 12 lattice units (1.09 fm), which is enough to avoid excited state contaminations for electromagnetic form factors [30]. Multiple source-sink pairs are employed by shifting them 12 lattice units in the temporal direction. All statistical errors are estimated by the single-elimination jackknife analysis. Momentum is inserted up to nine units: $(|p_x|, |p_y|, |p_z|) = (0,0,0), (1,0,0), (1,1,0), (1,1,1), (2,0,0), (2,1,0), (2,1,1), (2,2,0), (2,2,1)$ and averaged over equivalent momenta. Point-split lattice vector current is considered

$$j_{\mu} = \frac{1}{2} [\bar{q}(x + \mu) U_{\mu}^{\dagger} (1 + \gamma_{\mu}) q(x) - \bar{q}(x) U_{\mu} (1 - \gamma_{\mu}) q(x + \mu)]. \quad (5.23)$$

Since point-split lattice vector current is conserved by Wilson fermions, renormalization is not needed. Wall-source/sink method [83], providing a simultaneous extraction of all spin, momentum and projection components of the correlators is applied. On the other hand, the wall source/sink is a gauge-dependent object which requires fixing the gauge. Gauge is fixed to Coulomb, which gives better coupling to the ground state than Landau. By using the wall method, first, the shell and wall propagators are computed regardless of the current and momenta inserted. Then, the propagators are contracted to obtain the three-point correlators.

5.2 Numerical Results

We follow similar procedure in Section 4.2 for ground-state masses of Ξ_c and Ξ'_c . We extracted using the two-point correlation functions in Eq. (5.5). We used shell smeared source and point sink (shpt) two-point correlation functions for clean signal. Since the data may have been correlated, Jackknife resampling method is used. Details of Jackknife method is given in Appendix A.3. The obtained results are in lattice units, they must be multiplied with inverse lattice spacing a^{-1} for the physical results.

The results are given in Figs. (5.1a, 5.1b). In Table 5.2 the results are given along with their experimental values and those of other lattice collaborations. Since results are obtained with near physical values of light-quark masses, chiral extrapolations are not made. The results for the baryon masses are different from the experimental values by only 2%, while there is a good agreement for the mass splitting $m_{\Xi'_c} - m_{\Xi_c}$. This small difference

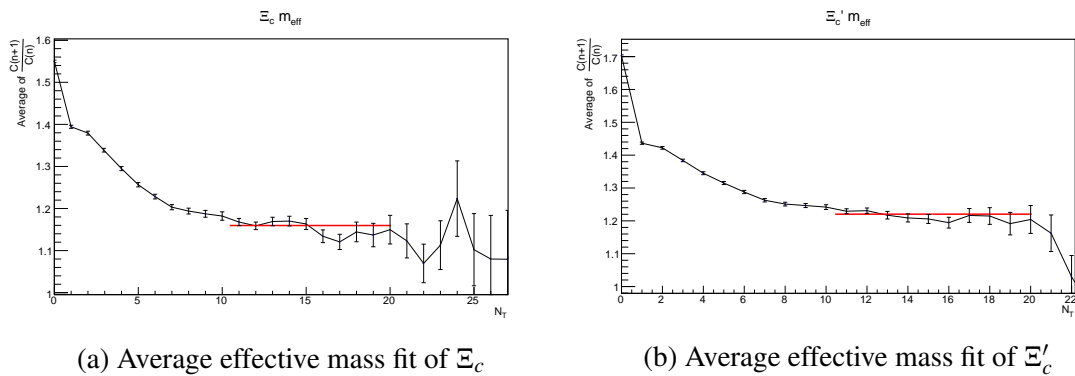


Figure 5.1 Effective mass plots of Ξ_c and Ξ'_c , red horizontal line indicates the fit region.

Table 5.2 The Ξ_c and Ξ'_c masses together with experimental values and those of other lattice collaborations.

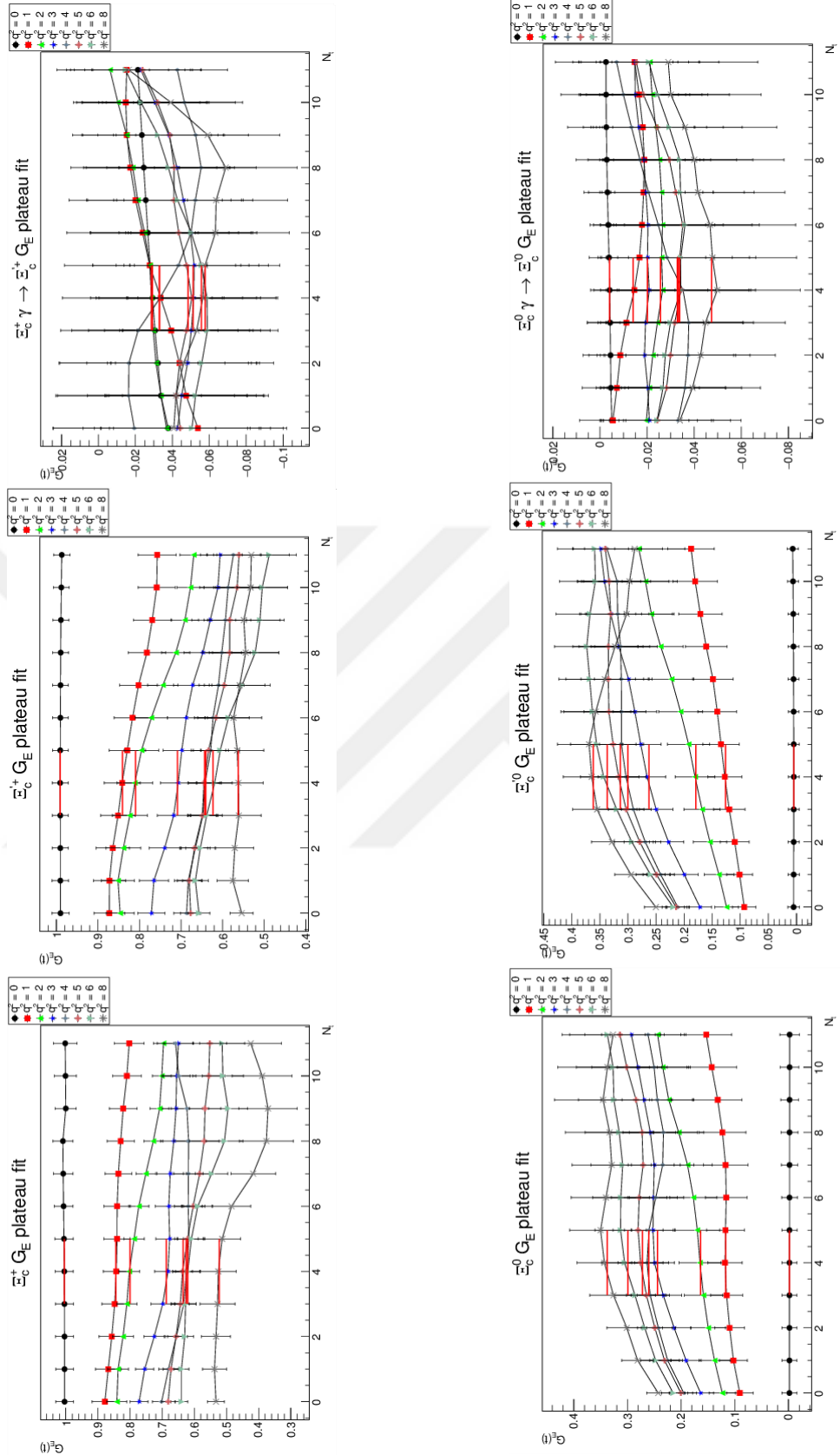
	This work	PACS-CS [38]	ETMC [5]	Briceno et al. [40]	Experiment [17]
m_{Ξ_c} [GeV]	2.519(15)	2.455(16)	2.469(28)	2.439(29)(25)(7)	2.470 (1)
$m_{\Xi'_c}$ [GeV]	2.646(17)	2.583(20)	2.542(27)	2.568(25)(12)(6)	2.577 (3)

can be attributed to Clover action, which is employed for the charm quarks. However, it has been confirmed in Ref. [131] that the mass of the triply charmed Ω_{ccc} baryon were calculated in very good agreement with other lattice determinations using relativistic heavy-quark actions. Such small discrepancy may be due to the choice of $\kappa_{\text{val}}^s = \kappa_{\text{sea}}^s = 0.13640$ which is chosen to be consistent with PACS-CS. This choice of κ values leads to an over-estimation of the $\Omega(sss)$ mass around 100 MeV as compared to its experimental value [4]. On the other hand, the form factor determinations are rather insensitive to mild changes in baryon masses, so at the current precision level and a discrepancy of 2% can be safely neglected.

The numerical calculation of $G_{E,M}(q^2)$ begins with constructing the ratio in Eq. (5.15). Next step is to extract the electric Sachs form factor (G_E) in Eq. (5.21). The selections are $\mu = 4$, $\Gamma' = 4$ and $\Gamma = 4$. At zero momentum transfer $q^2 = 0$, the electric Sachs form factor $G_E(q^2 = 0)$ gives the charge of the baryon. From experimental point of view there is a variation between source sink points for each configuration. Therefore, for each q^2 , the data must be plotted and fit the most probable ground state interval (see Figs. (5.2a) and (5.2b)).

Then G_E vs Q^2 plot can be drawn and it can be checked whether the plot fits the dipole form in Eq. (5.24). The form factors are calculated from individual quark contributions and the contributions combined using Eq. (5.25).

$$G_{E,M}(Q^2) = \frac{G_{E,M}(0)}{\left(1 + Q^2/\Lambda_{E,M}^2\right)^2}. \quad (5.24)$$



(a) Constant $G_E(t)$ fits of $\Xi_c^+ \gamma \rightarrow \Xi_c^+$, $\Xi_c^+ \gamma \rightarrow \Xi_c^+$ and $\Xi_c^+ \gamma \rightarrow \Xi_c^+$.

(b) Constant $G_E(t)$ fits of $\Xi_c^0 \gamma \rightarrow \Xi_c^0$, $\Xi_c^0 \gamma \rightarrow \Xi_c^0$ and $\Xi_c^0 \gamma \rightarrow \Xi_c^0$.

Figure 5.2 Constant fits for the electric form factors (a) Charged transitions of Ξ_c and Ξ_c' . (b) Neutral transitions of Ξ_c and Ξ_c' the fits made between 3-5 timesteps.

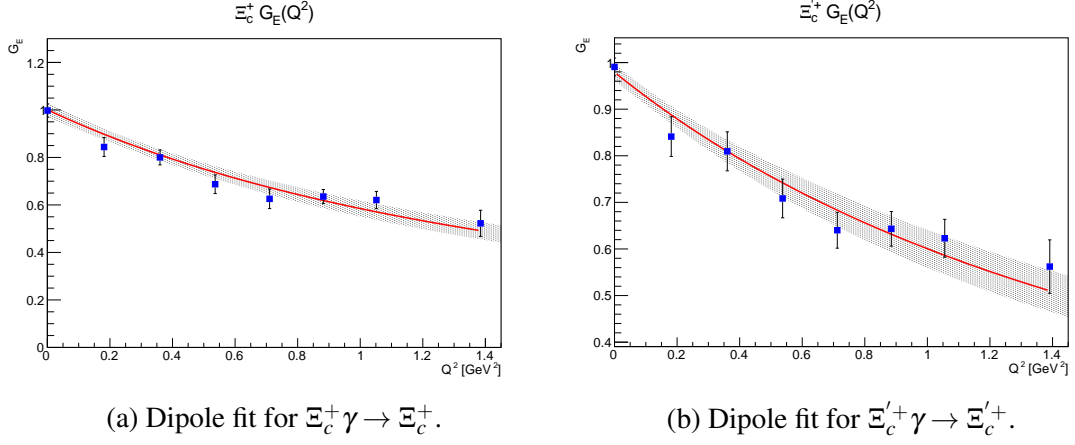


Figure 5.3 Dipole fits for Ξ_c' and Ξ_c . Red line indicates the fit function, black shadow indicates one σ error band.

The form factors can be calculated from individual quark contributions using

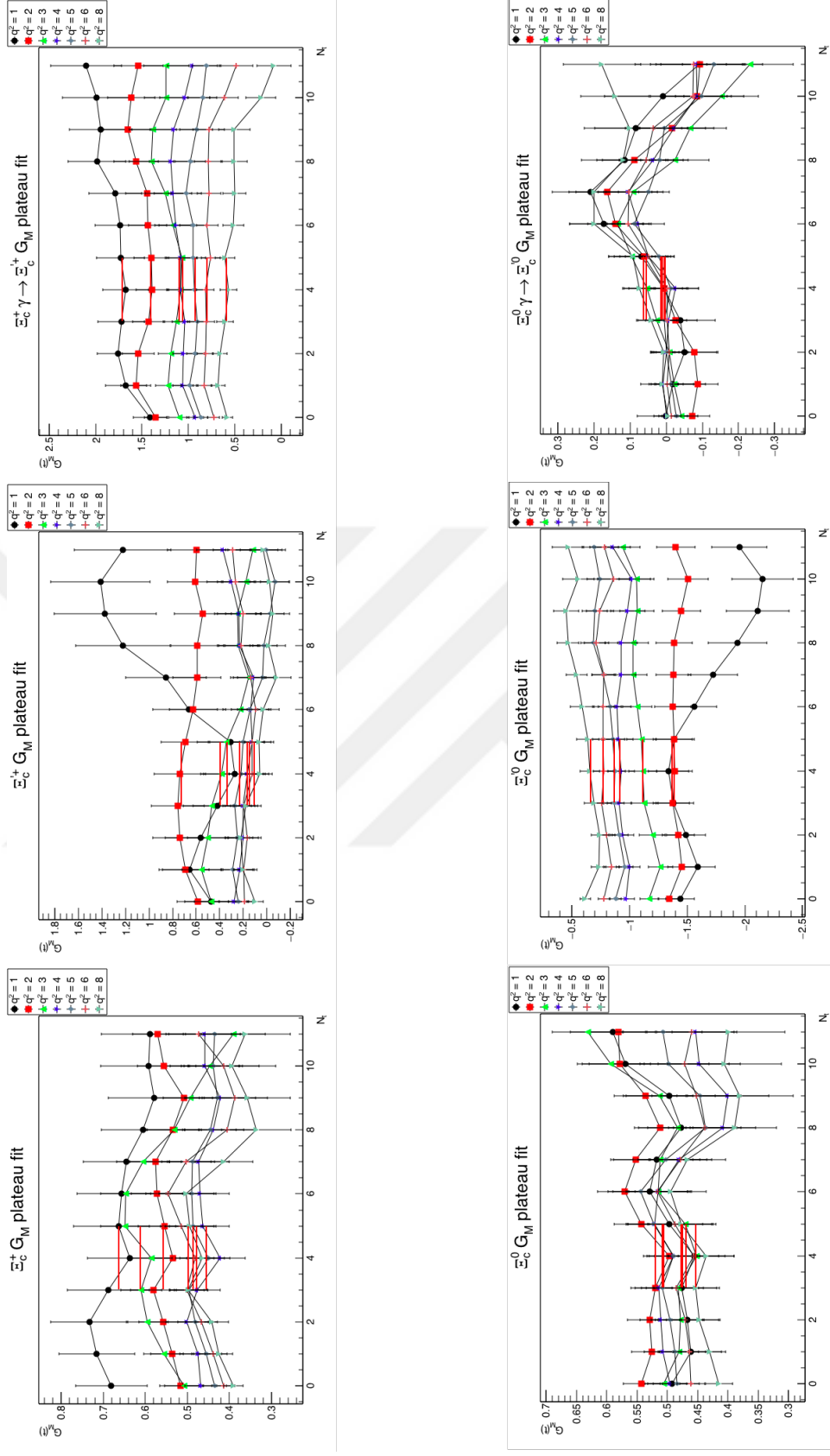
$$G_{E,M}(Q^2) = \frac{2}{3}G_{E,M}^c(Q^2) - \frac{1}{3}G_{E,M}^s(Q^2) + c_\ell G_{E,M}^\ell(Q^2), \quad (5.25)$$

where $c_\ell = -1/3$ for the d quark and $c_\ell = 2/3$ for the u quark.

In order to get G_M in Eq. (5.22) the selections are $\mu = i$, $\Gamma' = j$ and $\Gamma = 4$. Since there is Levi-Civita in Eq. (5.22) both i, j and k must be chosen differently. Similar to the $G_E(q^2)$ procedure weighted fit have to be applied between the most probable ground state interval Figs. (5.4a and 5.4b).

While the electric charge $G_E(0)$ can be computed directly with the formulation on the lattice magnetic form factor at zero momentum $G_M(0)$ cannot be directly measured. To this end, the dipole form in Eq. (5.24) is used to describe the Q^2 dependence of the form factors. The individual quark contributions are combined using Eq. (5.25) for each momentum transfer Q^2 , and extrapolated to $Q^2 = 0$.

In the SU(4) limit, each valence quark gives equal contributions to Ξ_c' form factors, similar to proton. However, SU(4) symmetry is badly broken and the quark contribution decreases as the quark mass increases. This is consistent with the observations in previous works on charmed baryons [83, 30, 131, 12]. This is also evident in Table 5.3, where individual contributions of u/d , s and c are listed separately for the transitions at all Q^2 . The heavy c -quark contribution is one order smaller than those of light u/d and s quarks.



(a) Constant $G_M(t)$ fits of $\Xi_c^+ \gamma \rightarrow \Xi_c^+$, $\Xi_c^+ \gamma \rightarrow \Xi_c^+$ and $\Xi_c^+ \gamma \rightarrow \Xi_c^+$. (b) Constant $G_M(t)$ fits of $\Xi_c^0 \gamma \rightarrow \Xi_c^0$, $\Xi_c^0 \gamma \rightarrow \Xi_c^0$ and $\Xi_c^0 \gamma \rightarrow \Xi_c^0$.

Figure 5.4 Constant fits for the electric form factors (a) Charged transitions of Ξ_c and Ξ_c' . (b) Neutral transitions of Ξ_c and Ξ_c' . The fits made between 3-5 timesteps.

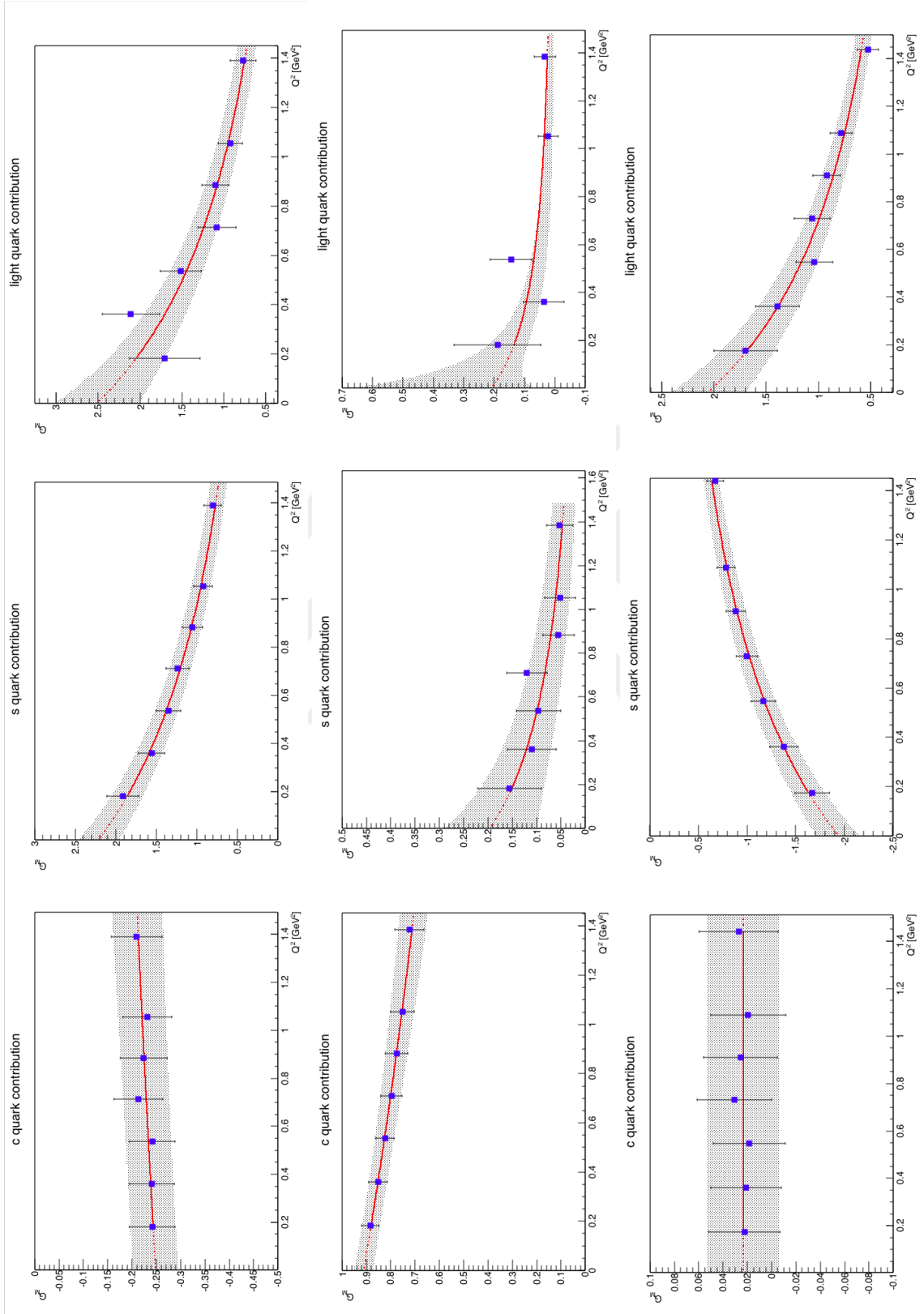


Figure 5.5 Individual quark (u/d , s and c) contributions of $\Xi'_c \gamma \rightarrow \Xi'_c$ (left), $\Xi_c \gamma \rightarrow \Xi_c$ (middle), $\Xi_c \gamma \rightarrow \Xi'_c$ (right) transitions. Black shadow indicates one σ error band.

Table 5.3 Individual quark contributions of $\Xi_c \gamma \rightarrow \Xi'_c$ transition to the magnetic form factor at different Q^2 values of all transitions.

Q^2 [GeV ²]		0	0.174	0.362	0.547
$\Xi_c \gamma \rightarrow \Xi'_c$	ℓ contr.	2.057(359)	1.696(304)	1.392(209)	1.040(176)
	s contr.	-1.943(223)	-1.669(179)	-1.378(148)	-1.169(127)
	c contr.	0.023(30)	0.022(29)	0.021(29)	0.018(29)
Q^2 [GeV ²]		0.730	0.911	1.089	1.439
$\Xi_c \gamma \rightarrow \Xi'_c$	ℓ contr.	1.062(171)	0.921(133)	0.783(105)	0.528(103)
	s contr.	-0.998(109)	-0.883(99)	-0.783(93)	-0.670(85)
	c contr.	0.031(30)	0.026(30)	0.019(31)	0.027(32)

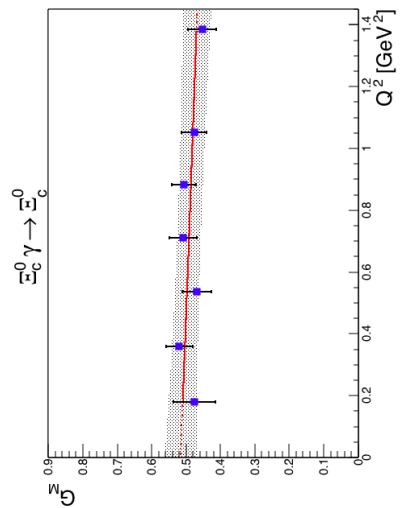
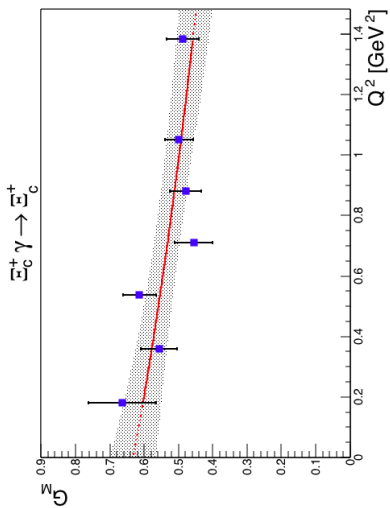
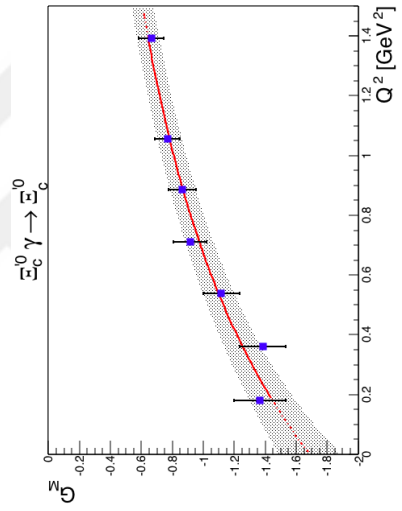
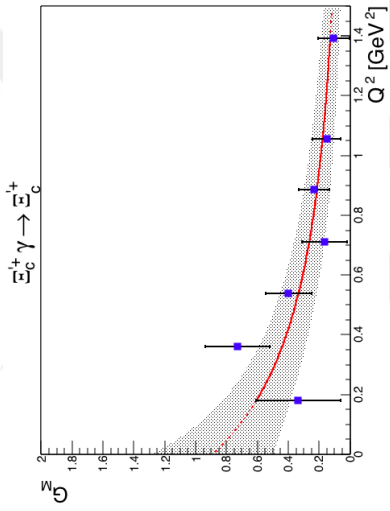
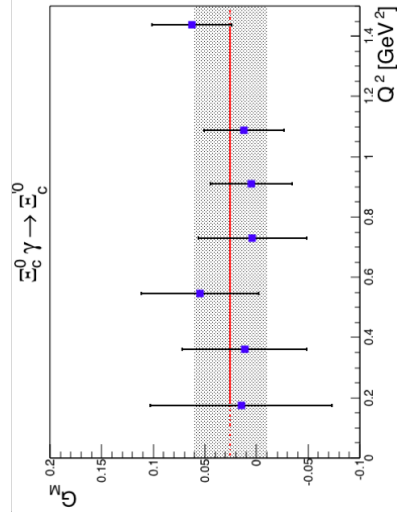
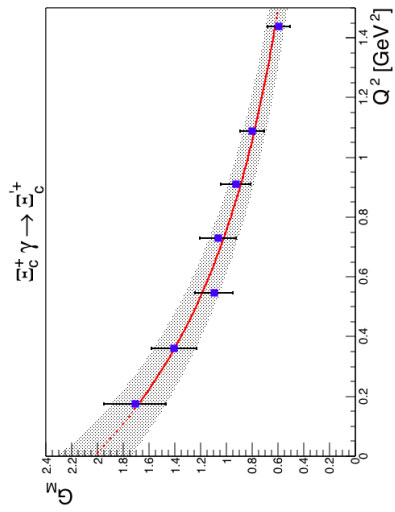
Table 5.4 Individual quark contributions of $\Xi_c \gamma \rightarrow \Xi_c$ transition to the magnetic form factor at different Q^2 values of all transitions.

Q^2 [GeV ²]		0	0.181	0.360	0.536
$\Xi_c \gamma \rightarrow \Xi_c$	ℓ contr.	0.209(272)	0.189(143)	0.038(67)	0.143(69)
	s contr.	0.195(91)	0.156(65)	0.110(50)	0.096(45)
	c contr.	0.912(39)	0.885(37)	0.853(37)	0.824(39)
Q^2 [GeV ²]		0.710	0.882	1.052	1.385
$\Xi_c \gamma \rightarrow \Xi_c$	ℓ contr.	-0.053(66)	-0.028(45)	0.023(32)	0.032(34)
	s contr.	0.120(41)	0.055(33)	0.052(31)	0.053(27)
	c contr.	0.796(44)	0.774(45)	0.752(49)	0.723(59)

This dominance of light quarks yields a soft core and the form factor decreases rapidly as Q^2 increases. Due to flavor asymmetry of Ξ_c baryon wave functions, the u/d - and s -quark contributions cancel each other to a great extent leading to a form factor dominantly determined by the c quark. This cancellation can be exact in the SU(3) symmetric limit. Since the Q^2 dependence of the Ξ_c form factors is controlled by the heavy c quark, it yields a hard core; and the form factor decreases less rapidly as Q^2 increases.

In the left two panels of Fig. (5.6a) and Fig. (5.6b), the magnetic form factors $G_M(Q^2)$ of the charged Ξ_c^+ , $\Xi_c'^+$ and neutral Ξ_c^0 , $\Xi_c'^0$ states are plotted as functions of Q^2 .

The light u/d - and s -quark contributions to the transition magnetic form factors of $\Xi_c \gamma \rightarrow$



(a) Q^2 dependence of the magnetic form factors of $\Xi_c^+ \gamma \rightarrow \Xi_c^+$, $\Xi_c'^+ \gamma \rightarrow \Xi_c'^+$ and $\Xi_c^+ \gamma \rightarrow \Xi_c^+$ (b) Q^2 dependence of the magnetic form factors of $\Xi_c^0 \gamma \rightarrow \Xi_c^0$, $\Xi_c'^0 \gamma \rightarrow \Xi_c'^0$ and $\Xi_c^0 \gamma \rightarrow \Xi_c^0$

Figure 5.6 Q^2 dependence of the magnetic form factors. Red line indicates the fit function, red dotted line indicates extrapolation. Black shadow indicates one σ error band.

Table 5.5 Individual contributions of $\Xi'_c \gamma \rightarrow \Xi'_c$ transition to the magnetic form factor at different Q^2 values of all transitions.

Q^2 [GeV ²]		0	0.181	0.360	0.537
$\Xi'_c \gamma \rightarrow \Xi'_c$	ℓ contr.	2.514(500)	1.703(421)	2.11(341)	1.515(245)
	s contr.	2.214(253)	1.913(200)	1.559(162)	1.348(148)
	c contr.	-0.249(47)	-0.241(468)	-0.241(46)	-0.242(47)
Q^2 [GeV ²]		0.712	0.885	1.056	1.391
$\Xi'_c \gamma \rightarrow \Xi'_c$	ℓ contr.	1.081(229)	1.098(162)	0.921(144)	0.772(153)
	s contr.	1.233(146)	1.054(127)	0.923(116)	0.804(108)
	c contr.	-0.213(50)	-0.224(48)	-0.232(49)	-0.209(52)

Ξ'_c are equal in magnitude and opposite in sign. On the other hand, the c quark has almost no effect. When the quark contributions are combined using the formula in Eq. (5.25), the u and s contributions to $\Xi'_c \gamma \rightarrow \Xi'_c$ have opposite signs, and they are multiplied with electric charges of opposite sign and add constructively. In contrast, the neutral transition $\Xi_c^0 \gamma \rightarrow \Xi_c^0$ is highly suppressed as a result of equal electric charges of the d and s quarks. According to U-spin flavor symmetry, assuming a degeneracy between two equally charged d and s quarks, a transition from Ξ_c^0 to Ξ_c^0 is forbidden. The results are in agreement with the prediction of U-spin flavor symmetry. As shown in Fig. (5.6b), the magnetic form factor of $\Xi_c^0 \gamma \rightarrow \Xi_c^0$ neutral transition is consistent with zero.

The finite-size effects should be negligible when $m_\pi L \geq 4$. On the other hand, in the $\kappa^\ell = 0.13781$ configurations used in the analysis, $m_\pi L = 2.3$ which is below the empirical bound. However, previous studies confirmed that the finite-size effects on this particular setup is under control for physical quantities related to strange and charmed baryons [131]. As discussed above, the magnetic form factor of $\Xi_c^0 \gamma \rightarrow \Xi_c^0$ should vanish due to U-spin flavor symmetry that assumes a degeneracy between d - and s -quarks. This is revealed in numerical calculations when the d - and s -quark contributions cancel each other so that the magnetic form factor is consistent with zero as shown in Fig. (5.6b). This indicates that the finite-size effects on the light quarks are either similar as compared to those of strange and charmed quarks. Any unaccounted effect is already hidden in the

statistical error of extracted quantities .

Table 5.6 The combined form factor as obtained using Eq. (5.25) and extrapolated to $Q^2 = 0$, together with the magnetic moments in units of nuclear magneton.

Transition	$G_M(0)$	Magnetic moment[μ_N]
$\Xi_c^+ \gamma \rightarrow \Xi_c^+$	0.631(68)	0.235(25)
$\Xi_c^0 \gamma \rightarrow \Xi_c^0$	0.516(46)	0.192(17)
$\Xi_c'^+ \gamma \rightarrow \Xi_c'^+$	0.889(397)	0.315(141)
$\Xi_c'^0 \gamma \rightarrow \Xi_c'^0$	-1.689(201)	-0.599(71)
$\Xi_c^+ \gamma \rightarrow \Xi_c'^+$	2.027(286)	0.729(103)
$\Xi_c^0 \gamma \rightarrow \Xi_c'^0$	0.025(36)	0.009(13)

Using the values of the magnetic form factors at $Q^2 = 0$ in Table 5.6, the magnetic moments are calculated in nuclear magnetons by using

$$\mu_B = G_M(0)(e/2m_B) = G_M(0)(m_N/m_B)\mu_N, \quad (5.26)$$

where m_N is the physical nucleon mass and m_B is the baryon mass obtained on the lattice. In Table 5.6, the magnetic moments are calculated using $G_M(0)$ in units of nuclear magneton.

The decay width of Ξ_c' baryon is related to the Pauli form factor $F_2(0)$ of $\Xi_c \gamma \rightarrow \Xi_c'$:

$$\Gamma_{B\gamma \rightarrow B'} = \frac{4 \alpha |\vec{q}|^3}{(m_{B'} + m_B)^2} |F_2(0)|^2 \quad \text{with} \quad |\vec{q}| = \frac{(m_{B'}^2 - m_B^2)}{2m_{B'}}. \quad (5.27)$$

In order to extract $F_2(0)$ from the Sachs form factors $G_E(Q^2)$ and $G_M(Q^2)$, the two equations in Eqs. (5.3) and (5.4) are solved simultaneously for all lattice data and extrapolated to $Q^2 = 0$. At zero momentum transfer, $G_E(0) = F_1(0)$ and obviously, if $F_1(0)$ is not zero, it is a very small value. Since $\Xi_c \gamma \rightarrow \Xi_c'$ cannot occur through electric transition, this implies $G_M(0) \simeq F_2(0)$. Consistently the Pauli form factors are

$$F_2(0) = 2.036(280) \quad \text{for} \quad \Xi_c^+ \gamma \rightarrow \Xi_c'^+, \quad (5.28)$$

$$F_2(0) = 0.039(46) \quad \text{for} \quad \Xi_c^0 \gamma \rightarrow \Xi_c'^0. \quad (5.29)$$

Using the formula in Eq. (5.27), the decay widths of Ξ_c baryons are obtained as follows:

$$\Gamma_{\Xi_c'^+} = 5.468(1.500) \text{ keV}, \quad \Gamma_{\Xi_c'^0} = 0.002(4) \text{ keV}. \quad (5.30)$$

The decay width can be translated into a lifetime using $\tau = \frac{1}{\Gamma}$;

$$\tau_{\Xi_c'^+} = 1.148(322) \times 10^{-19} \text{ s}. \quad (5.31)$$

Both neutral and charged transitions of $\Xi_c \gamma \rightarrow \Xi_c'$ were previously studied using QCD sum rules [132], heavy hadron chiral perturbation theory [133, 134, 135, 136, 137], quark model [138, 127] and bag model [139]. For the charged transition, lattice results for the transition form factor and decay width are in agreement with those from QCD sum rules [132], while other methods were predicted higher values. In the case of neutral transition, their predictions for the transition form factors were small but finite, while no signal is found on the lattice.

RESULTS AND DISCUSSION

Recent experimental observations of all the ground-state heavy baryons as predicted by the quark model makes it timely to study the structure and decays of these hadrons with theoretical methods. Baryons containing heavy quarks are interesting both from the theoretical and experimental points of view. Because the charm quark masses are greater than the intrinsic energy scale of QCD, approximate heavy-quark flavor and spin symmetries constrain the dynamics of heavy baryons [130]. The electromagnetic transitions of charmed baryons have been studied within QCD sum rules [132], heavy hadron chiral perturbation theory [133, 134, 135, 136, 137], quark model [138, 127] and bag model [139]. However the only method we know that provides a first-principles calculation of hadronic phenomena is LQCD, which is a valuable tool to determine the hadron form factors in a model-independent way [140]. State-of-the-art LQCD calculations can provide direct comparison with experiment [115]. In this thesis, we studied radiative transitions of $\Omega_c \gamma \rightarrow \Omega_c^*$ and $\Xi_c \gamma \rightarrow \Xi_c'$ in Lattice QCD. We have calculated form factors and extracted the decay width.

The existence of Ω_c has been predicted by the quark model, however experimental information about the Ω_c spectrum has been limited during the past decades. The literature on $\Xi_c \gamma \rightarrow \Xi_c'$ transition is also limited. Being motivated by the limited literature of these charmed baryons in the radiative decay mode, we focused on electromagnetic transition of single charmed baryons in LQCD. The results can shed light on the BEPCII, BES-III, the LHC and PANDA experiments which will help further investigate the heavy-baryon spectrum.

We first studied $\Omega_c \gamma \rightarrow \Omega_c^*$ transition. Since both Ω_c and Ω_c^* have s and c valance quarks it is relatively easy to make calculation on the lattice. The analysis was employed with near physical 2+1-flavor lattices that correspond to a pion mass of approximately 156 MeV. The $\Omega_c \gamma \rightarrow \Omega_c^*$ transition gives rise to three transition form factors, namely, the magnetic dipole ($M1$), the electric quadrupole ($E2$) and the electric charge quadrupole ($C2$). The data for electromagnetic transition form factors are noisier than those for elastic form factors, particularly for $C2$ form factor. Considering the analysis is done with limited number of gauge configurations at the smallest quark mass, $M1$ and $E2$ form factors are calculated for the lowest allowed lattice momentum transfer. The transition form factors at zero-momentum transfer are computed by assuming a simple scaling at low momentum transfer. The dominant contribution comes from the magnetic dipole form factor. The electric quadrupole transition is found in consistency with the quark model which is insignificantly small. Since strong decay channel is kinematically forbidden, the total decay width of Ω_c^* is almost entirely in terms of the photon decay mode. Eventually a significantly suppressed value of the Ω_c^* baryon decay width makes the Ω_c^* one of the longest living spin-3/2 charmed hadrons. The suppression in the decay width mainly attributed to the small mass splitting. The decay width is translated into a lifetime of $\tau = 1/\Gamma = 8.901(913) \times 10^{-18}$ sec. This transition is of particular interest because of its relevance to current and proposed experimental facilities such as LHCb, PANDA, Belle II, BESIII and J-PARC, which are expected to measure the electromagnetic decay widths of charmed baryons with a higher precision.

The $\Xi_c \gamma \rightarrow \Xi_c'$, $\Xi_c' \gamma \rightarrow \Xi_c'$, and $\Xi_c \gamma \rightarrow \Xi_c$ transitions are studied in 2+1-flavor LQCD. The magnetic Sachs and Pauli form factors have been extracted which gives the Ξ_c - Ξ_c' transition magnetic moment and the decay widths of Ξ_c' baryons. Individual quark contributions to the magnetic moments have been determined, which give an invaluable insight to the dynamics of u/d , s and c quarks having masses at different scales. In the case of Ξ_c' baryons the heavy quark contribution is much smaller than light quarks. On the other hand, due to antisymmetric flavor wave functions of the Ξ_c baryons, the u/d - and s -quark contributions cancel each other to a great extent leading to a form factor that is mostly

determined by heavy c quark. Using the Pauli form factor $F_2(Q^2 = 0)$, the decay widths of Ξ'_c baryons are extracted. The decay width of the charged Ξ'_c baryon on the lattice is determined as $\Gamma_{\Xi'_c^+} = 5.468(1.500)$ keV and no signal found for the neutral transition $\Xi_c^0 \gamma \rightarrow \Xi_c'^0$, which is suppressed by the U-spin flavor symmetry.

For future work we are planning to make chiral extrapolation with different light quark hopping parameters, $\kappa_{sea} = (0.13700, 0.13727, 0.13754, 0.13770)$ including the near physical $\kappa_{sea} = 0.13781$. This may be a good start to determine the systematic error concealed in statistical errors in the calculations. Moreover performing the simulations on lattices with different size will help us determine the systematic error which comes from finite lattice size effects. Examining the radiative charmed transitions that have not been observed by experiments may help to better understand the heavy quark effect. Finally, a breaking of the U-spin symmetry and a detailed examination of U-spin symmetry breaking might be an interesting study on lattice.

REFERENCES

- [1] Edwards, R. G. and Joo, B., (2005). “The Chroma software system for lattice QCD”, Nucl. Phys. Proc. Suppl., 140: 832.
- [2] Babich, R., Clark, M., Joo, B., Shi, G., Brower, R. and others, , (2011). “Scaling Lattice QCD beyond 100 GPUs”, .
- [3] Clark, M. A., Babich, R., Barros, K., Brower, R. C. and Rebbi, C., (2010). “Solving Lattice QCD systems of equations using mixed precision solvers on GPUs”, Comput. Phys. Commun., 181: 1517-1528.
- [4] Aoki, S., Ishikawa, K.-I., Ishizuka, N., Izubuchi, T., Kadoh, D., Kanaya, K., Kuramashi, Y., Namekawa, Y., Okawa, M., Taniguchi, Y., Ukawa, A., Ukita, N. and Yoshié, T., (2009). “2+1 Flavor Lattice QCD toward the Physical Point”, Phys. Rev. D, 79: 034503.
- [5] Alexandrou, C., Drach, V., Jansen, K., Kallidonis, C. and Koutsou, G., (2014). “Baryon spectrum with $N_f = 2 + 1 + 1$ twisted mass fermions”, Phys. Rev., D90: 074501.
- [6] Leinweber, D. B., Draper, T. and Woloshyn, R. M., (1993). “Baryon octet to decuplet electromagnetic transitions”, Phys. Rev., D48: 2230-2249.
- [7] Alexandrou, C., (2007). “Hadron deformation and form-factors from lattice QCD”, AIP Conf. Proc., 904: 49-64.
- [8] Richard, J.-M., (2012). “An introduction to the quark model”, Ferrara International School Niccolo Cabeo 2012: Hadronic spectroscopy Ferrara, Italy, May 21-26, 2012.
- [9] Colangelo, P. and Khodjamirian, A., (2012). QCD Sum Rules, a Modern Perspective, World Scientific.
- [10] Neubert, M., (2005). “Effective field theory and heavy quark physics”, Physics in $D \geq 4$. Proceedings, Theoretical Advanced Study Institute in elementary particle physics, TASI 2004, Boulder, USA, June 6-July 2, 2004.
- [11] Lepage, G. P., (1998). “Lattice QCD for novices”, Strong interactions at low and intermediate energies. Proceedings, 13th Annual Hampton University Graduate Studies, HUGS’98, Newport News, USA, May 26-June 12, 1998.

- [12] Bahtiyar, H., Can, K. U., Erkol, G. and Oka, M., (2015). “ $\Omega_c \gamma \rightarrow \Omega_c^*$ transition in lattice QCD”, Phys. Lett., B747: 281-286.
- [13] Bahtiyar, H., Can, K. U., Erkol, G., Oka, M. and Takahashi, T. T., (2016). “ $\Xi_c \gamma \rightarrow \Xi_c'$ transition in lattice QCD”, 1612.05722 (in Press), .
- [14] Shifman, M. A., Vainshtein, A. I. and Zakharov, V. I., (1979). “QCD and Resonance Physics. Theoretical Foundations”, Nucl. Phys., B147: 385-447.
- [15] Weinberg, S., (1979). “Phenomenological Lagrangians”, Physica, A96: 327-340.
- [16] Wilson, K. G., (1974). “Confinement of Quarks”, Phys. Rev., D10: 2445-2459.
- [17] Patrignani, C. and others, , (2016). “Review of Particle Physics”, Chin. Phys., C40: 100001.
- [18] Solovieva, E. and others, , (2009). “Study of Ω_c^0 and Ω_c^{*0} Baryons at Belle”, Phys. Lett., B672: 1-5.
- [19] Aubert, B. and others, , (2006). “Observation of an excited charm baryon Ω_c^* decaying to $\Omega_c^0 \gamma$ ”, Phys. Rev. Lett., 97: 232001.
- [20] Buchmann, A. J. and Henley, E. M., (2001). “Intrinsic quadrupole moment of the nucleon”, Phys. Rev., C63: 015202.
- [21] Mertz, C. and others, , (2001). “Search for quadrupole strength in the electroexcitation of the $\Delta(1232)$ ”, Phys. Rev. Lett., 86: 2963-2966.
- [22] Joo, K. and others, , (2002). “ Q^2 dependence of quadrupole strength in the $\gamma^* p \rightarrow \Delta^+(1232) \rightarrow p\pi^0$ transition”, Phys. Rev. Lett., 88: 122001.
- [23] Isgur, N., Karl, G. and Koniuk, R., (1982). “D waves in the nucleon: A test of color magnetism”, Phys. Rev. D, 25: 2394–2398.
- [24] Biagi, S. F. and others, , (1983). “Observation of a Narrow State at $2.46 - GeV/c^2$: A Candidate for the Charmed Strange Baryon A^+ ”, Phys. Lett., B122: 455.
- [25] Coteus, P. and others, , (1987). “Production of the Charmed Strange Baryon Ξ_c^+ by Neutrons”, Phys. Rev. Lett., 59: 1530.
- [26] Alam, M. S. and others, , (1989). “Measurement of the Isospin Mass Splitting $\Xi^+(c)\Xi^0(c)$ ”, Phys. Lett., B226: 401-404.
- [27] Jessop, C. P. and others, , (1999). “Observation of two narrow states decaying into $\Xi^+(c)\gamma$ and $\Xi^0(c)\gamma$ ”, Phys. Rev. Lett., 82: 492-496.
- [28] The BABAR Collaboration, and Aubert, B., (2006). “ Ξ_c' Production at BABAR”, ArXiv High Energy Physics - Experiment e-prints, .
- [29] Yelton, J. and others, , (2016). “Study of Excited Ξ_c States Decaying into Ξ_c^0 and Ξ_c^+ Baryons”, Phys. Rev., D94: 052011.

- [30] Can, K. U., Erkol, G., Isildak, B., Oka, M. and Takahashi, T. T., (2014). “Electromagnetic structure of charmed baryons in Lattice QCD”, JHEP, 05: 125.
- [31] Ziegler, V., (2011). “Charm baryon results from BaBar”, AIP Conf. Proc., 1374: 577-580.
- [32] Li, L., (2016). “Charm studies at Belle experiment”, J. Univ. Sci. Tech. China, 46: 347-357.
- [33] Yelton, J., (2000). “Recent CLEO results on charmed baryon spectroscopy”, AIP Conf. Proc., 549: 588-592.
- [34] Ogilvy, S., (2015). “Charmed baryons from LHCb”, 7th International Workshop on Charm Physics.
- [35] Aaij, R. and others, , (2017). “Observation of five new narrow Ω_c^0 states decaying to $\Xi_c^+ K^-$ ”, Phys. Rev. Lett., 118: 182001.
- [36] Lewis, R., Mathur, N. and Woloshyn, R. M., (2001). “Charmed baryons in lattice QCD”, Phys. Rev., D64: 094509.
- [37] Mathur, N., Lewis, R. and Woloshyn, R. M., (2002). “Charmed and bottom baryons from lattice NRQCD”, Phys. Rev., D66: 014502.
- [38] Namekawa, Y. and others, , (2013). “Charmed baryons at the physical point in 2+1 flavor lattice QCD”, Phys. Rev., D87: 094512.
- [39] Alexandrou, C., Carbonell, J., Christaras, D., Drach, V., Gravina, M. and Papinutto, M., (2012). “Strange and charm baryon masses with two flavors of dynamical twisted mass fermions”, Phys. Rev., D86: 114501.
- [40] Briceno, R. A., Lin, H.-W. and Bolton, D. R., (2012). “Charmed-Baryon Spectroscopy from Lattice QCD with $N_f = 2 + 1 + 1$ Flavors”, Phys. Rev., D86: 094504.
- [41] Alexandrou, C., Koutsou, G., Negele, J. W. and Tsapalis, A., (2006). “The Nucleon electromagnetic form factors from Lattice QCD”, Phys. Rev., D74: 034508.
- [42] Alexandrou, C., Brinet, M., Carbonell, J., Constantinou, M., Guichon, P., Harraud, P. A., Jansen, K., Kallidonis, C., Korzec, T. and Papinutto, M., (2011). “Nucleon form factors and moments of parton distributions in twisted mass lattice QCD”, PoS, EPS-HEP2011: 308.
- [43] Erkol, G., Oka, M. and Takahashi, T. T., (2010). “Axial Charges of Octet Baryons in Two-flavor Lattice QCD”, Phys. Lett., B686: 36-40.
- [44] Alexandrou, C. and Koutsou, G., (2007). “Pion and ρ -meson form-factors using four-point functions in $N_F = 2$ QCD”, PoS, LAT2007: 150.
- [45] Takahashi, T. T., Erkol, G. and Oka, M., (2010). “Pseudoscalar-Meson Octet-Baryon Coupling Constants from two-flavor Lattice QCD”, Nucl. Phys., A835: 346-349.

- [46] Aoki, S., Cossu, G., Feng, X., Hashimoto, S., Kaneko, T., Noaki, J. and Onogi, T., (2016). “Light meson electromagnetic form factors from three-flavor lattice QCD with exact chiral symmetry”, *Phys. Rev.*, D93: 034504.
- [47] Oka, M., Erkol, G. and Takahashi, T. T., (2009). “Recent QCD results on the strange hadron systems”, *PoS*, CD09: 021.
- [48] Can, K. U., Erkol, G., Isildak, B., Oka, M. and Takahashi, T. T., (2013). “Electromagnetic properties of doubly charmed baryons in Lattice QCD”, *Phys. Lett.*, B726: 703-709.
- [49] Can, K. U., Erkol, G., Oka, M. and Takahashi, T. T., (2017). “ $\Lambda_c \Sigma_c \pi$ coupling and $\Sigma_c \rightarrow \Lambda_c \pi$ decay in lattice QCD”, *Phys. Lett.*, B768: 309-316.
- [50] Griffiths, D. J., (2008). *Introduction to elementary particles*; 2nd rev. version, Wiley, New York, NY.
- [51] Fiedler, F., (2005). “Top quark production and properties at the Tevatron”, *Les Rencontres de physique de la Vall’ee d’Aoste*, results and perspectives in particle physics, La Thuile, Aoste Valley, February 27 - March 5, 2005.
- [52] Kodama, K. and others, , (2001). “Observation of tau neutrino interactions”, *Phys. Lett.*, B504: 218-224.
- [53] Chatrchyan, S. and others, , (2012). “Observation of a new boson at a mass of 125 GeV with the CMS experiment at the LHC”, *Phys. Lett.*, B716: 30-61.
- [54] Purcell, A., CERN Webfest, http://cds.cern.ch/record/1473657/files/SMinfographic_image.png, 05 May 2017.
- [55] Tong, D., *Quantum Field Theory Lecture notes*, <http://www.damtp.cam.ac.uk/user/tong/qft.html>, 05 October 2016.
- [56] Gasser, J. and Leutwyler, H., (1985). “Chiral Perturbation Theory: Expansions in the Mass of the Strange Quark”, *Nucl. Phys.*, B250: 465-516.
- [57] Durr, S. and others, , (2008). “Ab-Initio Determination of Light Hadron Masses”, *Science*, 322: 1224-1227.
- [58] Blossier, B., Boucaud, P., Brinet, M., De Soto, F., Du, X., Morenas, V., Pene, O., Petrov, K. and Rodriguez-Quintero, J., (2012). “The Strong running coupling at τ and Z_0 mass scales from lattice QCD”, *Phys. Rev. Lett.*, 108: 262002.
- [59] M. Creutz, C. R., (1979). “Monte Carlo study of Abelian lattice gauge theories”, *Phys. Rev. Lett.*, 20: 1915-1922.
- [60] DeGrand, T. A., (1996). “Nonperturbative quantum field theory on the lattice”, *Fields, strings and duality. Proceedings, Summer School, Theoretical Advanced Study Institute in Elementary Particle Physics, TASI’96, Boulder, USA, June 2-28, 1996.*
- [61] Feynman, R. P. and Hibbs, A. R., (1965). *Quantum mechanics and path integrals*, McGraw-Hill, New York, St. Louis, San Francisco.

- [62] Zee, A., (2003). Quantum Field Theory in a Nutshell, Princeton Univ. Press. Princeton, NJ.
- [63] Hausdorff, F., (1906). “Die symbolische Exponentialformel in der Gruppentheorie”, Ber. Verh. Kgl. Sächs. Ges. Wiss. Leipzig., Math.-phys. Kl., 58: 19-48.
- [64] Kogut, J. B. and Susskind, L., (1975). “Hamiltonian Formulation of Wilson’s Lattice Gauge Theories”, Phys. Rev., D11: 395-408.
- [65] Frezzotti, R., Grassi, P. A., Sint, S. and Weisz, P., (2000). “A Local formulation of lattice QCD without unphysical fermion zero modes”, Nucl. Phys. Proc. Suppl., 83: 941-946.
- [66] Frezzotti, R., Grassi, P. A., Sint, S. and Weisz, P., (2001). “Lattice QCD with a chirally twisted mass term”, JHEP, 08: 058.
- [67] Frezzotti, R., Sint, S. and Weisz, P., (2001). “O(a) improved twisted mass lattice QCD”, JHEP, 07: 048.
- [68] Kaplan, D. B., (1992). “A Method for simulating chiral fermions on the lattice”, Phys. Lett., B288: 342-347.
- [69] Furman, V. and Shamir, Y., (1995). “Axial symmetries in lattice QCD with Kaplan fermions”, Nucl. Phys., B439: 54-78.
- [70] Shamir, Y., (1993). “Chiral fermions from lattice boundaries”, Nucl. Phys., B406: 90-106.
- [71] Rothe, H. J., (2005). Lattice Gauge Theories: An Introduction; 3rd ed., World Scientific. Singapore.
- [72] Gattringer, C. and Lang, C. B., (2009). Quantum Chromodynamics on the Lattice: An Introductory Presentation, Springer.
- [73] Hasenfratz, A., Kunszt, Z., Hasenfratz, P. and Lang, C. B., (1982). “Hopping Parameter Expansion for the Meson Spectrum in SU(3) Lattice QCD”, Phys. Lett., B110: 289.
- [74] Symanzik, K., (1983). “Continuum Limit and Improved Action in Lattice Theories. 1. Principles and ϕ^4 Theory”, Nucl. Phys., B226: 187-204.
- [75] Symanzik, K., (1983). “Continuum Limit and Improved Action in Lattice Theories. 2. O(N) Nonlinear Sigma Model in Perturbation Theory”, Nucl. Phys., B226: 205-227.
- [76] Wu, C. S., Ambler, E., Hayward, R. W., Hoppes, D. D. and Hudson, R. P., (1957). “Experimental Test of Parity Conservation in Beta Decay”, Physical Review, 105: 1413-1415.
- [77] Aitchison, I. and Hey, A., (2002). Gauge Theories in Particle Physics, 1, IOP.
- [78] Gupta, R., (1997). “Introduction to lattice QCD: Course”, Probing the standard model of particle interactions. Proceedings, Summer School in Theoretical Physics, NATO Advanced Study Institute, 68th session, Les Houches, France, July 28-September 5, 1997. Pt. 1, 2.

- [79] Lin, H.-W. and Meyer, H. B., (2015). Lattice QCD for Nuclear Physics, 889, Springer.
- [80] Milford, F. J., (1955). “Projection Operator for the Rarita-Schwinger Equation”, Phys. Rev., 98: 1488–1488.
- [81] Metropolis, N., Rosenbluth, A. W., Rosenbluth, M. N., Teller, A. H. and Teller, E., (1953). “Equation of state calculations by fast computing machines”, J. Chem. Phys., 21: 1087-1092.
- [82] Gusken, S., (1990). “A Study of smearing techniques for hadron correlation functions”, Nucl. Phys. Proc. Suppl., 17: 361-364.
- [83] Can, K. U., Erkol, G., Oka, M., Ozpineci, A. and Takahashi, T. T., (2013). “Vector and axial-vector couplings of D and D* mesons in 2+1 flavor Lattice QCD”, Phys. Lett., B719: 103-109.
- [84] Di Pierro, M., El-Khadra, A. X., Gottlieb, S. A., Kronfeld, A. S., Mackenzie, P. B., Okamoto, M., Oktay, M. B. and Simone, J. N., (2004). “www.fermiqcd.net”, Nucl. Phys. Proc. Suppl., 129: 832-834.
- [85] Jung, C., (2014). “Overview of Columbia Physics System”, PoS, Lattice2013: 417.
- [86] Gottlieb, S. A. and Tamhankar, S., (2001). “Benchmarking MILC code with OpenMP and MPI”, Nucl. Phys. Proc. Suppl., 94: 841-845.
- [87] Wong, S. S. M., (1998). Introductory Nuclear Physics, New York, USA: Wiley (1998).
- [88] Bloom, E. D., Coward, D. H., Destaebler, H., Drees, J., Miller, G., Mo, L. W., Taylor, R. E., Breidenbach, M., Friedman, J. I., Hartmann, G. C. and Kendall, H. W., (1969). “High-Energy Inelastic e-p Scattering at 6° and 10° ”, Physical Review Letters, 23: 930-934.
- [89] Schwartz, M., (2013). Quantum Field Theory and the Standard Model, Cambridge University Press.
- [90] Ernst, F. J., Sachs, R. G. and Wali, K. C., (1960). “Electromagnetic form factors of the nucleon”, Phys. Rev., 119: 1105-1114.
- [91] Jones, H. and Scadron, M., (1973). “Multipole N to Delta form factors and resonant photo- and electroproduction”, Annals of Physics, 81: 1 - 14.
- [92] Wilcox, W., Draper, T. and Liu, K.-F., (1992). “Chiral limit of nucleon lattice electromagnetic form-factors”, Phys. Rev., D46: 1109-1122.
- [93] Ukita, N. and others, , (2008). “2+1 flavor lattice QCD simulation with $O(a)$ -improved Wilson quarks”, PoS, Lattice2008: 097.
- [94] Wang, M.-Z., (2016). “Study of Baryon Production at Belle and BaBar”, Nucl. Part. Phys. Proc., 273-275: 2091-2096.

- [95] Avery, P. and others, , (1989). “Observation of the Charmed Strange Baryon Ξ_c^0 ”, Phys. Rev. Lett., 62: 863.
- [96] Naik, P., (2016). “Charmed baryons at LHCb”, PoS, Charm2016: 047.
- [97] Cheng, H.-Y., (2015). “Charmed Baryons Circa 2015”, .
- [98] Cazzoli, E. G., Cnops, A. M., Connolly, P. L., Louttit, R. I., Murtagh, M. J., Palmer, R. B., Samios, N. P., Tso, T. T. and Williams, H. H., (1975). “Evidence for $\Delta S = -\Delta Q$ Currents or Charmed Baryon Production by Neutrinos”, Phys. Rev. Lett., 34: 1125-1128.
- [99] Aubert, B. and others, , (2005). “A precision measurement of the Λ_c^+ baryon mass”, Phys. Rev., D72: 052006.
- [100] Link, J. M. and others, , (2005). “Search for $\Lambda_c^+ \rightarrow pK^+\pi^-$ and $D_s^+ \rightarrow K^+K^+\pi^-$ using genetic programming event selection”, Phys. Lett., B624: 166-172.
- [101] Kushnirenko, A. and others, , (2001). “Precision measurements of the Λ_c^+ and D^0 lifetimes”, Phys. Rev. Lett., 86: 5243-5246.
- [102] Albrecht, H. and others, , (1988). “Observation of the Charmed Baryon Λ_c in e^+e^- Annihilation at 10-GeV”, Phys. Lett., B207: 109-114.
- [103] Skwarnicki, T., (1989). “CLEO results on charmed hadron spectroscopy”, New results in hadronic interactions. Proceedings, 24th Rencontres de Moriond, Les Arcs, France, March 12-18, 1989.
- [104] Aubert, B. and others, , (2004). “Measurements of Λ_c^+ branching fractions of Cabibbo-suppressed decay modes”, Proceedings, 32nd International Conference on High Energy Physics (ICHEP 2004): Beijing, China, August 16-22, 2004.
- [105] Abe, K. and others, , (2001). “Observation of $\Lambda_c^+ \rightarrow \Lambda^0 K^+$, $\Lambda_c^+ \rightarrow \Sigma^0 K^+$ and $\Lambda_c^+ \rightarrow \Sigma^+ K^+ \pi^-$ decays”, hep-ex/0108003.
- [106] Baltay, C. and others, , (1979). “Confirmation of the Existence of the Σ_c^{++} and Λ_c^+ Charmed Baryons”, Phys. Rev. Lett., 42: 1721.
- [107] Coteus, P. and others, , (1988). “Charm Hadroproduction Results from Fermilab E-400”, Nucl. Phys. Proc. Suppl., 1B: 317-328.
- [108] Crawford, G. D. and others, , (1993). “Observation of the charmed Baryon Σ_c^+ and measurement of the isospin mass splittings of the Σ_c ”, Phys. Rev. Lett., 71: 3259-3262.
- [109] Bowcock, T. J. V. and others, , (1985). “ $\Lambda(c)$ Production From e^+e^- Annihilation in the Υ Energy Region”, Phys. Rev. Lett., 55: 923.
- [110] Albrecht, H. and others, , (1988). “Observation of the Charmed Baryon $\Sigma(c)$ in e^+e^- Annihilations”, Phys. Lett., B211: 489-492.
- [111] Biagi, S. F. and others, , (1985). “Properties of the Charmed Strange Baryon A^+ and Evidence for the Charmed Doubly Strange Baryon T^0 at $2.74 - GeV/c^2$ ”, Z. Phys., C28: 175.

- [112] Patel, P. M., (1986). “First Observation of $\Omega\rho^0$ and $K^{0*}\bar{K}^{0*}$ Production in $\gamma\gamma$ Collisions at Argus”, Proceedings, High Energy Physics, Vol. 2: 1189-1192.
- [113] Dallapiccola, C., (1992). “Recent results on charmed baryons”, The Fermilab Meeting DPF 92. Proceedings, 7th Meeting of the American Physical Society, Division of Particles and Fields, Batavia, USA, November 10-14, 1992. Vol. 1, 2.
- [114] Abe, K. and others, , (2001). “Study of Ω_c^0 at Belle”, Lepton and photon interactions at high energies. Proceedings, 20th International Symposium, LP 2001, Rome, Italy, July 23-28, 2001.
- [115] Alexandrou, C., Forcrand, deP., Lippert, T., Neff, H., Negele, J. W., Schilling, K., Schroers, W. and Tsapalis, A., (2004). “N to Delta electromagnetic transition form-factors from lattice QCD”, Phys. Rev., D69: 114506.
- [116] El-Khadra, A. X., Kronfeld, A. S. and Mackenzie, P. B., (1997). “Massive fermions in lattice gauge theory”, Phys. Rev., D55: 3933-3957.
- [117] Zichichi, A., (1977). New Phenomena in Subnuclear Physics: Part A, Springer US.
- [118] Sheikholeslami, B. and Wohlert, R., (1985). “Improved Continuum Limit Lattice Action for QCD with Wilson Fermions”, Nucl. Phys., B259: 572.
- [119] Mohler, D. and Woloshyn, R. M., (2011). “D and D_s meson spectroscopy”, Phys. Rev., D84: 054505.
- [120] Isgur, N., Karl, G. and Koniuk, R., (1982). “D Waves in the Nucleon: A Test of Color Magnetism”, Phys. Rev., D25: 2394.
- [121] Buchmann, A. J., Hernandez, E. and Faessler, A., (1997). “Electromagnetic properties of the $\Delta(1232)$ ”, Phys. Rev., C55: 448-463.
- [122] Buchmann, A., Hernandez, E. and Yazaki, K., (1991). “Gluon and pion exchange currents in the nucleon”, Phys. Lett., B269: 35-42.
- [123] Butler, M. N., Savage, M. J. and Springer, R. P., (1993). “ E_2/M_1 mixing ratio of $\Delta \rightarrow N\gamma$ and hyperon resonance radiative decay”, Phys. Lett., B304: 353-358.
- [124] Savage, M. J., (1995). “ E_2 strength in the radiative charmed baryon decay $\Sigma_c^* \rightarrow \Lambda_c\gamma$ ”, Phys. Lett., B345: 61-66.
- [125] Nozawa, S., Blankleider, B. and Lee, T. S. H., (1990). “A Dynamical Model of Pion Photoproduction on the Nucleon”, Nucl. Phys., A513: 459-510.
- [126] Sato, T. and Lee, T. S. H., (2001). “Dynamical study of the Δ excitation in N ($e, e'\pi$) reactions”, Phys. Rev., C63: 055201.
- [127] Dey, J., Shevchenko, V., Volkovitsky, P. and Dey, M., (1994). “Radiative decays of S wave charmed baryons”, Phys. Lett., B337: 185-188.
- [128] Franklin, J., (1997). “Mixing of $\Xi_c - \Xi_c'$ baryons”, Phys. Rev., D55: 425-426.

- [129] Aliev, T. M., Ozpineci, A. and Zamiralov, V., (2011). “Mixing Angle of Hadrons in QCD: A New View”, *Phys. Rev.*, D83: 016008.
- [130] Brown, Z. S., Detmold, W., Meinel, S. and Orginos, K., (2014). “Charmed bottom baryon spectroscopy from lattice QCD”, *Phys. Rev.*, D90: 094507.
- [131] Can, K. U., Erkol, G., Oka, M. and Takahashi, T. T., (2015). “Look inside charmed-strange baryons from lattice QCD”, *Phys. Rev. D*, 92: 114515.
- [132] Aliev, T. M., Barakat, T. and Savci, M., (2016). “Analysis of the radiative decays $\Sigma_Q \rightarrow \Lambda_Q \gamma$ and $\Xi'_Q \rightarrow \Xi_Q \gamma$ in light cone sum rules”, *Phys. Rev.*, D93: 056007.
- [133] Cheng, H.-Y., Cheung, C.-Y., Lin, G.-L., Lin, Y. C., Yan, T.-M. and Yu, H.-L., (1993). “Chiral Lagrangians for radiative decays of heavy hadrons”, *Phys. Rev.*, D47: 1030-1042.
- [134] Banuls, M. C., Pich, A. and Scimemi, I., (2000). “Electromagnetic decays of heavy baryons”, *Phys. Rev.*, D61: 094009.
- [135] Jiang, N., Chen, X.-L. and Zhu, S.-L., (2015). “Electromagnetic decays of the charmed and bottom baryons in chiral perturbation theory”, *Phys. Rev.*, D92: 054017.
- [136] Cheng, H.-Y., Cheung, C.-Y., Lin, G.-L., Lin, Y. C., Yan, T.-M. and Yu, H.-L., (1994). “Corrections to chiral dynamics of heavy hadrons: SU(3) symmetry breaking”, *Phys. Rev. D*, 49: 5857–5881.
- [137] Cheng, H.-Y., Cheung, C.-Y., Lin, G.-L., Lin, Y. C., Yan, T.-M. and Yu, H.-L., (1997). “Erratum: Corrections to chiral dynamics of heavy hadrons: SU(3) symmetry breaking [Phys. Rev. D 49, 5857 (1994)]”, *Phys. Rev. D*, 55: 5851–5852.
- [138] Ivanov, M. A., Korner, J. G., Lyubovitskij, V. E. and Rusetsky, A. G., (1999). “Strong and radiative decays of heavy flavored baryons”, *Phys. Rev.*, D60: 094002.
- [139] Bernotas, A. and Āimonis, V., (2013). “Radiative M1 transitions of heavy baryons in the bag model”, *Phys. Rev.*, D87: 074016.
- [140] Erkol, G., Oka, M. and Takahashi, T. T., (2009). “Pseudoscalar-meson–octet-baryon coupling constants in two-flavor lattice QCD”, *Phys. Rev.*, D79: 074509.
- [141] Deliduman, C., (2015). Lecture notes in Quantum Field Theory, Mimar Sinan Fine Arts University.
- [142] Peskin, M. E. and Schroeder, D. V., (1995). *An Introduction to Quantum Field Theory*, Westview Press.
- [143] Zinn-Justin, J., (2002). *Quantum Field Theory and Critical Phenomena*; 4th ed., Clarendon Press. Oxford.
- [144] Berezin, F. A., (1966). “The method of second quantization”, *Pure Appl. Phys.*, 24: 1-228.

- [145] Wasserman, L., (2006). All of Nonparametric Statistics (Springer Texts in Statistics), Springer-Verlag New York, Inc., Secaucus, NJ, USA.
- [146] Quenouille, M. H., (1949). “Problems in Plane Sampling”, The Annals of Mathematical Statistics, 20: 355–375.
- [147] Tukey, J. W., (1958). “Bias and confidence in not quite large samples”, Ann. Math. Statist., 29: 614–623.
- [148] Roepstorff, G., (1996). Path Integral Approach to Quantum Physics, Springer.
- [149] Costa, G. and Fogli, G., (2012). Symmetries and Group Theory in Particle Physics, Springer.
- [150] Keller, D., (2010). U-Spin Symmetry Test of the Σ^{*+} Electromagnetic Decay, Ohio U., .
- [151] Buchmann, A. J., (2007). “Charge form factors and nucleon shape”, AIP Conf. Proc., 904: 110-125.

APPENDIX-A

DEFINITIONS AND ALGEBRAS

A.1 Gamma Matrices

This appendix explains the properties of γ -matrices. The Euclidean gamma matrices $\gamma_\mu, \mu = 1, 2, 3, 4$ can be constructed from the Minkowski gamma matrices $\gamma_\mu^M, \mu = 0, 1, 2, 3$.

$$\gamma_1 = -i\gamma_1^M, \gamma_2 = -i\gamma_2^M, \gamma_3 = -i\gamma_3^M, \gamma_4 = \gamma_0^M. \quad (\text{A.1})$$

The Euclidean anti-commutation relations are

$$\{\gamma_\mu, \gamma_\nu\} = 2g_{\mu\nu}\mathbb{1}, \quad (\text{A.2})$$

where $g_{\mu\nu}$ is metric tensor given by $g_{\mu\nu} = \text{diag}(1, 1, 1, 1)$ and $\mathbb{1}$ is the 4×4 unit matrix. Besides product of the matrices is defined as γ_5 ;

$$\gamma_5 = \gamma_1 \gamma_2 \gamma_3 \gamma_4. \quad (\text{A.3})$$

The Euclidean gamma matrices can be written as

$$\begin{aligned} \gamma_1 &= \begin{bmatrix} 0 & 0 & 0 & -i \\ 0 & 0 & -i & 0 \\ 0 & i & 0 & 0 \\ i & 0 & 0 & 0 \end{bmatrix}, \gamma_2 = \begin{bmatrix} 0 & 0 & 0 & -1 \\ 0 & 0 & 1 & 0 \\ 0 & 1 & 0 & 0 \\ -1 & 0 & 0 & 0 \end{bmatrix}, \gamma_3 = \begin{bmatrix} 0 & 0 & -i & 0 \\ 0 & 0 & 0 & i \\ i & 0 & 0 & 0 \\ 0 & -i & 0 & 0 \end{bmatrix}, \\ \gamma_4 &= \begin{bmatrix} 0 & 0 & 1 & 0 \\ 0 & 0 & 0 & 1 \\ 1 & 0 & 0 & 0 \\ 0 & 1 & 0 & 0 \end{bmatrix}, \gamma_5 = \begin{bmatrix} 1 & 0 & 0 & 0 \\ 0 & 1 & 0 & 0 \\ 0 & 0 & -1 & 0 \\ 0 & 0 & 0 & -1 \end{bmatrix}. \end{aligned} \quad (\text{A.4})$$

The gamma matrices also obey the relation

$$\gamma_\mu = \gamma_\mu^\dagger = \gamma_\mu^{-1}. \quad (\text{A.5})$$

A.2 Grassmann Algebra and Grassmann Integrals

This appendix briefly explains the Grassmann algebra and Grassmann integrals. The gaussian form of Grassmann integral arises in the fermionic calculations. The appendix

is written by using lecture notes in Reference [141]. Detailed information are available at [142] and [143]. Amplitudes as path integrals of fermionic fields are expressed as classical analogs of \hat{x} and $\hat{\psi}$. These are Grassmann numbers that obey Grassmann algebra,

$$\{\chi_m, \psi_n\} = 0 = \{\chi_m, \chi_n\} = \{\psi_m, \chi_n\}, \quad (\text{A.6})$$

Grassmann field is the function of spacetime whose values are Grassmann numbers,

$$\psi(x) = \sum_i \psi_i \phi_i(x), \quad (\text{A.7})$$

where $\phi_i(x)$ are complete set of orthogonal functions and ψ_i are Grassmann numbers. Associative algebra U over \mathbb{R} or \mathbb{C} are constructed from unit $\mathbb{1}$ and set of generators θ_i with anti-commuting products,

$$\{\theta_i, \theta_j\} = 0 \quad \forall i, j. \quad (\text{A.8})$$

Examining Grassmann algebra under the parity operator helps to understand the behavior of the fermions,

$$\begin{aligned} P\theta_i &= -\theta_i \Rightarrow P^2 = \mathbb{1}, \\ P(\theta_{i_1}\theta_{i_2}\dots\theta_{i_p}) &= (-1)^p \theta_{i_1}\theta_{i_2}\dots\theta_{i_p}. \end{aligned} \quad (\text{A.9})$$

P divides U into two parts,

$P(x) = x \Rightarrow x \in U^+ : x$ contains even number of θ 's

$P(x) = -x \Rightarrow -x \in U^- : x$ contains odd number of θ 's.

U^+ is the sub-algebra of commuting elements in which two fermions act like boson. To perform calculations, it is necessary to define derivative and integral operations in Grassmann algebra. Starting from a Grassmann function as a function of single θ_i ,

$$F = F_1 + \theta_i F_2 \quad (\text{A.10})$$

F_1 and F_2 may contain other θ_j ($j \neq i$), the side of derivation is important. There are two derivative operators:

Left Derivative,

$$\frac{\partial F}{\partial \theta_i} = F_2, \quad (\text{A.11})$$

and Right Derivative, $F = F_1 + \tilde{F}_2 \theta_i$

$$\frac{\partial F}{\partial \theta_i} = \tilde{F}_2. \quad (\text{A.12})$$

In fermionic calculations, usually left derivative is used. In 1966 Berezin showed that, in Grassmannian algebra the left derivative operator equals to integration [144]

$$\int d\theta_i F = \frac{\partial F}{\partial \theta_i} \quad (\text{A.13})$$

the integral is written,

$$I = \int d\theta f(\theta), \quad (\text{A.14})$$

$f(\theta) = f_1 + \theta f_2$ so

$$I = \int d\theta (f_1 + \theta f_2) = f_2, \quad (\text{A.15})$$

change of variables, $\theta = a\theta' + b$, $d\theta = Jd\theta'$

$$\begin{aligned} I &= \int Jd\theta' f(\theta) = \int Jd\theta' (f_1 + (a\theta' + b)f_2) \\ &= aJf_2 \Rightarrow J = 1/a. \end{aligned} \quad (\text{A.16})$$

Jacobian is inverted compared to commuting numbers. More generally, the Jacobian is

$$\begin{aligned} d\theta_1 d\theta_2 \dots d\theta_n &= J\theta'_1 d\theta'_2 \dots d\theta'_n, \\ \Rightarrow J^{-1} &= \det \begin{pmatrix} \theta_i \\ \theta'_i \end{pmatrix} \end{aligned} \quad (\text{A.17})$$

if $\frac{\theta_i}{\theta'_i}$ is invertible. Fermions obey the Grassmann algebra. Generally, Gaussian integrals are encountered in calculations, so the Gaussian integral in the Grassmann algebra must be solved. Beginning with a Grassmann algebra consists two sets of generators:

$$Z(M) = \int d\bar{\theta}_1 d\theta_1 d\bar{\theta}_2 d\theta_2 \dots d\bar{\theta}_n d\theta_n e^{-\sum_{i,j} [d\bar{\theta}_i M_{ij} d\theta_j]}, \quad (\text{A.18})$$

change of variables

$$\sum_i M_{i,j} \theta_j = \theta'_i \Rightarrow J = \det[M] \Rightarrow J = \det\left(\frac{\partial \theta_i}{\partial \theta'_j}\right), \quad (\text{A.19})$$

then the integration becomes

$$\begin{aligned} Z(M) &= \det[M] \int d\bar{\theta}_1 d\theta'_1 d\bar{\theta}_2 d\theta'_2 \dots d\bar{\theta}_n d\theta'_n e^{-\sum_{i,j} [d\bar{\theta}_i d\theta'_j]} \\ &= \det[M] \int d\bar{\theta}_1 d\theta'_1 d\bar{\theta}_2 d\theta'_2 \dots d\bar{\theta}_n d\theta'_n \prod_i e^{-[d\bar{\theta}_i d\theta'_i]} \\ &\xrightarrow[\text{expansion}]{\text{Taylor}} \det[M] \int \prod_i d\bar{\theta}_i d\theta'_i (1 - \bar{\theta}_i \theta'_i) \end{aligned} \quad (\text{A.20})$$

the $\int \prod_i d\bar{\theta}_i d\theta'_i 1 = 0$.

$$\begin{aligned} Z(M) &= \det[M] \int \prod_i d\bar{\theta}_i d\theta'_i \theta'_i \bar{\theta}_i, \\ &= \det[M]. \end{aligned} \quad (\text{A.21})$$

The integral, is called as generating functional

$$Z_G[\eta, \bar{\eta}] = \int \prod_i d\bar{\theta}_i d\theta_i e^{-\sum_{i,j}^n [d\bar{\theta}_i M_{ij} d\theta_j + \sum_i^n (\bar{\eta}_i \theta_i + \bar{\theta}_i \eta_i)]} \quad (\text{A.22})$$

change of variables

$$\theta_i = \theta'_i - \sum_j (M^{-1})_{ij} \eta_j \quad , \quad \bar{\theta}_i = \bar{\theta}'_i - \sum_j \bar{\eta}_j (M^{-1})_{ji} \quad (\text{A.23})$$

after changing variables and using the Eq. (A.21), the integral becomes

$$Z_G[\eta, \bar{\eta}] = \det[M] \int e^{\left[\sum_{ij} \bar{\eta}_i (M^{-1})_{ij} \eta_j \right]}, \quad (\text{A.24})$$

before calculating the integral, there is one more key formula to understand and complete the Gaussian integral part, which is called as Wick's theorem,

$$\begin{aligned} \det[M] \langle \theta_{i_1} \bar{\theta}_{j_1} \dots \theta_{i_n} \bar{\theta}_{j_n} \rangle &= \int \prod_i d\bar{\theta}_i d\theta_i (\theta_{i_1} \bar{\theta}_{j_1} \dots \theta_{i_n} \bar{\theta}_{j_n}) e^{-\sum_{i,j} \bar{\theta}_i M_{ij} \theta_j} \\ &= \left[\frac{\delta}{\delta \eta_{j_1}} \frac{\delta}{\delta \bar{\eta}_{i_1}} \dots \frac{\delta}{\delta \eta_{j_n}} \frac{\delta}{\delta \bar{\eta}_{i_n}} \right] Z_G[\eta, \bar{\eta}] \Big|_{\eta=\bar{\eta}=0} \\ &= (-1)^n \sum_{P(1,2,\dots,n)} \text{sign}[P] (M^{-1})_{i_1 j_{P_1}} (M^{-1})_{i_2 j_{P_2}} \dots (M^{-1})_{i_n j_{P_n}}. \end{aligned} \quad (\text{A.25})$$

$P(1,2,\dots,n)$ is the permutation of numbers from 1 to n, and $\text{sign}[P]$ is the sign of permutation. Using the Wick's theorem, the $2n$ function becomes

$$\begin{aligned} \langle \theta_{i_1} \bar{\theta}_{j_1} \dots \theta_{i_n} \bar{\theta}_{j_n} \rangle &= \left[\frac{\delta}{\delta \eta_{j_1}} \frac{\delta}{\delta \bar{\eta}_{i_1}} \dots \frac{\delta}{\delta \eta_{j_n}} \frac{\delta}{\delta \bar{\eta}_{i_n}} \right] e^{\left[-\sum_{i,j} \bar{\eta}_i M_{ij} \eta_j \right]} \\ &= \det[M_{i_k j_l}^{-1}] = \det \langle \theta_{i_k} \bar{\theta}_{j_l} \rangle \end{aligned} \quad (\text{A.26})$$

Using Wick's theorem in Eq. (A.26), $2n$ functions can be written as 2 point functions. This is useful for calculating observables. For Dirac field

$$\begin{aligned} \langle 0 | T[\psi(x_1) \bar{\psi}(x_2)] | 0 \rangle &= \frac{\int \mathcal{D}\bar{\psi} \mathcal{D}\psi \psi(x_1) \bar{\psi}(x_2) e^{i \int d^4x \bar{\psi}(i\partial - m)\psi}}{\int \mathcal{D}\bar{\psi} \mathcal{D}\psi e^{i \int d^4x \bar{\psi}(i\partial - m)\psi}} \\ &= \frac{1}{\det[-i(i\partial - m)]} \left(-i \frac{\delta}{\delta \bar{\eta}} \right) \left(-\frac{\delta}{\delta \eta} \right) Z[\eta, \bar{\eta}] \Big|_{\eta=\bar{\eta}=0} = S_F(x_1 - x_2), \end{aligned} \quad (\text{A.27})$$

where

$$Z[\eta, \bar{\eta}] = \det[-i(i\partial - m)] e^{-\int d^4x d^4y \bar{\eta}(x) S_F(x-y) \eta(y)}, \quad (\text{A.28})$$

the Feynman propagator is

$$S_F(x-y) = \det[-i(i\partial - m)]^{-1}. \quad (\text{A.29})$$

The Eq. (A.29) shows that the propagator is inversion of Dirac operator. In LQCD this is a matrix, calculating the propagator means inverting the Dirac operator matrix, that is a time consuming process.

A.3 Jackknife Resampling Method

Jackknife is a nonparametric methods for computing standard errors and confidence intervals [145]. It is especially useful for variance and bias estimation. The Jackknife technique was invented by Maurice Quenouille in 1949 [146] as a tool for bias reduction. John Tukey in 1958 [147] showed the Jackknife technique is useful in reducing the bias as well as in estimating the variance. Moreover Tukey proposed the name "Jackknife" to imply that the method is an all-purpose statistical tool.

The Jackknife samples are created by deleting a data from the original data set, i th variable of Jackknife sample is defined as

$$\tilde{x}_i = \frac{1}{n-1} \sum_{j \neq i}^n x_j, \quad (\text{A.30})$$

where \tilde{x}_i is Jackknife estimation of i th variable, x_j is variable in original dataset. Variance of Jackknife is defined as

$$\sigma^2 = \frac{n-1}{n} \sum_{i=1}^n (\tilde{x}_i - \tilde{x}_{avg}). \quad (\text{A.31})$$

\tilde{x}_{avg} is the estimator based on all of the subsamples, defined as

$$\tilde{x}_{avg} = \frac{1}{n} \sum_i^n \tilde{x}_i. \quad (\text{A.32})$$

APPENDIX-B

PATH INTEGRAL ON THE LATTICE

To understand the path integral on lattice, it is useful to begin with scalar field theory. By considering a scalar field $\Phi(t, x)$ and employing the Euler-Lagrange equation, the Klein Gordon equation is derived as

$$\partial_\mu(\partial^\mu\Phi) + m^2\Phi = 0. \quad (\text{B.1})$$

By adding a potential, $V(\Phi)$, the system is quantized via canonical quantization. Hamiltonian of the system is written as

$$H = \int d^3x \left(\frac{1}{2}\Pi(t, x)^2 + \frac{1}{2}(\nabla\Phi(t, x))^2 + \frac{m^2}{2}\Phi(t, x)^2 + V(\Phi(t, x)) \right), \quad (\text{B.2})$$

where in the quantum language, the classical fields are replaced by corresponding operators, viz.,

$$\hat{H} = \int d^3x \left(\frac{1}{2}\hat{\Pi}^2 + \frac{1}{2}(\nabla\hat{\Phi})^2 + \frac{m^2}{2}\hat{\Phi}^2 + V(\hat{\Phi}) \right). \quad (\text{B.3})$$

In order to eliminate infinities in continuum quantum field theory calculations, an ultraviolet regulator must be used. Usual methods are Pauli-Villars or dimensional regularization or using a momentum cutoff. In LQCD, space is replaced by a 3D lattice Λ so that it acts as a momentum cutoff. The space vector \mathbf{x} is replaced by $a\mathbf{n}$, where \mathbf{n} is the lattice site coordinate and a is the lattice spacing. In turn, operators are defined only on lattice sites $\hat{\Phi}(x) \Rightarrow \hat{\Phi}(\mathbf{n})$ and $\hat{\Pi}(x) \Rightarrow \hat{\Pi}(\mathbf{n})$. In the $a \rightarrow 0$ limit, derivatives in Eq. (B.2) can be replaced by the finite difference

$$\partial_i\hat{\Phi}(x) = \frac{\hat{\Phi}(n+i) - \hat{\Phi}(n-i)}{2a} + \mathcal{O}(a^2). \quad (\text{B.4})$$

With the replacement of the integral over the spatial volume by a sum over all lattice points, the discrete Hamiltonian becomes

$$\hat{H}(n) = a^3 \sum_{n \in \Lambda} \left(\frac{1}{2}\hat{\Pi}(n)^2 + \frac{1}{2} \sum_{i=0}^3 \left(\frac{\hat{\Phi}(n+i) - \hat{\Phi}(n-i)}{2a} \right)^2 + \frac{m^2}{2}\hat{\Phi}(n)^2 + V(\hat{\Phi}(n)) \right), \quad (\text{B.5})$$

where $\mathcal{O}(a^2)$ terms have been omitted and the the momentum operator is

$$\widehat{\Pi}(n) = \frac{-i}{a^3} \frac{\partial}{\partial \Phi(n)}. \quad (\text{B.6})$$

The discrete Klein-Gordon hamiltonian may be split into a free, H_0 , and interaction, H_I , part

$$\begin{aligned} \widehat{H}_0 &= \frac{-1}{2a^3} \sum_{n \in \Lambda} \frac{\partial^2}{\partial \Phi(n)^2}, \\ \widehat{H}_I &= a^3 \sum_{n \in \Lambda} \left(\frac{1}{2} \sum_{i=0}^3 \left(\frac{\widehat{\Phi}(n+i) - \widehat{\Phi}(n-i)}{2a} \right)^2 + \frac{m^2}{2} \widehat{\Phi}(n)^2 + V(\widehat{\Phi}(n)) \right). \end{aligned} \quad (\text{B.7})$$

Such a separation is particularly useful when calculating the correlators. Assuming time steps, ε , are infinitesimal interaction part H_I is split symmetrically,

$$e^{-\varepsilon \widehat{H}} = e^{-\varepsilon \widehat{H}_I/2} e^{-\varepsilon \widehat{H}_0} e^{-\varepsilon \widehat{H}_I/2} + (1 + \mathcal{O}(\varepsilon)). \quad (\text{B.8})$$

This equation can be derived by, Taylor expanding the both sides of equation so that the left hand side is

$$e^{-\varepsilon \widehat{H}} \xrightarrow[\text{expansion}]{\text{Taylor}} (1 - \varepsilon \widehat{H} + \dots) \Rightarrow (1 - \varepsilon \widehat{H}_0 - \varepsilon \widehat{H}_I) + \mathcal{O}(\varepsilon), \quad (\text{B.9})$$

and the right hand side is given by

$$\begin{aligned} e^{-\varepsilon \widehat{H}_I/2} e^{-\varepsilon \widehat{H}_0} e^{-\varepsilon \widehat{H}_I/2} &\xrightarrow[\text{expansion}]{\text{Taylor}} (1 - \varepsilon \widehat{H}_I/2 + \dots)(1 - \varepsilon \widehat{H}_0 + \dots)(1 - \varepsilon \widehat{H}_I/2 + \dots), \\ &\Rightarrow \left(1 - \varepsilon \widehat{H}_0 - \varepsilon \frac{\widehat{H}_I}{2} + \varepsilon^2 \widehat{H}_0 \frac{\widehat{H}_I}{2} - \varepsilon \frac{\widehat{H}_I}{2} + \varepsilon^2 \widehat{H}_0 \frac{\widehat{H}_I}{2} + \varepsilon^2 \frac{\widehat{H}_I}{2} \frac{\widehat{H}_I}{2} \right. \\ &\quad \left. - \varepsilon^3 \widehat{H}_0 \frac{\widehat{H}_I}{2} \frac{\widehat{H}_I}{2} \right). \end{aligned} \quad (\text{B.10})$$

Using the Trotter formula [148], one obtains [72]

$$\langle \Phi' | e^{-t \widehat{H}} | \Phi \rangle = \lim_{n_t \rightarrow \infty} \langle \Phi' | \widehat{W}_\varepsilon^{n_t} | \Phi \rangle, \quad (\text{B.11})$$

where new operator is defined

$$\widehat{W}_\varepsilon = e^{-\varepsilon \widehat{H}_I/2} e^{-\varepsilon \widehat{H}_0} e^{-\varepsilon \widehat{H}_I/2} + (1 + \mathcal{O}(\varepsilon)). \quad (\text{B.12})$$

Similar to the procedure in Eq. (2.16), complete set of states is inserted, $n_t - 1$ times and focus on one term only

$$\langle \Phi_{i+1} | \widehat{W}_\varepsilon | \Phi_i \rangle = \langle \Phi_{i+1} | e^{-\varepsilon \widehat{H}_I/2} e^{-\varepsilon \widehat{H}_0} e^{-\varepsilon \widehat{H}_I/2} | \Phi_i \rangle. \quad (\text{B.13})$$

\widehat{W}_ε acts on states, returning eigenvalues

$$\langle \Phi_{i+1} | \widehat{W}_\varepsilon | \Phi_i \rangle = e^{-\varepsilon \frac{\widehat{H}_I(\Phi_{i+1})}{2}} \langle \Phi_{i+1} | e^{-\varepsilon \widehat{H}_0} | \Phi_i \rangle e^{-\varepsilon \frac{\widehat{H}_I(\Phi_i)}{2}}, \quad (\text{B.14})$$

which reduces to a Gaussian integral

$$\langle \Phi_{i+1} | \widehat{W}_\varepsilon | \Phi_i \rangle = \left(\sqrt{\frac{a^3}{2\pi\varepsilon}} \right)^{N^3} e^{-\varepsilon \frac{\widehat{H}_I(\Phi_i) - \frac{a^3}{2\varepsilon} \sum_n (\Phi(n)_i - \Phi(n)_{i+1})^2 - \varepsilon \frac{\widehat{H}_I(\Phi_{i+1})}{2}}. \quad (\text{B.15})$$

It is now straightforward to compute the correlator

$$\langle O_2(t) O_1(0) \rangle_T = \frac{1}{Z_T} \int \mathcal{D}[\Phi] e^{-S_E[\Phi]} O_2[\Phi(\cdot, n_t)] O_1[\Phi(\cdot, 0)], \quad (\text{B.16})$$

where $Z_T = \int \mathcal{D}[\Phi] e^{-S_E[\Phi]}$ is the partition function and $\Phi(\cdot, 0)$ and $\Phi(\cdot, n_t)$ are functionals whose time arguments are fixed; but spatial arguments are varied. The Euclidean action, S_E , is

$$S_E[\Phi] = a^4 \sum_{n \in \Lambda} \left(\frac{1}{2} \sum_{\mu=1}^4 \left(\frac{\Phi(n + \widehat{\mu}) - \Phi(n - \widehat{\mu})}{2a} \right)^2 + \frac{m^2}{2} \Phi(n)^2 + V(\Phi(n)) \right). \quad (\text{B.17})$$

However, the LQCD is not a scalar theory, it begins from the QCD action. For this reason, defining the QCD action will be descriptive for the reader. The procedures set above are followed to define the discrete, Euclidean QCD action. The QCD action is written as the combination of a fermionic and a gauge part. These actions can be examined separately. In the continuum notation, quark fields are written as, $\psi^{(f)}(x)_\alpha, \bar{\psi}^{(f)}(x)_\alpha$, where x is the space-time coordinate, $\alpha = 1, \dots, 4$ is the Dirac index, $c = 1, 2, 3$ is the color index and f is the flavor index that denotes 6 different flavors. $\bar{\psi}$ is an anti-fermion field described as, $\bar{\psi} = \psi^\dagger \gamma_0$. Gauge (gluon) fields are written as; $A_\mu(x)_{cd}$, where μ is Lorentz index.

Fermionic part of the QCD action is written as

$$\int d^4x \bar{\psi}(x) \left(\gamma_\mu (\partial_\mu + iA_\mu(x) + m) \right) \psi(x). \quad (\text{B.18})$$

In order to ensure the gauge invariance of the action, a covariant derivative is introduced,

$$D_\mu(x) = \partial_\mu + iA_\mu(x). \quad (\text{B.19})$$

It is easier to prove gauge invariance of QCD action when splitting the fermionic and gauge part of the action.

$$S_F[\psi, \bar{\psi}, A_\mu] = \int d^4x \bar{\psi}(x) \left(\gamma_\mu (\partial_\mu + iA_\mu(x) + m) \right) \psi(x). \quad (\text{B.20})$$

New fields are defined as

$$\begin{aligned} \psi(x) &\rightarrow \psi'(x) = \Omega(x) \psi(x), \\ \bar{\psi}(x) &\rightarrow \bar{\psi}'(x) = \bar{\psi}(x) \Omega^\dagger(x). \end{aligned} \quad (\text{B.21})$$

action is written in terms of new fields

$$S_F[\psi', \bar{\psi}', A'_\mu] = \int d^4x \bar{\psi}'(x) \Omega^\dagger(x) \left(\gamma_\mu (\partial_\mu + iA'_\mu(x) + m) \right) \Omega(x) \psi'(x). \quad (\text{B.22})$$

Mass part of the action is $m\Omega^\dagger(x)\Omega(x)\bar{\psi}(x)\psi(x)$ gauge invariant. Examining the gauge invariance of kinetic part

$$\begin{aligned} & \Omega^\dagger(x)(\partial_\mu + iA'_\mu(x))\Omega(x), \\ & = \partial_\mu + \Omega^\dagger(x)(\partial_\mu\Omega(x)) + i\Omega^\dagger(x)A'_\mu(x)\Omega(x). \end{aligned} \quad (\text{B.23})$$

In order to provide gauge invariance $A'_\mu(x)$ must be transformed as the following form,

$$A_\mu(x) \rightarrow A'_\mu(x) = \Omega(x)A_\mu(x)\Omega^\dagger(x) + i(\partial_\mu\Omega(x))\Omega^\dagger(x). \quad (\text{B.24})$$

There is also new definition of derivative operator

$$D_\mu(x) = \partial_\mu + iA_\mu(x), \quad (\text{B.25})$$

it is called as covariant derivative. The gauge invariance of covariant derivative is

$$D_\mu(x) \rightarrow D'_\mu(x) = \partial_\mu + iA'_\mu(x) = \Omega(x)D_\mu(x)\Omega^\dagger(x). \quad (\text{B.26})$$

The gauge part of the action is written as

$$S_g[A'] = \frac{1}{2g^2} \int d^4x \text{tr}[F_{\mu\nu}(x)F^{\mu\nu}(x)], \quad (\text{B.27})$$

the field strength tensor is defined as

$$F_{\mu\nu}(x) = -i[D_\mu(x), D_\nu(x)], \quad (\text{B.28})$$

examining the gauge invariance of field strength tensor

$$\begin{aligned} F_{\mu\nu}(x) \rightarrow F'_{\mu\nu}(x) & = -i[D'_\mu(x), D'_\nu(x)] = -i[\Omega(x)D_\mu(x)\Omega^\dagger(x), \Omega(x)D_\nu(x)\Omega^\dagger(x)] \\ & = -i(\Omega(x)D_\mu(x)D_\nu(x)\Omega^\dagger(x) - \Omega(x)D_\nu(x)D_\mu(x)\Omega^\dagger(x)) \\ & = \Omega(x)F_{\mu\nu}\Omega^\dagger(x). \end{aligned} \quad (\text{B.29})$$

The gauge part of the action is also gauge invariant.

APPENDIX-C

U-SPIN SYMMETRY

In general, in the hadrons classification for $SU(3)_f$, $SU(2)$ isospin subgroup is used. Isospin (I) subgroup commutes with hypercharge (Y), through this classification, $SU(3)_f$ can be written in terms of $SU(2)_I \times U(1)_Y$. In fact there are alternative ways to label $SU(3)_f$.

When the generators of $SU(3)$ group are examined, it is seen that they are formed with 8 Gell-Mann matrices. These Gell-Mann matrices can be written as three subsets. Thus $SU(3)$ group can be expressed in three different $SU(2)$ s. It should be noted that the three different $SU(2)$ s do not commute with each other. Thus, there cannot be three $SU(2)$ s in $SU(3)$, but $SU(3)$ can be expressed as three different $SU(2)$. One of them the is well-known isospin and hypercharge.

$$I_i = \frac{1}{2}\lambda_i (i = 1, 2, 3), \quad (C.1)$$

here λ_i are Gell-Mann matrices, the commutation relations of isospin are

$$[I_i, I_j] = i\varepsilon_{ijk}I_k, \quad (C.2)$$

the commutation relation of isospin and hypercharge is

$$[I_i, Y] = 0. \quad (C.3)$$

As described earlier, $SU(3)$ can be written as three different $SU(2)$. First set is the set of isospin and hypercharge. The remaining two sets can be written as follows [149],

$$\begin{aligned} U_1 &= \frac{1}{2}\lambda_6, \\ U_2 &= \frac{1}{2}\lambda_7, \\ U_3 &= \frac{1}{4}(\sqrt{3}\lambda_8 - \lambda_3), \end{aligned} \quad (C.4)$$

called as U-spin ($SU(2)_U$) and

$$\begin{aligned} V_1 &= \frac{1}{2}\lambda_4, \\ V_2 &= \frac{1}{2}\lambda_5, \\ V_3 &= \frac{1}{4}(\lambda_3 + \sqrt{3}\lambda_8), \end{aligned} \tag{C.5}$$

called as V-Spin ($SU(2)_V$). The commutation relations are

$$\begin{aligned} [U_i, U_j] &= i\epsilon_{ijk}U_k, \\ [V_i, V_j] &= i\epsilon_{ijk}V_k. \end{aligned} \tag{C.6}$$

The ladder operators of U-spin and V-spin defined as

$$\begin{aligned} U_{\pm} &= U_1 \pm iU_2, \\ V_{\pm} &= V_1 \pm iV_2, \end{aligned} \tag{C.7}$$

The U-spin generators commute with electric charge Q ($Q = I_3 + \frac{1}{2}(B + S) = I_3 + \frac{1}{2}Y$)

$$[U_i, Q] = 0, \tag{C.8}$$

By analogy to the definition of isospin, $SU(3)_f$ can be written in terms of $SU(2)_U \times U(1)_Q$. Furthermore Q and U_3 axis can be set up like Y and I_3 axis. U_3 values can be written in terms of isospin and hypercharge,

$$U_3 = \frac{1}{2}\left(\frac{3}{2}Y - I_3\right). \tag{C.9}$$

In U-spin symmetry, doublets can be written same as in the isospin symmetry. In the isospin symmetry, the quarks in this doublet are u and d quarks. Since the mass difference between u and d quarks is very small, chiral symmetry is assumed as not broken. On the other hand, in the isospin symmetry, charge symmetry is not preserved; since the charges of the quarks are not the same. In U-spin symmetry, the charge symmetry is preserved, because the doublets have s and d quarks that are in same charge, but the mass difference between these quarks is much larger than the isospin symmetry,

$$SU(2)_I \begin{bmatrix} u \\ d \end{bmatrix} \rightarrow SU(2)_U \begin{bmatrix} s \\ d \end{bmatrix}. \tag{C.10}$$

Since in electromagnetic transitions the charge is conserved, U-spin symmetry is a handy symmetry for these type of transitions. Some decay channels are also forbidden by U-spin symmetry. The electromagnetic transitions of octet - octet and decuplet - octet baryon, gives a prediction of the degree of U-spin symmetry breaking [150].

Fig. (C.1), illustrates that there are two U-spin doublets, Σ^+ , p and Ξ^- , Σ^- . There is one triplet (n , Σ^0 and Ξ^0) and finally one singlet with Λ^0 . Some care is needed when switching between isospin multiplets and U-spin multiplets. The connection between Σ_u^0 , Λ_u^0 and Σ^0 ,

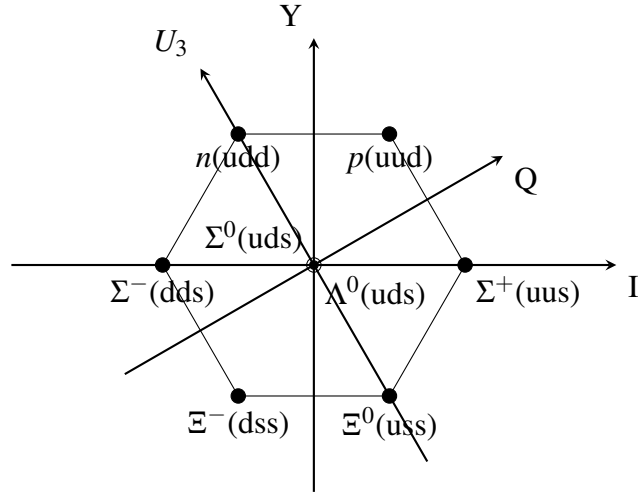


Figure C.1 U-spin and I-spin for octet baryons.

Λ^0 can be obtained as

$$\begin{aligned}\Sigma^0 &= \frac{1}{\sqrt{2}} \text{tr}(B\lambda_3), \\ \Lambda^0 &= \frac{1}{\sqrt{2}} \text{tr}(B\lambda_8).\end{aligned}\tag{C.11}$$

The states Σ_u^0 and Λ_u^0 are obtained by applying the rotation described in Fig. (C.1) and new axes are defined as

$$\begin{aligned}\lambda'_3 &= -\frac{1}{2}\lambda_3 + \frac{\sqrt{3}}{2}\lambda_8, \\ \lambda'_8 &= \frac{\sqrt{3}}{2}\lambda_3 + \frac{1}{2}\lambda_8.\end{aligned}\tag{C.12}$$

The new states in terms of new-axes are

$$\begin{aligned}\Sigma_u^0 &= \frac{1}{\sqrt{2}} \text{tr}(B\lambda'_3), \\ \Lambda_u^0 &= \frac{1}{\sqrt{2}} \text{tr}(B\lambda'_8).\end{aligned}\tag{C.13}$$

Comparing the Eq. (C.12) and Eq. (C.13), the states Σ_u^0 and Λ_u^0 describe the mixing between the neutral ground states:

$$\begin{aligned}\Sigma_u^0 &= -\frac{1}{2}\Sigma^0 + \frac{\sqrt{3}}{2}\Lambda^0, \\ \Lambda_u^0 &= \frac{\sqrt{3}}{2}\Sigma^0 + \frac{1}{2}\Lambda^0\end{aligned}\tag{C.14}$$

Here Σ_u^0 and Λ_u^0 are mixed states, they are combinations of $U=1$ (Σ^0), and $U=0$ (Λ^0) states. The $SU(3)_f$ decuplet can be examined similarly, When the charm quark is considered, the U-spin doublet remains the same. However octet baryons become 20-plet and one anti four plet. While the decuplet baryons also form a 20-plet. The exact $SU(3)$ U-spin

U-spin	Charge	Baryons
$U = 0$	$Q = 0$	(Λ^0)
$U = \frac{1}{2}$	$Q = 1$	(p, Σ^+)
$U = \frac{1}{2}$	$Q = -1$	(Ξ^-, Σ^-)
$U = 1$	$Q = 0$	(n, Ξ^0, Σ^0)

Table C.1 U-spin numbers for octet baryons.

U-spin	Charge	Baryons
$U = 0$	$Q = 2$	(Δ^{++})
$U = \frac{1}{2}$	$Q = 1$	(Δ^+, Σ^{*+})
$U = 1$	$Q = 0$	$(\Delta^0, \Sigma^{*0}, \Xi^{*0})$
$U = \frac{3}{2}$	$Q = -1$	$(\Delta^-, \Sigma^{*-}, \Xi^{*-}, \Omega^{*-})$

Table C.2 U-spin numbers for decuplet baryons.

symmetry forbids the two neutral electromagnetic decays $\Xi_c^0 \gamma \rightarrow \Xi_c^{\prime 0}$ and $\Xi_c^0 \gamma \rightarrow \Xi_c^{*0}$.

U-spin	Charge	Baryons
$U = 0$	$Q = 2$	(Σ_c^{++})
$U = \frac{1}{2}$	$Q = 1$	(Σ_c^+, Ξ_c^+)
$U = 1$	$Q = 0$	$(\Sigma_c^0, \Xi_c^0, \Omega_c^0)$
$U = 0$	$Q = 0$	$(\Xi_c^{\prime 0})$
$U = \frac{1}{2}$	$Q = 1$	$(\Lambda_c^+, \Xi_c^{\prime +})$
$U = 0$	$Q = 2$	(Ξ_{cc}^{++})
$U = \frac{1}{2}$	$Q = 1$	$(\Omega_{cc}^+, \Xi_{cc}^+)$

Table C.3 U-spin numbers for triply charmed, doubly charmed and single charmed spin $\frac{1}{2}$ baryons

U-spin	Charge	Baryons
U = 0	Q = 2	(Ω_{ccc}^{*+++})
U = 0	Q = 2	(Ξ_{cc}^{*+++})
U = $\frac{1}{2}$	Q = 1	$(\Xi_{cc}^{*+}, \Omega_{cc}^{*+})$
U = 0	Q = 2	(Σ_c^{*+++})
U = $\frac{1}{2}$	Q = 1	$(\Xi_c^{*+}, \Sigma_c^{*+})$
U = 1	Q = 0	$(\Xi_c^{*0}, \Sigma_c^{*0}, \Omega_c^{*0})$

Table C.4 U-spin numbers for triply charmed, doubly charmed and single charmed spin $\frac{3}{2}$ baryons

D.1 Hopping Part Invariance Under Parity Transformation

The parity transformation of hopping part can be examined more easily when splitting the temporal and spatial parts, spatial part, transforms as

$$\frac{a^4}{2a} \sum_{n,n_4} \sum_{i=\pm 1}^{\pm 3} \bar{\psi}(n, n_4)^{\mathcal{P}} (\mathbb{1} - \gamma_i) U_i(n, n_4)^{\mathcal{P}} \psi(n + \hat{i}, n_4)^{\mathcal{P}}, \quad (\text{D.1})$$

Using the transformation rules from the Eq. (2.95), the spatial hopping part is

$$\frac{a^4}{2a} \sum_{n,n_4} \sum_{i=\pm 1}^{\pm 3} \bar{\psi}(-n, n_4) \gamma_4 (\mathbb{1} - \gamma_i) \gamma_4 U_i(-n - \hat{i}, n_4)^{\dagger} \psi(-n - \hat{i}, n_4), \quad (\text{D.2})$$

using the relation $U_i(n - \hat{i})^{\dagger} \equiv U_{-i}(n)$ and setting the $m = -n$, the spatial hopping part is

$$\frac{a^4}{2a} \sum_{m,n_4} \sum_{i=\pm 1}^{\pm 3} \bar{\psi}(m, n_4) \gamma_4 (\mathbb{1} - \gamma_i) \gamma_4 U_{-i}(m, n_4) \psi(m - \hat{i}, n_4), \quad (\text{D.3})$$

from gamma matrices relations $\gamma_4 \gamma_i \gamma_4 = -\gamma_i = \gamma_{-i}$,

$$\frac{a^4}{2a} \sum_{m,n_4} \sum_{i=\pm 1}^{\pm 3} \bar{\psi}(m, n_4) \gamma_4 (\mathbb{1} - \gamma_{-i}) \gamma_4 U_{-i}(m, n_4) \psi(m - \hat{i}, n_4), \quad (\text{D.4})$$

after setting the $i = -i$, the spatial hopping part becomes invariant

$$\frac{a^4}{2a} \sum_{m,n_4} \sum_{i=\pm 1}^{\pm 3} \bar{\psi}(m, n_4) \gamma_4 (\mathbb{1} - \gamma_i) \gamma_4 U_i(m, n_4) \psi(m + \hat{i}, n_4). \quad (\text{D.5})$$

For the temporal hopping part, the calculation is straightforward,

$$\frac{a^4}{2a} \sum_{n,n_4} \sum_{\mu=\pm 4} \bar{\psi}(n, n_4)^{\mathcal{P}} (\mathbb{1} - \gamma_{\mu}) U_{\mu}(n, n_4)^{\mathcal{P}} \psi(n, n_4 \pm 1)^{\mathcal{P}}, \quad (\text{D.6})$$

using the transformation rules from the Eq. (2.95),

$$\frac{a^4}{2a} \sum_{n,n_4} \sum_{\mu=\pm 4} \bar{\psi}(-n,n_4)(\mathbb{1} - \gamma_\mu)U_\mu(-n,n_4)\psi(-n,n_4 \pm 1), \quad (\text{D.7})$$

setting the $m = -n$,

$$\frac{a^4}{2a} \sum_{n,n_4} \sum_{\mu=\pm 4} \bar{\psi}(m,n_4)(\mathbb{1} - \gamma_\mu)U_\mu(m,n_4)\psi(m,n_4 \pm 1). \quad (\text{D.8})$$

Thus it is shown that the hopping part is invariant under parity transformations.

D.2 Hopping Part Invariance Under Charge Conjugation Transformation

The hopping part transforms as

$$\frac{a^4}{2a} \sum_n \sum_{\mu=\pm 1}^{\pm 4} \bar{\psi}(n)^C(\mathbb{1} - \gamma_\mu)U_\mu(n)^C\psi(n + \hat{\mu})^C, \quad (\text{D.9})$$

the transformation of link variable under charge conjugation is given in Eq. (2.98), transformation of the fermion fields are given in Eq. (2.97). Using these two transformations the hopping part becomes

$$-\frac{a^4}{2a} \sum_n \sum_{\mu=\pm 1}^{\pm 4} \bar{\psi}(n)^T C(\mathbb{1} - \gamma_\mu)C^{-1}(U_\mu(n)^\dagger)^T \psi(n + \hat{\mu})^T, \quad (\text{D.10})$$

from the charge conjugation relation $C\gamma_\mu C^{-1} = -\gamma_\mu^T$.

$$-\frac{a^4}{2a} \sum_n \sum_{\mu=\pm 1}^{\pm 4} \bar{\psi}(n)^T (\mathbb{1} + \gamma_\mu^T)(U_\mu(n)^\dagger)^T \psi(n + \hat{\mu})^T. \quad (\text{D.11})$$

The equation can be written as the transpose of the product of the matrices and spinors in reverse order. It should be noted that the fermionic fields obey the Grassmann algebra, therefore when they replace, a negative sign appears.

$$\frac{a^4}{2a} \sum_n \sum_{\mu=\pm 1}^{\pm 4} \bar{\psi}(n + \hat{\mu})(\mathbb{1} + \gamma_\mu)U_\mu(n)^\dagger \psi(n), \quad (\text{D.12})$$

define a new node $m = n + \mu$, the equation is

$$\frac{a^4}{2a} \sum_m \sum_{\mu=\pm 1}^{\pm 4} \bar{\psi}(m)(\mathbb{1} + \gamma_\mu)U_\mu(m - \hat{\mu})^\dagger \psi(m - \hat{\mu}), \quad (\text{D.13})$$

using the relation $U_\mu(m - \hat{\mu})^\dagger \equiv U_{-\mu}(m)$,

$$\frac{a^4}{2a} \sum_m \sum_{\mu=\pm 1}^{\pm 4} \bar{\psi}(m)(\mathbb{1} - \gamma_{-\mu})U_{-\mu}(m)^\dagger \psi(m - \hat{\mu}), \quad (\text{D.14})$$

setting the $\mu \equiv -\mu$, finally the equation becomes

$$\frac{a^4}{2a} \sum_m \sum_{\mu=\pm 1}^{\pm 4} \bar{\psi}(m) (\mathbb{1} - \gamma_\mu) U_\mu(m)^\dagger \psi(m + \hat{\mu}), \quad (\text{D.15})$$

the equation shows that the hopping part is invariant under charge conjugation.

D.3 Hopping Part Invariance Under Time-Reversal

The hopping part transforms as

$$\begin{aligned} \frac{1}{2a} \sum_{\mu=\pm 1}^{\pm 4} (\mathbb{1} - \gamma_\mu)_{\alpha\beta} U_\mu(n)_{ab} \delta_{n+\hat{\mu},m} &\rightarrow \frac{1}{2a} \sum_{\mu=\pm 1}^{\pm 4} (\gamma_5 (\mathbb{1} - \gamma_\mu) \gamma_5)_{\alpha\beta} U_\mu(n)_{ab} \delta_{n+\hat{\mu},m}, \\ &= \frac{1}{2a} \sum_{\mu=\pm 1}^{\pm 4} (\mathbb{1} + \gamma_\mu)_{\alpha\beta} U_\mu(n)_{ab} \delta_{n+\hat{\mu},m}, \\ &= \frac{1}{2a} \sum_{\mu=\pm 1}^{\pm 4} (\mathbb{1} - \gamma_\mu)_{\alpha\beta} U_{-\mu}(n)_{ab} \delta_{n-\hat{\mu},m}, \\ &= \frac{1}{2a} \sum_{\mu=\pm 1}^{\pm 4} (\mathbb{1} - \gamma_\mu)_{\alpha\beta} U_\mu(n - \hat{\mu})_{ab}^\dagger \delta_{n-\hat{\mu},m}, \end{aligned} \quad (\text{D.16})$$

eventually $\delta_{n-\hat{\mu},m}$ makes $n - \hat{\mu} = m$. Additionally $U_\mu(m)_{ab}^\dagger$ which is a hermitian of link variable interchanges the $n \leftrightarrow m$. The hopping part becomes

$$= \frac{1}{2a} \sum_{\mu=1}^4 (\mathbb{1} - \gamma_\mu)_{\alpha\beta} U_\mu(m)_{ab}^\dagger \delta_{m,n+\hat{\mu}}. \quad (\text{D.17})$$

VERTEX FUNCTION AND FORM FACTORS

E.1 Calculation of Vertex Function

The vertex function is defined as

$$iM_0^\mu = -ie\bar{u}(p')\gamma^\mu u(p), \quad (\text{E.1})$$

where u it is spinor of electron. The photon momentum is $q^\mu = p'^\mu - p^\mu$. The gamma matrix is stressed using the sigma tensor relations,

$$\begin{aligned} \sigma^{\mu\nu} &= \frac{i}{2}[\gamma^\mu, \gamma^\nu], \\ i\sigma^{\mu\nu} &= \gamma^\nu\gamma^\mu - g^{\mu\nu}. \end{aligned} \quad (\text{E.2})$$

Then putting this result between spinors the equation becomes

$$\begin{aligned} \bar{u}(p')i\sigma^{\mu\nu}(p'_\nu - p_\nu)u(p) &= \bar{u}(p')[(\gamma^\nu\gamma^\mu - g^{\mu\nu})(p'_\nu - p_\nu)]u(p), \\ &= \bar{u}(p')[(\gamma^\nu\gamma^\mu) - g^{\mu\nu}]p'_\nu(\gamma^\nu\gamma^\mu) - g^{\mu\nu}p_\nu]u(p), \\ &= \bar{u}(p')[\not{p}'\gamma^\mu - (p' + p)^\mu + \gamma^\mu\not{p}]u(p). \end{aligned} \quad (\text{E.3})$$

From the Dirac equation $\bar{u}(p')\not{p}' = mu(p')$ and $\not{p}u(p) = mu(p)$, the equation becomes

$$\begin{aligned} \bar{u}(p')i\sigma^{\mu\nu}(p'_\nu - p_\nu)u(p) &= \bar{u}(p')[2m\gamma^\mu - (p' + p)^\mu]u(p). \\ \frac{\bar{u}(p')i\sigma^{\mu\nu}(p'_\nu - p_\nu)u(p)}{2m} &= \bar{u}(p')\gamma^\mu u(p) - \frac{\bar{u}(p')[\not{(p' + p)}^\mu]u(p)}{2m}. \end{aligned} \quad (\text{E.4})$$

Finally, the vertex function can be written by using the $q^\mu = p'^\mu - p^\mu$

$$-ie\bar{u}(p')\gamma^\mu u(p) = -ie\bar{u}(p')\left[\frac{(p' + p)^\mu}{2m}\right]u(p) - \frac{ie}{2m}\sigma^{\mu\nu}(q^\nu)u(p). \quad (\text{E.5})$$

E.2 Form Factors of spin $\frac{1}{2}$ particles in Lattice QCD

In this section, CHROMA's [1] documentation will be followed. Electromagnetic form factors can be calculated by the baryon matrix elements of the electromagnetic vector

current $J_\mu = e\bar{q}(x)\gamma_\mu q(x)$. Sachs electric and magnetic form factors are defined as

$$\begin{aligned} G_E(q^2) &= F_1(q^2) - \frac{q^2}{4m_N^2} F_2(q^2), \\ G_M(q^2) &= F_1(q^2) + F_2(q^2). \end{aligned} \quad (\text{E.6})$$

Sachs form factors can be found by selecting proper variables of the matrix elements

$$\begin{aligned} \langle \chi(p', s') | J_\mu | \chi(p, s) \rangle &= \Gamma^{\beta\alpha} \left[(i\not{p}' + M)^\alpha \gamma_\mu (i\not{p} + M)^\beta \right] F_1(q^2) \\ &\quad - \Gamma^{\beta\alpha} \left[(i\not{p}' + M)^\alpha \frac{\sigma_{\mu\nu} q_\nu}{2M} (i\not{p} + M)^\beta \right] F_2(q^2), \end{aligned} \quad (\text{E.7})$$

The summation over the indices give traces. For ease of writing, the formulas can be abbreviated,

$$\begin{aligned} A_\mu &= \left[(i\not{p}' + M)^\alpha \gamma_\mu (i\not{p} + M)^\beta \right] \\ B_\mu &= \left[(i\not{p}' + M)^\alpha \frac{\sigma_{\mu\nu} q_\nu}{2M} (i\not{p} + M)^\beta \right]. \end{aligned} \quad (\text{E.8})$$

The equation becomes,

$$\langle \chi(p', s') | J_\mu | \chi(p, s) \rangle = \text{tr} \left[\Gamma^{\beta\alpha} A_\mu \right] F_1(q^2) - \text{tr} \left[\Gamma^{\beta\alpha} B_\mu \right] F_2(q^2). \quad (\text{E.9})$$

$$\text{tr} \left[\Gamma^{\beta\alpha} A_\mu \right] = \text{tr} \left[\Gamma^{\beta\alpha} (i\not{p}' + M)^\alpha \gamma_\mu (i\not{p} + M)^\beta \right], \quad (\text{E.10})$$

$$\text{tr} \left[\Gamma^{\beta\alpha} B_\mu \right] = \text{tr} \left[\Gamma^{\beta\alpha} (i\not{p}' + M)^\alpha \frac{\sigma_{\mu\nu} q_\nu}{2M} (i\not{p} + M)^\beta \right]. \quad (\text{E.11})$$

For μ is selected as 4, Γ' is selected as 4 and Γ is selected as 4 the ratio gives Sachs electric form factor, where Γ_4 is defined as $\begin{bmatrix} 1 & 0 \\ 0 & 0 \end{bmatrix}$;

$$\text{tr} \left[\Gamma^{\beta\alpha} A_4 \right] = \text{tr} \left[\Gamma^{\beta\alpha} (i\not{p}' + M)^\alpha \gamma_4 (i\not{p} + M)^\beta \right], \quad (\text{E.12})$$

$$\text{tr} \left[\Gamma^{\beta\alpha} B_4 \right] = \text{tr} \left[\Gamma^{\beta\alpha} (i\not{p}' + M)^\alpha \frac{\sigma_{4\nu} q_\nu}{2M} (i\not{p} + M)^\beta \right]. \quad (\text{E.13})$$

Splitting the energy and three momentum parts

$$\not{p}' = \vec{p}' \cdot \vec{\gamma} - iE_{p'} \gamma_4, \quad (\text{E.14})$$

$$\not{p} = \vec{p} \cdot \vec{\gamma} - iE_p \gamma_4, \quad (\text{E.15})$$

putting in E.10 and E.11

$$\begin{aligned} A_4 &= \left[\gamma_4 (E_{p'} + \gamma_4 M) (E_p + \gamma_4 M) - i(E_p - \gamma_4 M) \vec{p}' \cdot \vec{\gamma} - i(E_{p'} - \gamma_4 M) \vec{p} \cdot \vec{\gamma} - 2\gamma_4 i \sigma_{kj} p'_k p_j \right. \\ &\quad \left. + \gamma_4 \vec{p} \cdot \vec{p}' \right], \end{aligned} \quad (\text{E.16})$$

$$B_4 = \frac{\gamma_4}{2M} \left[- (E_{p'} + \gamma_4 M) i \vec{\gamma} \cdot \vec{q} (E_p + \gamma_4 M) - \vec{q}^2 \gamma_4 (E_p + \gamma_4 M) - \vec{p} \cdot \vec{q} \gamma_4 (E_p - E_{p'}) + \right. \\ \left. i \left((\vec{p} + \vec{p}') \vec{q} \cdot \vec{\gamma} \cdot \vec{p} + \vec{p}^2 \vec{\gamma} \cdot \vec{q} + 2\gamma_4 \sigma_{kj} p_k q_j (E_p + E_{p'} + 2\gamma_4 M) \right) \right]. \quad (\text{E.17})$$

Setting $\Gamma' = 4$ and taking the trace

$$\text{tr}[\Gamma_4 A_4] = 2 \left[2E_p E_{p'} + M(E_p + E_{p'}) - \frac{q^2}{2} \right], \quad (\text{E.18})$$

$$\text{tr}[\Gamma_4 B_4] = 2 \left[\frac{-q^2}{4M^2} M(E_p + E_{p'} + 2M) - \frac{1}{2} (E_{p'} - E_p)^2 \right]. \quad (\text{E.19})$$

The two point function is

$$\langle F^{NN}(t; p; \Gamma_4) \rangle = \sum_{B,s} e^{-E_p t} \frac{Z_B^2}{2E_p} \text{tr} \left[\Gamma_4 i \not{p} + M \right]. \quad (\text{E.20})$$

Taking the trace

$$\langle F^{NN}(t; p; \Gamma_4) \rangle = \sum_{B,s} e^{-E_p t} \frac{Z_B^2 (E + M)}{2E_p}. \quad (\text{E.21})$$

With help of these the ratio becomes

$$\Pi(0, -q, \Gamma_4, \Gamma'_4, \mu = 4) = \sqrt{\frac{(E + M)}{2E}} G_E(q^2). \quad (\text{E.22})$$

For $\mu = i$, $\Gamma' = j$ and $\Gamma = 4$ the ratio gives Sachs Magnetic Form Factor,

$$A_i = (i \not{p}' + M)^\alpha \gamma_i (i \not{p} + M)^\beta, \quad (\text{E.23})$$

$$B_i = (i \not{p}' + M)^\alpha \frac{\sigma_{i\nu} q_\nu}{2M} (i \not{p} + M)^\beta. \quad (\text{E.24})$$

Splitting the energy and three momentum parts, adding $\Gamma' = j$ and taking the trace

$$\text{tr}[\Gamma_j A_i] = 2\varepsilon_{ijk} \left[p'_k (E_p + M) - p_k (E_{p'} + M) \right], \quad (\text{E.25})$$

$$\text{tr}[\Gamma_j B_i] = \frac{1}{M} \left[\varepsilon_{ijk} p'_k (E_p + M)^2 - \varepsilon_{ijk} p_k (2ME'_p + M^2) \right. \\ \left. + \vec{p} \vec{p}' - p_j \varepsilon_{ilm} p_l p'_m - p'_j \varepsilon_{ilm} p_l p'_m \right]. \quad (\text{E.26})$$

Putting together in to ratio

$$\Pi(0, -q, \Gamma_4, \Gamma'_j, \mu = i) = \sqrt{\frac{1}{2E(E + M)}} \varepsilon_{ijk} q_k G_M(q^2). \quad (\text{E.27})$$

E.3 $N\gamma \rightarrow \Delta$ Electromagnetic Form Factors

The matrix element of $N\gamma \rightarrow \Delta$ transition is written as

$$\langle \chi^\Delta(p', s') | J_\mu | \chi(p, s) \rangle = i\sqrt{2/3} \bar{u}_\tau(\vec{p}', s') \mathcal{O}^{\tau\mu} u(\vec{p}, s), \quad (\text{E.28})$$

where $\chi^\Delta(p', s')$ denotes Δ wave function, $u_\tau(p, s)$ is spin vector in Rarita-Schwinger formalism. The vertex tensor $\mathcal{O}^{\tau\mu}$ is written in terms of Sachs form factors [91],

$$\mathcal{O}^{\tau\mu} = G_{M1}(q^2)K_{M1}^{\tau\mu} + G_{E2}(q^2)K_{E2}^{\tau\mu} + G_{C2}(q^2)K_{C2}^{\tau\mu}. \quad (\text{E.29})$$

In this equation the G_{M1}, G_{E2}, G_{C2} form factors are called as the magnetic dipole, the electric quadrupole and the electric charge quadrupole respectively. At low momentum transfers, M1 transition has been found to dominate. The M1 transition can be explained as the spin and isospin flip of a single quark [151]. The small but non-vanishing values of E2 and C2 multipoles give information about deformation of the geometric shape of nucleon. E2 and C2 can be explained as double spin flip involving two interacting quarks [121]. The kinematical factors of vertex tensor in Eq. (E.29) are

$$\begin{aligned} K_{M1}^{\tau\mu} &= -\frac{3}{(m_\Delta + m_N)^2 + q^2} \frac{(m_\Delta + m_N)}{2m_N} i \epsilon^{\tau\mu\alpha\beta} P_\alpha q_\beta, \\ K_{E2}^{\tau\mu} &= -K_{M1}^{\tau\mu} + 6\Omega^{-1}(q^2) \frac{(m_\Delta + m_N)}{2m_N} i \gamma_5 \epsilon^{\tau\lambda\alpha\beta} P_\alpha q_\beta \epsilon^{\mu\lambda\rho\delta} (2P_\rho + q_\rho) q_\delta, \\ K_{C2}^{\tau\mu} &= -6\Omega^{-1}(q^2) \frac{(m_\Delta + m_N)}{2m_N} i \gamma_5 q_\tau (q^2 P_\mu - q \cdot P q_\mu), \end{aligned} \quad (\text{E.30})$$

$\Omega(q^2) = [(m_\Delta + m_N)^2 + q^2][(m_\Delta - m_N)^2 + q^2]$ and $P^\mu = \frac{(p_f^\mu + p_i^\mu)}{2}$, when Eq. (E.28) has been put into Eq. (3.91)

$$\begin{aligned} \langle F_\sigma^{NJ\mu\Delta}(t_2, t_1; p', p; \Gamma) \rangle &= \sum_{s, s'} i \sqrt{\frac{2}{3}} \frac{m_\Delta m_N}{E_\Delta(\vec{p}') E_N(\vec{p})} e^{-E_\Delta(\vec{p}')(t_2 - t_1)} e^{-E_N(\vec{p})(t_1)} \Gamma^{\beta\alpha} u_\sigma(\vec{p}', s') \\ &\quad \bar{u}_\tau(\vec{p}', s') \mathcal{O}^{\tau\mu} u(\vec{p}, s) \bar{u}(\vec{p}, s). \end{aligned} \quad (\text{E.31})$$

When Eqs. (3.20) and (3.29) are used

$$\begin{aligned} \langle F_\sigma^{NJ\mu\Delta}(t_2, t_1; p', p; \Gamma) \rangle &= i \sqrt{\frac{2}{3}} \frac{e^{-(t_2 - t_1)E_\Delta(\vec{p}')} e^{-(t_1)E_N(\vec{p})}}{4E_\Delta(\vec{p}')E_N(\vec{p})} \\ &\quad \left[M_{\sigma\mu}^{M1} G_{M1}(q^2) + M_{\sigma\mu}^{E2} G_{E2}(q^2) + M_{\sigma\mu}^{C2} G_{C2}(q^2) \right], \end{aligned} \quad (\text{E.32})$$

where,

$$\begin{aligned}
M_{\sigma\mu}^{M1} &= \text{Tr} \left(\Gamma (i\not{p}' + m_\Delta) \left[\delta_{\sigma\tau} + \frac{2p'_\sigma p'_\tau}{3m_\Delta^2} + i \frac{p'_\sigma \gamma_\tau - p'_\tau \gamma_\sigma}{3m_\Delta} - \frac{1}{3} \gamma_\sigma \gamma_\tau \right] \right. \\
&\quad \left. K_{M1}^{\tau\mu} (i\not{p} + m_N) \right), \\
M_{\sigma\mu}^{E2} &= \text{Tr} \left(\Gamma (i\not{p}' + m_\Delta) \left[\delta_{\sigma\tau} + \frac{2p'_\sigma p'_\tau}{3m_\Delta^2} + i \frac{p'_\sigma \gamma_\tau - p'_\tau \gamma_\sigma}{3m_\Delta} - \frac{1}{3} \gamma_\sigma \gamma_\tau \right] \right. \\
&\quad \left. K_{E2}^{\tau\mu} (i\not{p} + m_N) \right), \\
M_{\sigma\mu}^{C2} &= \text{Tr} \left(\Gamma (i\not{p}' + m_\Delta) \left[\delta_{\sigma\tau} + \frac{2p'_\sigma p'_\tau}{3m_\Delta^2} + i \frac{p'_\sigma \gamma_\tau - p'_\tau \gamma_\sigma}{3m_\Delta} - \frac{1}{3} \gamma_\sigma \gamma_\tau \right] \right. \\
&\quad \left. K_{C2}^{\tau\mu} (i\not{p} + m_N) \right). \tag{E.33}
\end{aligned}$$

To extract the form factors and to eliminate the exponential terms, a ratio should be defined as

$$R_\sigma(t_2, t_1, p', p, \Gamma, \mu) = \frac{\langle F_\sigma^{\Delta\mu N}{}_{shwl}(t_2, t_1; p', p; \Gamma) \rangle}{\langle \delta_{ij} F_{ij}^{\Delta\Delta}{}_{shwl}(t_2; p'; \Gamma_4) \rangle} \left[\frac{\langle \delta_{ij} F_{ij}^{\Delta\Delta}{}_{shsh}(2t_1; p'; \Gamma_4) \rangle}{\langle F_{shsh}^{NN}(2t_1; p; \Gamma_4) \rangle} \right]^{\frac{1}{2}}. \tag{E.34}$$

The ratio has been chosen among several alternatives used in the literature, because of the signal quality. The three Sachs form factors $G_{M1}(q^2)$, $G_{E2}(q^2)$ and $G_{C2}(q^2)$ can be singled out by choosing the appropriate combinations of Lorentz direction μ , gamma matrices Γ and initial momenta. When momentum is inserted in one spatial direction ($\Gamma = \Gamma_j$) the kinematical factors becomes

$$\begin{aligned}
M_{\sigma\mu}^{M1} &= \frac{-(m_N + m_\Delta) p_\alpha p'_\beta}{m_N((m_N + m_\Delta)^2 + q^2)} \\
&\quad \left[(E_\Delta + m_\Delta)(E_N + m_N) \varepsilon_{\tau\mu\alpha\beta} \varepsilon_{j\sigma\tau} (1 - \delta_{4\tau}) \right. \\
&\quad + \left((E_N + m_N) p'_k - (E_\Delta + m_\Delta) p_k \right) \frac{p'_\sigma}{m_\Delta} (1 - \delta_{4\tau}) \varepsilon_{\tau\mu\alpha\beta} \varepsilon_{jk\tau} \\
&\quad + i \left((E_N + m_N) p'_k - (E_\Delta + m_\Delta) p_k \right) \varepsilon_{\tau\mu\alpha\beta} (\delta_{4\tau} (1 - \delta_{4\sigma}) \varepsilon_{jk\sigma} - \delta_{4\sigma} (1 - \delta_{4\tau}) \varepsilon_{jk\tau}) \\
&\quad + p'_k p_l \varepsilon_{jkl} \left(3\varepsilon_{\sigma\mu\alpha\beta} + i \frac{p'_\sigma}{m_\Delta} \varepsilon_{4\mu\alpha\beta} - \varepsilon_{4\mu\alpha\beta} \delta_{4\sigma} \right) \\
&\quad \left. - p'_k p_l \varepsilon_{\tau\mu\alpha\beta} (1 - \delta_{4\sigma}) (1 - \delta_{4\tau}) (\delta_{jk} \varepsilon_{\sigma\tau l} + \delta_{\sigma\tau} \varepsilon_{jkl} + \delta_{\tau l} \varepsilon_{jk\sigma} - \delta_{\sigma l} \varepsilon_{jk\tau}) \right] \tag{E.35}
\end{aligned}$$

$$\begin{aligned}
M_{\sigma\mu}^{E2} = & -M_{\sigma\mu}^{M1} + \left[-2iK_{\sigma\mu} \left((E_N + m_N)p'_j - (E_\Delta + m_\Delta)p_j \right) \right. \\
& + K_{4\mu} \left(-\delta_{\sigma j}(E_N + m_N)(E_\Delta + m_\Delta) - \frac{p'_j p'_\sigma}{m_\Delta}(E_N + m_N) \right. \\
& \left. \left. - \frac{p_j p'_\sigma}{m_\Delta}(E_\Delta + m_\Delta) + p'_j p_\sigma - \delta_{j\sigma} \vec{p} \cdot \vec{p}' + p_j p'_\sigma \right) \right. \\
& + K_{j\mu} \left(\left(\delta_{4\sigma} - \frac{ip'_\sigma}{m_\Delta} \right) (E_N + m_N)(E_\Delta + m_\Delta) + ip'_\sigma (E_N + m_N)(1 - \delta_{4\sigma}) \right. \\
& \left. \left. + ip_\sigma (E_\Delta + m_\Delta)(1 - \delta_{4\sigma}) + \frac{ip'_\sigma}{m_\Delta} \vec{p} \cdot \vec{p}' + \delta_{4\sigma} \vec{p} \cdot \vec{p}' \right) \right], \tag{E.36}
\end{aligned}$$

$$\begin{aligned}
M_{\sigma\mu}^{C2} = & \frac{i(m_N + m_\Delta)}{m_N} \Omega^{-1} \left(q^2 (p + p')_\mu - q \cdot (p + p') q_\mu \right) \\
& \left[(m_N + E_N) p'_j \left(-3p_\sigma + \frac{p'_\sigma}{m_\Delta} \left(m_N - \frac{2p \cdot p'}{m_\Delta} \right) - i\delta_{4\sigma} \left(m_N + \frac{p \cdot p'}{m_\Delta} \right) \right) \right. \\
& - (m_\Delta + E_\Delta) p_j \left(-3p_\sigma + \frac{p'_\sigma}{m_\Delta} \left(m_N - \frac{2p \cdot p'}{m_\Delta} \right) + i\delta_{4\sigma} \left(m_N + \frac{p \cdot p'}{m_\Delta} \right) \right) \\
& + \delta_{j\sigma} (m_N + E_N)(m_\Delta + E_\Delta) \left(m_N + \frac{p \cdot p'}{m_\Delta} \right) \\
& \left. + (1 - \delta_{4\sigma}) \left(m_N + \frac{p \cdot p'}{m_\Delta} \right) \left(p_\sigma p'_j - \vec{p} \cdot \vec{p}' \delta_{j\sigma} + p_j p'_\sigma \right) \right], \tag{E.37}
\end{aligned}$$

when μ is selected as 4 and initial particle are at rest $\vec{p} = 0$

$$\begin{aligned}
M_{\sigma\mu}^{M1} &= 0, \\
M_{\sigma\mu}^{E2} &= 0, \\
M_{\sigma\mu}^{C2} &= \frac{m_N + m_\Delta}{m_\Delta} \left[q_j q_\sigma \left(1 + \frac{2E_\Delta}{m_\Delta} \right) - \vec{q}^2 \delta_{\sigma j} \right]. \tag{E.38}
\end{aligned}$$

From $\delta_{\sigma j}$, σ must be equal to j . Hence the Coulomb electric quadrupole form factor becomes

$$G_{C2}(q^2) = 2\sqrt{6} \frac{E_\Delta m_\Delta}{m_N + m_\Delta} \sqrt{1 + \frac{m_\Delta}{E_\Delta}} \sqrt{1 + \frac{q^2}{3m_\Delta^2}} \frac{2m_\Delta}{q^2} R_j(q, 0, i\Gamma_j; 4). \tag{E.39}$$

For $\Gamma = j$ the momentum polarization $\sigma \neq 4$ and photon polarization $\mu \neq 4$, kinematical factors are

$$\begin{aligned}
M_{\sigma\mu}^{M1} &= -i \left(\frac{m_N + m_\Delta}{m_\Delta + E_\Delta} \right) q_k \epsilon_{l\mu k} \left((E_\Delta + m_\Delta) \epsilon_{j\sigma l} + \frac{q_\sigma q_l}{m_\Delta} \epsilon_{jml} \right), \\
M_{\sigma\mu}^{E2} &= -M_{\sigma\mu}^{(1)} + i(m_N + m_\Delta) \left[4q_j \left(\delta_{\sigma\mu} - \frac{q_\sigma q_\mu}{\vec{q}^2} \right) + 3 \frac{E_\Delta}{m_\Delta} q_\sigma \right. \\
& \left. \left(\delta_{j\mu} - \frac{q_j q_\mu}{\vec{q}^2} \right) \right], \tag{E.40}
\end{aligned}$$

Putting kinematical factors into the Eq. (E.34), the magnetic dipole $G_{M1}(q^2)$ and electric quadrupole $G_{E2}(q^2)$ form factors can be extracted

$$G_{M1}(q^2) = 2\sqrt{6} \frac{E_{\Delta} m_{\Delta}}{m_N + m_{\Delta}} \sqrt{1 + \frac{m_{\Delta}}{E_{\Delta}}} \sqrt{1 + \frac{q^2}{3m_{\Delta}^2}} \frac{1}{|q|} \left[R_{\sigma}(q_j, 0, \Gamma_j; \sigma) - \frac{m_{\Delta}}{E_{\Delta}} R_{\sigma}(q_{\sigma}, 0, \Gamma_j; j) \right] \quad (\text{E.41})$$

$$G_{E2}(q^2) = 2\sqrt{6} \frac{E_{\Delta} m_{\Delta}}{m_N + m_{\Delta}} \sqrt{1 + \frac{m_{\Delta}}{E_{\Delta}}} \sqrt{1 + \frac{q^2}{3m_{\Delta}^2}} \frac{1}{|q|} \left[R_{\sigma}(q_j, 0, \Gamma_j; \sigma) + \frac{m_{\Delta}}{E_{\Delta}} R_{\sigma}(q_{\sigma}, 0, \Gamma_j; j) \right] \quad (\text{E.42})$$

APPENDIX-F

TABLES FOR ALL PROBABLE q^2 VALUES

Table F.1 Table for probabilities q^2 up to 6

q^2	p_x	p_y	p_z	q^2	p_x	p_y	p_z	q^2	p_x	p_y	p_z	q^2	p_x	p_y	p_z		
1	1	0	0	3	-1	-1	-1	5	-2	-1	0	6	-2	-1	-1		
	0	1	0		-1	-1	1		-2	0	-1		-2	-1	1		
	0	0	1		-1	1	-1		-2	0	1		-2	1	-1		
	-1	0	0		-1	1	1		-2	1	0		-2	1	1		
	0	-1	0		1	-1	-1		-1	-2	0		-1	-2	-1		
	0	0	-1		1	1	1		-1	0	-2		-1	-2	1		
2	-1	-1	0	4	-2	0	0	5	-1	0	2	6	-1	-1	-2		
	-1	0	-1		0	-2	0		-1	2	0		-1	2	-1	-1	2
	-1	0	1		0	0	-2		0	-2	-1		-1	1	-2		
	-1	1	0		0	0	2		0	-2	1		-1	1	2		
	0	-1	-1		0	2	0		0	0	-1		-2	-1	2	-1	
	0	-1	1		2	0	0		0	0	-1		2	1	-1	2	1
	0	1	-1						0	1	-2		-1	1	-2	-1	
	0	1	1						0	1	2		1	-2	1		
	1	-1	0						0	2	-1		1	-1	-2		
	1	0	-1						0	2	1		1	-1	2		
	1	0	1						1	-2	0		1	1	-2		
	1	1	0						1	0	-2		1	1	2		
							1	0	2	1	2	-1					
							1	2	0	1	2	1					
							2	-1	0	2	-1	-1					
							2	0	-1	2	-1	1					
							2	0	1	2	1	-1					
							2	1	0	2	1	1					

Table F.2 Table for probabilities q^2 7-8

q^2	p_x	p_y	p_z
7	-	-	-
	-2	-2	0
	-2	0	-2
	-2	0	2
	-2	2	0
	0	-2	-2
	0	-2	2
8	0	2	-2
	0	2	2
	2	-2	0
	2	0	-2
	2	0	2
	2	2	0

CURRICULUM VITAE

PERSONAL INFORMATION

Name Surname : Huseyin Bahtiyar
Date of birth and place : June 01, 1984 – İstanbul
Foreign Languages : English
E-mail : huseyinbahtiyar@gmail.com

EDUCATION

Degree	Department	University	Date of Graduation
Masters	Physics Engineering	Istanbul Technical University	2012
Undergraduate	Physics	Yildiz Technical University	2010

WORK EXPERIENCE

Year	Corporation/Institution	Enrollment
2011-...	Mimar Sinan Fine Arts University	Research Assistant

PUBLISHERMENTS

1. $\Omega_c \gamma \rightarrow \Omega_c^*$ transition in lattice QCD, Phys. Lett. B747 (2015).
2. $\Xi_c \gamma \rightarrow \Xi_c'$ transition in lattice QCD, arXiv:1612.05722 (in Press) (2017).

Conference Papers

1. Study of charge particle production at simulated 0.9 and 14 TeV P-P collision at LHC ALICE.